ABSTRACT

EMPIRICAL RENORMALIZATION OF SHELL-MODEL HAMILTONIANS and MAGNETIC DIPOLE MOMENTS OF sd-SHELL NUCLEI

By

Wilton Chung

A refinement of the technique of using energy-level data to renormalize shell-model Hamiltonians is described. The one- and two-body matrix elements of the Hamiltonian are treated as parameters and determined by an iterative least-squares fit to experimental energy-level data. To overcome the problems associated with the large number of correlated parameters involved, the least-squares fit is reformulated in terms of orthogonal linear combinations of the one- and two-body matrix elements. Empirical Hamiltonians for full $0d_{5/2}$-$1s_{1/2}$-$0d_{3/2}$ model space shell-model calculations are determined by the described technique using energy-level data at either the lower or upper end of the sd-shell. For the lower end of the sd-shell, the Hamiltonian is renormalized with respect to 197 measured level energies in the A=17-24 region. For the upper end, the data set is comprised of 134 measured level energies in the A=32-39 region. In either case, the initial Hamiltonians are of the realistic variety of Kuo. A single

mass independent (1+2)-body Hamiltonian is found to be inadequate to simultaneously fit the data sets at both ends of the sd-shell. Results of fits to both the upper and lower ends of the sd-shell show that in each case only a few orthogonal parameters are very well determined, and less than half of the orthogonal parameters are at all well determined by the data sets. The dominant result of the empirical renormalization obtained for the Kuo matrix elements is a reduction in attractiveness of the $d_{5/2}$-$s_{1/2}$, $d_{5/2}$-$d_{3/2}$, and $s_{1/2}$-$d_{3/2}$ diagonal two-body matrix elements. Ground-state binding energies and low-lying spectra of a number of sd-shell nuclei are calculated with the renormalized Hamiltonians. The agreement with experiment is very good, except for some missing levels in a few active particles or active holes systems which are presumably intruder states. Band shifting in which entire excited bands are predicted overbound with respect to the ground state, the main defect of present interactions, is corrected and the improvement is found to extend beyond the region of nuclei from which the data sets were taken in the least-squares fits. Ground-state wave functions of nuclei in the middle of the sd-shell also look more "normal" than the results of realistic interactions as is shown by the wave functions generated for ^{28}Si. It is hoped that the two sets of renormalized Hamiltonians will complement each other to give a good description of all nuclei in the sd-shell region.

Using wave functions generated from the renormalized Hamiltonians, magnetic dipole moments of some ground and excited states of sd-shell nuclei are calculated. Results are given both for using the bare-nucleon values of the single-particle reduced μ matrix elements and values obtained by a fit to available precise measured magnetic moments. Agreement with experiment is good with either operator for A=17-26. However, for A=28-39, results agree less well with experiment using the bare-nucleon operator than using the fitted operator. Effective orbital g-factors and intrinsic moments are also obtained from the fitted operators.

EMPIRICAL RENORMALIZATION OF SHELL-MODEL HAMILTONIANS and MAGNETIC DIPOLE MOMENTS OF sd-SHELL NUCLEI

By

Wilton Chung

A DISSERTATION

Submitted to
Michigan State University
in partial fulfillment of the requirements
for the degree of

DOCTOR OF PHILOSOPHY

Department of Physics

1976

ACKNOWLEDGMENTS

I wish to express my deepest appreciation to my thesis adviser, Professor Hobson Wildenthal, whose influence goes beyond this work, for introducing me to the many areas of current interest in nuclear physics, especially the shell model and this study, and for his guidance and continuing help and encouragement throughout the course of this work and the writing of the thesis.

I am grateful to Dr. Jerzy Borysowicz for the enlightening discussions on least-squares fitting and error analysis.

To the members of the Cyclotron Laboratory computer staff, especially to Mr. Richard Au and Mr. Robert Howard, go my thanks for their excellent maintenance of the computer and computer assistance, without whom this study would have been impossible. The patience of the entire professional staff of the Cyclotron Laboratory is also appreciated.

Special thanks go to Dr. Rex Whitehead and Dr. Sandy Watt for their generosities in making the Glasgow Shell-Model Code readily available.

Parts of this work were done with the computer facilities at Oak Ridge National Laboratory, Brookhaven National Laboratory, Glasgow University in Scotland, and Rutherford Laboratory in England. I wish to express my appreciation, especially to Dr. Joe McGrory and Dr. Duane Larson at Oak Ridge National Laboratory, and Dr. Sandy Watt at Glasgow University for their help and assistance.

I also acknowledge the financial support of the National Science Foundation throughout my graduate career at M.S.U.

TABLE OF CONTENTS

LIST OF TABLES

LIST OF FIGURES

I. EMPIRICAL RENORMALIZATION OF SHELL-MODEL HAMILTONIANS (FOR sd-SHELL NUCLEI)

I.1. Introduction

Shell-model calculations have proved to be successful in describing not only energy levels of nuclei, but other properties such as spectroscopic factors, electromagnetic transitions and moments as well.[1-12] However, a serious limitation of the method is the rapid increase in the dimensions of the model space as the number of particles considered active is increased. Present calculations have to be done in well-chosen truncated spaces. The major problem is then that of finding an appropriate effective Hamiltonian for the model space.

For mass A=18-38 "s-d shell" nuclei, many aspects of nuclear properties can be well reproduced by treating the three orbits $0d_{5/2}$, $1s_{1/2}$, $0d_{3/2}$ as active while the $0s_{1/2}$, $0p_{3/2}$, $0p_{1/2}$ orbits are filled, forming an inactive ^{16}O core.[1-3, 5-8] The model space is spanned by all Pauli-allowed states formed from distributing A-16 active nucleons in the three active orbits. The effective Hamiltonian is assumed to consist of only one-and two-body parts. The one-body terms represent the interaction

energies of the active nucleons with the core, while the two-body terms represent the residual effective interactions among the active nucleons. For each A,J,T combination, the many-body Hamiltonian is constructed and diagonalized in the model basis space. The eigenvalues are interpreted as energy levels and compared with corresponding experimentally observed levels. The associated eigenvectors are used to calculate other experimentally measured nuclear properties.

The advent of sophisticated computer codes like the J-T coupling code of French et al.[13] (Oak Ridge-Rochester) and the M-scheme code of Whitehead[14] (Glasgow) have made shell-model calculations relatively straightforward in a computational sense. Nuclei of the sd-shell have since been extensively studied[1-8] with various effective interactions obtained by different techniques. First, there are realistic effective interactions derived from nucleon-nucleon scattering data, such as those of Kuo and Brown[15] and Kuo.[16] The successes and failures of this type of interactions have been discussed extensively for a few particles (A=18-22),[1] and a few holes (A=34-38)[2] in the sd-shell; and more recently for more than 6 active nucleons (A=23-31) in the sd-shell.[5-8] Secondly, the residual two-nucleon interaction may be assumed to have a simple general functional dependence. The variables in the function are then adjusted to best reproduce the experimental level energies. For example, the depths of the

various spin-isospin components of a potential with a gaussian radial dependence,[17] or the strengths of the two isospin components of surface-delta or modified surface-delta interactions[18] can be varied to best reproduce the experimental level energies. Finally, the one- and two-body matrix elements of the Hamiltonian can be treated as basic parameters of the model,[19] independent of concern about any underlying potential, and determined empirically from available experimental level energies.

The technique of direct empirical determination of the two-body matrix elements had early successes with nuclear levels approximately described by models of one or two "j" orbits.[9,10,20,21,22] The problem inherent in this technique is the rapid increase in the number of two-body matrix elements (2bme parameters) with larger model spaces. For example, the Hamiltonian for the $(f_{7/2})^n$ model space is specified by only eight 2bme, while the $1s_{1/2}$-$0d_{3/2}$ model space requires fifteen. For the full sd-shell model space, sixty-three 2bme are needed to specify the Hamiltonian. Attempts[1,3] have previously been made to empirically improve some features of the realistic interactions of Kuo.[16] However, these attempts circumvented the problem of "too many" parameters by adjusting only selected 2bme. Specifically, the Preedom-Wildenthal (PW) interaction[3] was fitted to 72 experimental level energies in the A=18-22 region by adjusting only the 2bme which do not involve the

$d_{3/2}$ orbit together with only the centroids of the $d_{5/2}$-$d_{3/2}$ and $d_{3/2}$-$d_{3/2}$ interactions. The success of the PW interaction in the A>22 region, as shown by recent full sd-shell calculations[5-8] by the Glasgow group, is encouraging. The problem remains of how to manage the larger number of parameters in an optimum way. A more systematic method of extracting as much information as possible from the level-energy data while at the same time varying the right number of two-body matrix elements is certainly desirable.

In the following, the formulation of theoretical binding energies in terms of one- and two-body matrix elements is briefly outlined and, from this, expressions for the least-squares fit to experimental energies are derived. A method is described in which the least-squares fit problem is reformulated in terms of uncorrelated linear combinations of the one- and two-body matrix elements or parameters. The uncorrelated parameters are reordered according to increasing uncertainty, and the well determined separated from the poorly determined. The well determined uncorrelated parameters are varied while the poorly determined uncorrelated parameters are kept fixed. A new set of one- and two-body matrix elements is derived by applying the inverse transformation to the uncorrelated parameters.

Applications of the technique are then described. An attempt was initially made to obtain an empirical Hamiltonian for the whole sd-shell region by least-squares

fitting to level energies in A=18-24 and A=32-38 simultaneously. This attempt was not successful. The problem was then divided into two separate least-squares fits, in the A=18-24 and A=32-38 regions, respectively. Results of the empirical Hamiltonians obtained are presented and compared to the realistic Hamiltonians of Kuo[16] used as the starting sets. Ground-state binding energies of sd-shell nuclei, and spectra of A=18-24, ^{25}Mg, ^{26}Al and A=32-38 are also presented. Mass excesses of neutron-rich nuclei are compared with predictions using other mass formulae.

I.2. Method

The Hamiltonian is assumed to consist of one- and two-body matrix elements only:[23]

$$H = \Sigma e_i a_i^+ a_i + \Sigma V_{klmn} a_k^+ a_l^+ a_m a_n \qquad (1)$$

where e_i are the single particle energies, V_{klmn} are the two-body matrix elements, and a_i and a_i^+ are the single particle annihilation and creation operators, respectively. For a more compact definition, we use:

$$x = e_i \text{ or } V_{klmn}$$

and

$$\theta_l = a_i^+ a_i \text{ or } a_k^+ a_l^+ a_m a_n$$

equation (1) becomes:

$$H = \sum_1^p x_l \theta_l \ , \qquad (2)$$

where p is the total number of one- and two-body matrix elements.

Let ϕ_i^k denote the i^{th} pure configuration basis state where k stands for a set of quantum numbers, e.g, A-16 number of particles, angular momentum J, isospin T, and parity π. One- and two-body operator matrix elements can be defined as:

$$\rho_{ijl}^k = \langle\phi_i^k|\theta_l|\phi_j^k\rangle \quad . \tag{3}$$

Note that the operator matrix elements are independent of the interaction and only dependent on the model space. A matrix element of the many-body Hamiltonian can then be expressed as:

$$\begin{aligned} H_{ij}^k &= \langle\phi_i^k|H|\phi_j^k\rangle \\ &= \sum_l^p \langle\phi_i^k|\theta_l|\phi_j^k\rangle x_l \\ &= \sum_l^p \rho_{ijl}^k x_l \quad . \end{aligned} \tag{4}$$

Let Ψ^k be an eigenstate with corresponding eigenvalue λ^k. Ψ^k can be expressed as a linear combination of the basis states ϕ_i^k;

$$\Psi^k = \sum_i^D \alpha_i^k \phi_i^k \tag{5}$$

where α_i^k are the amplitudes of the wavefunction, and D is the dimension of the state k in the model space. Equations (4) and (5) give:

$$\lambda^k = \langle\psi^k|H|\psi^k\rangle$$

$$= \sum_{ij} \alpha_i^k \alpha_j^k \langle\phi_i^k|H|\phi_j^k\rangle$$

$$= \sum_{ij} \alpha_i^k \alpha_j^k \rho_{ijl}^k \; x_l \qquad (6)$$

Summing over i and j first gives

$$\lambda^k = \sum_{l}^{p} \beta_l^k \; x_l \qquad (7)$$

where

$$\beta_l^k = \sum_{ij} \alpha_i^k \alpha_j^k \rho_{ijl}^k \qquad (8)$$

Equation (7) expresses the eigenvalue λ^k as a linear expression of the one- and two-body matrix elements. The β_l^k's are just combinations of the operator matrix elements and amplitudes of the wavefunction. It should be noted that the β's, unlike the ρ's, depend on the Hamiltonian through the amplitudes α's.

Changes in the one- and two-body matrix elements which improve the agreement of the λ^k with experimental level-energies can be obtained by minimizing the quantity:

$$\chi^2 = \sum_{k}^{n} (E_{exp}^k - \lambda^k)^2 \qquad (9)$$

where E^k_{exp}'s are experimental level energies corresponding to the λ^k's for the shell-model eigenstates Ψ^k's, and n is the total number of such level energy data. E^k_{exp} is the binding energy relative to the model core, with Coulomb energies extracted. The p number of parameters in the Hamiltonian gives p equations of

$$\frac{\partial \chi^2}{\partial x_m} = 0 \qquad m=1,2,3,\ldots,p \qquad (10)$$

Equations (7), (9) and (10) give:

$$\sum_k^n (E^k_{exp} - \sum_1^p \beta^k_1 x_1) \frac{\partial \sum_{1'}^p \beta^k_{1'} x_{1'}}{\partial x_m} = 0$$

$$m=1,2,3,\ldots,p \qquad (11)$$

It has been pointed out that the β's depend indirectly on the interaction through the α's. However, the α's change slowly with the interaction. For small changes in the interaction, the β's can be treated as constants; more precisely, with an assumption of approximate linearity of equation (7), the minimization of equation (9) can be done iteratively until the interaction converges. Equation (11) then becomes

$$\sum_k^n (E^k_{exp} - \sum_1^p \beta^k_1 x_1) \beta^k_m = 0 \qquad m=1,2,3,\ldots,p \qquad (12)$$

Defining $$\gamma_{ml} = \sum_{k}^{n} \beta_l^k \beta_m^k \tag{13}$$

and $$\varepsilon_m^{exp} = \sum_{k}^{n} E^k_{exp} \beta_m^k \tag{14}$$

Equation (12) becomes:

$$\sum_{l}^{p} \gamma_{ml} x_l = \varepsilon_m^{exp} \qquad m=1,2,3,\ldots,p \tag{15}$$

The least-squares fit reduces to that of solving p equations for p unknowns. Equation (15) in more compact matrix notation becomes

$$GX = \tilde{\varepsilon} \tag{16}$$

where G is a pxp matrix whose matrix elements are the γ_{ml}'s; X is a vector composed of the (unknown) parameters, and $\tilde{\varepsilon}$ is a vector derived from the experimental level-energies. It should be pointed out here that the single-particle energies and/or some of the two-body matrix elements may be fixed in the least-squares fit; in this case p would denote the number of free parameters, not necessarily the total number of one- and two-body matrix elements. For the rest of this section, however, p is taken to be equal to the number of two-body matrix elements.

The procedure commonly followed in the past in solving equation (16) has been to solve for G^{-1} by numerical methods. This would then be followed by a matrix

multiplication $G^{-1}\tilde{\epsilon}$ to obtain the parameters X. However, the problems of the large number of parameters (or equivalently the correlations among the parameters), and an insufficient data set, make it difficult to do the minimization effectively. In previous cases, some additional assumptions were usually made. For example, certain parameters were assumed to be poorly determined by the data set and were fixed at prior theoretical values. In determining the PW interaction, for example, blocks of parameters were assumed to vary by only one single additive constant rather than independently. The centroids of the $d_{5/2}$-$d_{3/2}$ and $d_{3/2}$-$d_{3/2}$ interactions were adjusted in this way.

MacFarlane has previously compared[24] empirically determined 2bme with realistic effective interactions. He noted that the eigenvectors of the error matrix give uncorrelated linear combinations of the two-body matrix elements, and that the corresponding eigenvalues give the uncertainties in these linear combinations. From the error matrix for the p-shell calculation of Cohen and Kurath,[9] MacFarlane found that of the 11 independent two-body parameters, only seven were well determined. Similar results were found in other shell-model least-squares fits, with an increasing proportion of poorly determined linear combinations as the number of two-body matrix elements increased.

In view of the difficulty in thus determining a large number of two-body matrix elements, the question may be asked whether the χ^2 can be minimized in terms of uncorrelated linear combinations of the two-body matrix elements. The mutual independence of the parameters should then make the problem more manageable. In others words, can the G in equation (16) be diagonalized as in the case of the error matrix investigated by MacFarlane. The eigenvectors thus derived would give uncorrelated linear combinations of the two-body matrix elements.

It follows from equation (13) that $\gamma_{ml} = \gamma_{lm}$, so that G is a symmetric matrix. It can be diagonalized with the same numerical method used to diagonalize the symmetric Hamiltonian in shell-model calculations. The least-squares fit can then be reformulated in terms of uncorrelated linear combinations of the two-body matrix elements or for a shorter name "orthogonal parameters."

Let A be the transformation matrix formed from the eigenvectors of G. Matrix A being orthogonal, A^{-1} is just A^T. Let D be

$$D = AGA^T \tag{17}$$

It is interesting to note that the uncorrelated linear combinations obtained here are exactly the same as those obtained by MacFarlane from the error matrix. This is easily seen by getting the inverse of D, in which case

$$D^{-1} = A\, G^{-1} A^{T}$$

where G^{-1} is just the error matrix. The eigenvalues of the matrix D are just the inverses of the eigenvalues of the error matrix. The same transformation is applied to the right hand side of equation (16)

$$\tilde{C} = A\tilde{\varepsilon} \tag{18}$$

A new set of orthogonal parameters is then obtained by

$$Y = C/D \tag{19}$$

where the matrix division denotes dividing each component of C by the corresponding diagonal matrix element of D. Applying the inverse transformation immediately gives a new set of fitted two-body matrix elements, i.e.,

$$X = A^{T}Y \tag{20}$$

The above procedure merely replaces the inversion of G by the diagonalization of G, it does not solve all problems of the least-squares fit. We next note that since the eigenvalues of the error matrix are the squares of the uncertainties of the corresponding orthogonal parameters, the eigenvalues of the D matrix are just the inverses of the squared uncertainties. The orthogonal parameters can then be ordered according to the increasing or decreasing certainty with which the data set determines them, and the

well determined orthogonal parameters separated from the poorly determined orthogonal parameters.

In Figure 1 are plotted the eigenvalues d_m of the D^{-1} error matrix, and the deviations between corresponding starting and fitted orthogonal parameters. The fitted orthogonal parameters are derived from the least-squares fit, i.e., Y in equation (19). The starting orthogonal parameters are derived by applying the same transformation on the starting Hamiltonian for the iteration.

It is clear that the deviations for the very well determined orthogonal parameters are systematically much smaller than the others. The deviations for the poorly determined orthogonal parameters are large and randomly distributed, a large part of which must be contributed from round-off errors. For these parameters with large uncertainties, the starting orthogonal parameters are as "good" as the fitted orthogonal parameters in terms of fitting the data set. To avoid the round-off errors, and in the spirit of the linear approximation of equation (17), i.e., keeping the change in the interaction small in each iterative least-squares fit, the procedure in obtaining a new interaction is modified. First, the transformation A is applied on the starting Hamiltonian, i.e.,

$$Y^S = A\ X^S \qquad (21)$$

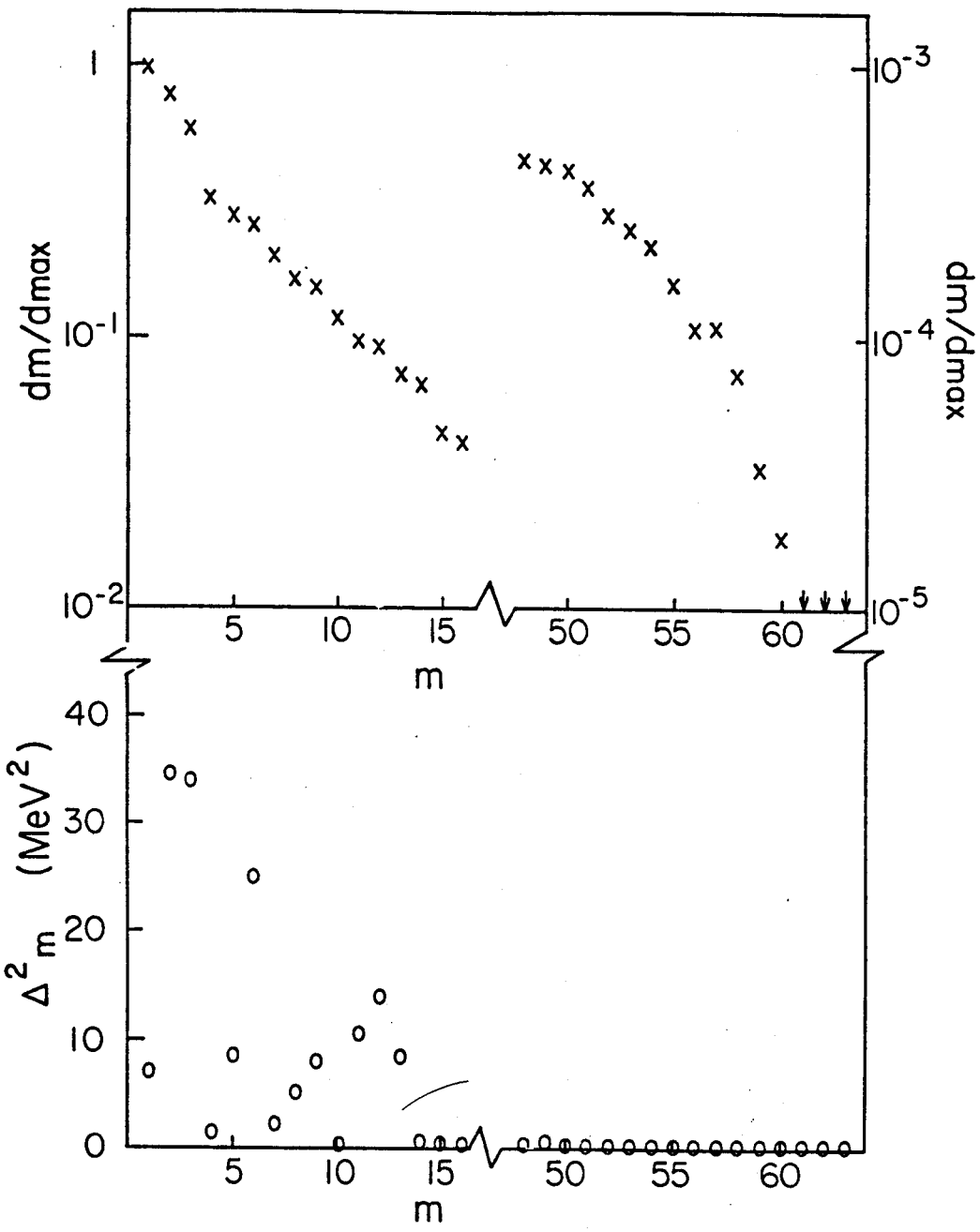

Figure 1. Eigenvalues d_m of the D^{-1} error matrix and the deviations between corresponding starting and fitted orthogonal parameters.

where X^s specifies the starting Hamiltonian and Y^s is the vector of starting orthogonal parameters. A new vector Y' is defined by:

$$Y' = Y(\delta \geq d_m) + Y^s \ (\delta < d_m) \tag{22}$$

The δ is an arbitrarily set uncertainty level, and the d_m's are the diagonal matrix elements of the D^{-1} matrix. The vector Y' is made up of components from Y if the corresponding d_m is less than or equal to the uncertainty level δ; otherwise, components from Y^s are used. The d_m's are the squared uncertainties of the corresponding orthogonal parameters, so that the δ in effect sets a limit on the uncertainties of the orthogonal parameters. A new interaction for the iteration is then derived by applying the inverse transformation on Y',

$$X' = A^T Y' \tag{23}$$

As a result of the modification of equation (22) some constraints have been added to the least-squares fit. Ideally, the fitted interaction is held to the starting interaction except for the parts that are well determined by the data set.

The above procedure describes one iteration of the least-squares fit. The process is repeated until the interaction converges, i.e., until the differences between the $(n+1)^{th}$ set and n^{th} set of matrix elements are negligibly small. A reasonable realistic interaction,

e.g., Kuo's matrix elements[16] derived from the Hamada-Johnston potential,[25] or a schematic interaction, e.g., the MSDI,[18] is usually used as the initial Hamiltonian for the process. The many-body Hamiltonian matrices are created and diagonalized in the shell-model space to obtain the level energies and corresponding eigenvectors. The β's, and so the γ's, are calculated from the eigenvectors. A new interaction $X^{(1)}$ is then derived from the least-squares fit. A new set of level energies, eigenvectors and hence the β's and γ's are calculated from the interaction $X^{(1)}$. From the ensuing new least-squares fit a new and further improved interaction $X^{(2)}$ is derived. Again, a third set of interaction $X^{(3)}$ is calculated from $X^{(2)}$, $X^{(4)}$ from $X^{(3)}$, and so on, until the interaction converges.

The diagonalization of the G matrix, or the reformulation of the least-squares problem in terms of orthogonal parameters, attacks the main problems of the minimization of χ^2, namely those of the large number of correlated matrix elements and the insufficiency of the data set. The matrix elements of G are calculated from the eigenvectors of the Hamiltonians, so that the data set indirectly determines the orthogonal linear combinations of the two-body matrix elements, and separates the well determined from the poorly determined parameters. The least-squares problem boils down to having a reasonable initial Hamiltonian for the shell-model space and of fixing the uncertainty level.

There exist now many realistic interactions calculated from potentials derived from nucleon-nucleon scattering data, such as the Hamada-Johnston potential[25] or the Reid potential.[26] Schematic interactions, such as the MSDI,[18] have also been shown to reproduce nuclear observables quite well. The uncertainty level δ allows the fixing of the parameters to be varied. Only very well determined orthogonal parameters may be varied, thus only making slight improvements in the interactions. In the other extreme, even poorly determined orthogonal parameters may be varied with the possible inclusion of round-off errors. A compromise between the two is possible by setting the δ at an intermediate level. The parameters are found to converge in at most two iterations for a fixed uncertainty level. Thus, varying the δ does not affect the total number of iterations needed for the whole calculation. In fact, it is useful in that the change in the interactions can be kept small in each iteration, in line with the linear approximation of equation (7).

I.3. Details of the Calculation

I.3.A. Initial Attempt, "Intruder States" and Coulomb Energies

The A=18=22 and 34-38 regions have previously been investigated extensively in shell-model studies[1,2] with a full sd-shell model space, i.e., with (A-16) active particles distributed in the $0d_{5/2}$, $1s_{1/2}$, $0d_{3/2}$ orbits. Comparisons were made between experiments and results of

realistic, schematic, and limited-fit interactions for which only a few matrix elements were varied to fit experimental energy data. In general, the results were inconclusive as to which interaction was better. Preedom and Wildenthal[3] further expanded the shell-model least-squares fit in the A=18-22 region by allowing more degrees of freedom in the two-body matrix elements. All two-body matrix elements which did not involve the $d_{3/2}$ orbit, plus the centroids of the $d_{5/2}$-$d_{3/2}$ and $d_{3/2}$-$d_{3/2}$ interactions were varied. As the active particles are mainly filling the $d_{5/2}$ orbit in the A=18-22 region, the matrix elements involving the $d_{3/2}$ orbit are hence not well fixed by the data set. Quantitatively, the PW interaction results were found to agree better with experiment relative to results from previous interactions in essentially all cases in the A=18-22 region. More recent calculations[5-8] in the full sd-shell model space by the Glasgow group showed that the improvement extends beyond the A=18-22 region.

Under the stimulation of the success of the PW interaction, the initial purpose of the present study was to find a single empirically determined interaction for the whole sd-shell region. The Glasgow shell-model developments have made it possible to include more measured level energies in the least-squares fit. Specifically, the two sd-shell regions previously studied can now be expanded to include measured level energies of A=23,24 and A=32,33 in the fit.

More measured level energies will presumably determine more matrix elements of the Hamiltonian. Using the above described least-squares method, a single mass-independent (1+2)-body Hamiltonian was fitted simultaneously to measured level energies in both the expanded A=17-24 and A=32-39 regions, with the level binding energies corrected relative to ^{16}O and with Coulomb energies extracted. It was found that the least-squares χ^2 was fairly constant as the number of data points increased in the A=17-24 region. However, adding more measured level energies from the A=32-39 region into the fit increased the χ^2 by almost a factor of 2. Besides the poorer fit, nuclear observables calculated from wave functions derived from the fitted interaction thus obtained were in poorer agreement with experiment than was the case when the process was confined to one or the other subsets of the data. A single set of mass-independent (1+2)-body Hamiltonian was hence found to be inadequate for the description of the entire sd-shell model space. Accordingly, the least-squares fit was divided into two parts; the A=17-24 region and the A=32-39 region.

Before discussing the two least-squares fits separately, it is appropriate here to comment on how "intruder states" and the extraction of Coulomb energies are treated in the present study. By "intruder states," we mean experimentally observed states which cannot be even qualitatively described by a (1+2)-body Hamiltonian in a $(0s)^4(0p)^{12}(1s,0d)^{A-16}$ shell-model space. Trivially, these

include the negative-parity states, for which the model cannot yield theoretical partners. More important, there are certain positive-parity states which appear to be dominated by configurations from outside of the sd-shell model space. Examples are core-excited states where 2,4 or more particles are excited out of the ^{16}O core, or states where 2,4 or more active particles are excited out of the sd-shell and into the (0f,1p) orbits. For states in the A=18-20 and A=36-38 regions, i.e., close to the boundaries of the model space, those levels suspected to be intruder states or to involve large admixtures of intruder states are not included in the least-squares fits. For example, the second observed 1^+, first observed 2^+ and second observed 3^+ levels in ^{18}F are not included in the fits. The only exceptions are the second and third observed 0^+ in ^{18}O, and the second and third observed 2^+ in ^{38}Ar. In these cases, an approximate centroid for the two states is used. However, for states in the A=21-24 and A=32-35 regions, i.e., farther away from the model space boundaries, intruder state problems are generally ignored. The low-lying observed positive-parity states are taken to have a one-to-one correspondence with the calculated results, the inherent assumptions being that these states have only small and constant admixtures of intruder states. A fundamental assumption is that this sort of effect can be treated by a renormalization of the Hamiltonian through the least-squares fit.

The Hamiltonian used in the least-squares fit includes no Coulomb terms. Hence the measured level binding energies have to be corrected by removal of the Coulomb component. However, only estimates can be made of the Coulomb part of the binding energies. In most previous work, the Coulomb part of the binding energies was parameterized in some form, for example[23]

$$E_{Coul}(A,Z)=CZ + \frac{1}{2}aZ(Z-1)+b[\frac{Z}{2}] \quad ,$$

where Z is the number of active protons, $[\frac{Z}{2}]$ is the largest integer $\leq \frac{Z}{2}$ and C, a, b are parameters which depend on the active orbits in which the protons are distributed. The energy differences between mirror nuclei having either $T_z=\pm T=\pm 1/2$ or $T_z=\pm T=\pm 1$ is then given by

$$\Delta_1(A) = C + Za + \frac{1}{2}\{1-(-1)^Z\}b \quad ,$$

and

$$\Delta_2(A) = 2C + (2Z + 1)a + b \quad ,$$

respectively.

The parameters C, a, b are determined by a least-squares fit to measured energy differences between mirror nuclei.[22] The Coulomb part of the binding energies can then be estimated as a function of A and Z.

Other estimates of the empirical binding energies minus the Coulomb part are possible with the use of $T_> = T_o+1$ and $T_{>>} = T_o+2$ analogue states in T_o nuclei. At present, all T=1 analogue states in T=0 odd-odd nuclei, and

all T=1 and T=2 analogue states in T=0 even-even nuclei, corresponding to the ground states of neighboring nuclei, are known in the sd-shell region.[27,29] For example, the corrected ground-state binding energy E_{corr} of the A=18, T=1 system can be obtained by taking the difference between measured binding energies of ^{16}O and ^{18}O. From reference 28:

$$E_{corr}(A=18,\ T=1) = B.E.(^{18}O) - B.E.(^{16}O)$$
$$= -139.813 + 127.624$$
$$= -12.189 \qquad (MeV).$$

The E_{corr} of the A=18, T=0 system is estimated from the excitation energy of the T=1 analogue state in ^{18}F, corresponding to the ground state of ^{18}O, i.e., from reference 29:

$$E_{corr}(A=18,\ T=0) = E_{corr}(A=18,\ T=1) - Ex.E.(^{18}F,\ T=1)$$
$$= -12.189 - 1.042$$
$$= -13.231 \qquad (MeV).$$

Assuming the difference in measured binding energies of ^{18}O and ^{18}Ne to be due to the Coulomb contribution, the E_{corr} of A=20, T=0 system is obtained from the difference in measured binding energies of ^{18}Ne and ^{20}Ne, i.e.,

$$E_{corr}(A=20,\ T=0) = B.E.(^{20}Ne) - B.E.(^{18}Ne) + E_{corr}(A=18,\ T=1)$$

$$= -160.651 + 132.146 - 12.189$$

$$= -40.694 \quad \text{(MeV)}.$$

The process is repeated with ^{20}Ne to obtain the E_{corr} of ^{22}Na, ^{24}Mg and so on. The E_{corr} of the odd-A nuclei and other even-A nuclei with higher isospin are obtained from the differences in the measured binding energies of the corresponding isotopes.

However, the above estimate for E_{corr} of ^{20}Ne is not unique; there are other possibilities. Use can be made of the T=1 analogue state in ^{20}Ne corresponding to the ground state of ^{20}F, then:

$$E_{corr}(A=20,\ T=1) = E_{corr}(A=18,\ T=0) + B.E.(^{20}F) - B.E.(^{18}F)$$

$$= -13.231 - 154.407 + 137.375$$

$$= -30.263 \quad \text{(MeV)},$$

and

$$E_{corr}(A=20,\ T=0) = E_{corr}(A=20,\ T=1) - Ex.E.(^{20}Ne,\ T=1)$$

$$= -30.26 - 10.26$$

$$= -40.52 \quad \text{(MeV)}.$$

Or use can also be made of the T=2 analogue state in ^{20}Ne corresponding to the ground state of ^{20}O, in which case:

$$E_{corr}(A=20,\ T=2) = B.E.(^{20}O) - B.E.(^{16}O)$$

$$= -151.374 + 127.624$$

$$= -23.750 \qquad \text{(MeV)}.$$

and

$$E_{corr}(A=20,\ T=0) = E_{corr}(A=20,\ T=2) - Ex.E.(^{20}Ne,\ T=2)$$

$$= -23.750 - 16.728$$

$$= -40.478 \qquad \text{(MeV)},$$

and

$$E_{corr}(A=20,\ T=1) = E_{corr}(A=20,\ T=0) + Ex.E.(^{20}Ne,\ T=1)$$

$$= -40.48 + 10.26$$

$$= -30.22 \qquad \text{(MeV)}.$$

The above described procedures are schematically shown in the following diagram:

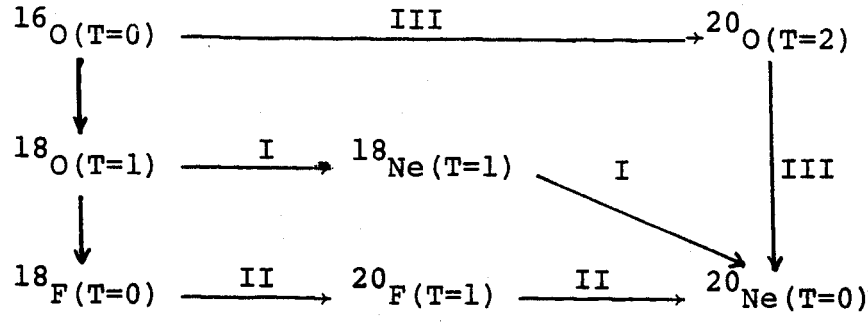

where the procedures are numbered I, II and III. It is noted that the three procedures give different estimates of E_{corr} of ^{20}Ne. The discrepancy between the two extremes, i.e., I and III, is more than 200 keV. It does raise the

question of which is the best estimate. It should be remarked here that the above procedures do not exhaust all possibilities of estimates of Coulomb energies. Other analogue states, such as T=2 states in T=1 nuclei, or T=3/2 states in T=1/2 nuclei and so on, if experimentally known, offer many more alternatives to the above procedures. Qualitatively, part of the discrepancies may be accounted for as due to the effects of different numbers of active neutrons in the different nuclei used in the procedures. However, a full understanding of the differences is a problem to which a solution is not attempted in the present study.

Arbitrarily, procedure III was adopted for the estimate of corrected ground-state binding energies. The only exception is that of deriving E_{corr} of ^{40}Ca from ^{36}Ar. Use of procedure III would entail use of the unmeasured binding energy of ^{36}Ca. Procedure I is used instead, with an additional 200 keV correction for the discrepancy between procedure I and III which is found to be quite general in the sd-shell region. The corrected ground-state binding energies of odd-A nuclei, and even-A nuclei with higher isospin were obtained from the differences in measured binding energies of the corresponding isotopes.

I.3.B. "Particle" Hamiltonian (A=17-24 fit)

The word "Particle" will henceforth refer to the least-squares fit in the A=17-24 region simply because these shell-model calculations were done in the particle formalism. The fit in the A=32-39 region will correspondingly be referred to with the word "Hole"; as will be discussed later, the shell-model calculations there were done in the hole formalism (relative to ^{40}Ca).

The corrected binding energies of 197 experimentally observed states included in the data set for the "Particle" least-squares fit are tabulated in Table 1, together with their excitation energies. The considerations for intruder states and the procedure for the correction of measured binding energies relative to ^{16}O for Coulomb contributions are as described above. The present least-squares fit including level energies of A=23 and 24 involves diagonalizing Hamiltonians of large orders. These can be as large as 2000 in the j-j coupling scheme (Oak Ridge Code) or 13000 in the m-scheme (Glasgow Code). Large amounts of computer time and data storage are required not only for the diagonalization, but as well for the calculation of the coefficients β of equation (7). As a time and storage saving step, the data set was slightly reduced except for the last iteration.

The above time and storage considerations, the linear approximation in the formulation requiring only a

TABLE 1.--Binding and excitation energies of states comprising the data set used to determine the "Particle" Hamiltonian (MeV).

A	2J	2T	ν	Ex	EB[a]	A	2J	2T	ν	Ex	EB[a]
17	01	01	1	0.87	- 3.27		00	02	1	3.53	-26.69
	03	01	1	5.74	+ 1.60[b]		02	02	1	1.06	-29.16
	05	01	1	0.00	- 4.14				2	3.49	-26.73
									3	4.08	-26.14
18	02	00	1	0.00	-13.23		04	02	1	0.00	-30.22
			2	3.72	- 9.51				2	2.04	-28.18
	04	00	1	3.84	- 9.39		06	02	1	0.66	-29.56
	06	00	1	0.94	-12.29				2	2.20	-28.02[g]
			2	4.12	- 9.11				3	2.97	-27.25[g]
	10	00	1	1.12	-12.11		08	02	1	0.82	-29.40[h]
									2	3.68	-26.54[g]
	00	02	1	0.00	-12.19		10	02	1	1.82	-28.40[h]
			2	4.80	- 7.39[c]		12	02	1	4.51	-25.71[i]
	04	02	1	1.98	-10.21		14	02	1	4.59	-25.63[i]
			2	3.92	- 8.27						
	06	02	1	5.37	- 6.82		00	04	1	0.00	-23.75
	08	02	1	3.55	- 8.64				2	4.45	-19.30
							04	04	1	1.67	-22.08
19	01	01	1	0.00	-23.68				2	4.07	-19.68
			2	5.34	-18.34[d]		08	04	1	3.57	-20.18
	03	01	1	1.56	-22.12						
	05	01	1	0.22	-23.46	21	01	01	1	2.80	-44.44
			2	4.56	-19.12				2	5.78	-41.46[j]
	07	01	1	4.38	-19.30		03	01	1	0.00	-47.24
			2	5.46	-18.22				2	4.69	-42.55[k]
	09	01	1	2.79	-20.89				3	5.34	-41.90[ℓ]
	11	01	1	6.50	-17.18				4	5.55	-41.69[k]
			2	7.94	-15.74		05	01	1	0.35	-46.89
	13	01	1	4.65	-19.03				2	3.74	-43.50
									3	4.53	-42.71[ℓ]
	01	03	1	1.47	-14.67		07	01	1	1.75	-45.49
	03	03	1	0.10	-16.04				2	5.43	-41.81[ℓ]
			2	3.07	-13.07[e]		09	01	1	2.67	-44.37
			3	5.46	-10.68[f]		11	01	1	4.43	-42.81
	05	03	1	0.00	-16.14		13	01	1	6.45	-40.79[m]
			2	3.15	-12.99						
			3	4.71	-11.43		01	03	1	0.28	-38.11
	07	03	1	2.78	-13.36[e]		03	03	1	1.73	-36.66[n]
	09	03	1	2.37	-13.77[e]				2	3.51	-34.88
							05	03	1	0.00	-38.39
20	00	00	1	0.00	-40.48				2	3.43	-34.96
			2	6.72	-33.76		09	03	1	1.76	-36.63[n]
	04	00	1	1.63	-38.85						
			2	7.46	-33.02	22	02	00	1	0.58	-57.65
	08	00	1	4.25	-36.23				2	1.94	-56.29
	12	00	1	8.78	-31.70				3	3.94	-54.29
	16	00	1	11.95	-28.53		04	00	1	3.06	-55.17

TABLE 1.--Continued.

A	2J	2T	ν	Ex	EB[a]
	04	00	2	4.36	-53.87
	06	00	1	0.00	-58.23
			2	1.98	-56.25[o]
			3	2.97	-55.26
	08	00	1	0.89	-57.34
			2	4.77	-53.46
	10	00	1	1.53	-56.70
			2	4.71	-53.52
			3	5.83	-52.40
	12	00	1	3.71	-54.52[o]
			2	6.58	-51.65[p]
	14	00	1	4.52	-53.71[p]
			2	9.05	-49.18[p]
	16	00	1	8.60	-49.63[p]
	18	00	1	9.86	-48.37[p]
			2	12.62	-45.61[p]
	20	00	1	13.58	-44.65[p]
	00	02	1	0.00	-57.61
			2	6.24	-51.37[q]
			3	7.34	-50.27[q]
	02	02	1	5.34	-52.27[r]
			2	6.86	-50.75[r]
	04	02	1	1.28	-56.33
			2	4.46	-53.15
			3	5.36	-52.25
			4	5.92	-51.69
	06	02	1	5.64	-51.97
	08	02	1	3.36	-54.25
			2	5.52	-52.09
	12	02	1	6.35	-51.26
	16	02	1	11.01	-46.60[s]
	08	04	1	0.00	-43.56[t]
23	01	01	1	2.39	-68.37
			2	4.43	-66.33
			3	6.31	-64.45
	03	01	1	0.00	-70.76
			2	2.98	-67.78
	05	01	1	0.44	-70.32
			2	3.91	-66.85
			3	5.38	-65.38[u]
	07	01	1	2.08	-68.68
			2	4.78	-65.98
			3	5.77	-64.99
	09	01	1	2.70	-68.06
	11	01	1	5.53	-65.23[v]
	13	01	1	6.23	-64.53[v]
	15	01	1	9.04	-61.72[w]
	19	01	1	14.24	-56.52[x]
	01	03	1	1.02	-61.78
			2	3.84	-58.96[y]
	03	03	1	1.83	-60.97
			2	3.44	-59.36[z]
			3	3.99	-58.81[z]
	05	03	1	0.00	-62.80
			2	2.31	-60.49[z]
			3	3.83	-58.97[aa]
	07	03	1	1.70	-61.10
			2	4.43	-58.37[aa]
	09	03	1	2.52	-60.28[bb]
	11	03	1	4.27	-58.53
	05	05	1	0.00	-51.10[aa]
24	00	00	1	0.00	-87.11
			2	6.44	-80.67
	02	00	1	7.75	-79.36
			2	9.83	-77.28
	04	00	1	1.37	-85.74
			2	4.23	-82.88
			3	7.35	-79.76
			4	8.65	-78.46
	06	00	1	5.23	-81.88
	08	00	1	4.12	-82.99
			2	6.01	-81.10
			3	8.44	-78.67
	10	00	1	7.81	-79.30[cc]
	12	00	1	8.12	-78.99[cc]
			2	9.53	-77.58[cc]
	16	00	1	11.86	-75.25[dd]
			2	13.21	-73.90[cc]
			3	14.14	-72.97[dd]
	02	02	1	0.47	-77.18
			2	1.35	-76.30
	04	02	1	0.56	-77.09
			2	1.34	-76.31[ee]
			3	1.85	-75.80[ee]
	06	02	1	1.34	-76.31[ee]
			2	1.89	-75.76[ee]
	08	02	1	0.00	-77.65
	10	02	1	1.51	-76.14[ee]
	00	04	1	0.00	-71.67
			2	4.76	-66.91
	04	04	1	1.98	-69.69
			2	3.87	-67.80
			3	5.58	-66.09
	08	04	1	3.96	-67.71

TABLE 1.--Continued.

A	2J	2T	ν	Ex	EB[a]	A	2J	2T	ν	Ex	EB[a]
25	01	05	1	0.00	-75.97[ff]	33	03	05	1	0.00	-175.14[ll]
26	02	04	1	0.24	-92.04[gg]	35	03	01	1	0.00	-215.34[mm]
	04	04	1	0.10	-92.18[gg]						
			2	0.48	-91.80[gg]		01	05	1	0.00	-200.48[nn]
	06	04	1	0.00	-92.28[hh]						
						38	06	00	1	0.00	-251.19[mm]
28	02	06	1	0.00	-102.66[ii]						
							00	02	1	0.00	-251.06[mm]
29	03	07	1	0.00	-106.94[ii,jj]		04	02	1	2.17	-248.89[mm]
	05	07	1	0.00	-106.94[ii,jj]						
						39	03	01	1	0.00	-264.22[mm]
31	05	05	1	0.00	-148.62[kk]		01	01	1	2.50	-261.72[mm]
							05	01	1	6.71	-257.51[mm,oo]

[a]Unless otherwise noted, the ground-state binding energies are taken from reference 28, corrected for Coulomb energies and relative to ^{16}O; the spin assignments and excitation energies are taken from references 27 and 29.

[b]Reference 30, see text for discussion.

[c]Spectroscopic-factors-weighted centroid of second and third observed 0^+ state.

[d]Reference 38.

[e]Reference 39.

[f]Reference 40.

[g]Reference 41.

[h]References 41 and 42.

[i]Reference 43.

[j]Reference 44.

[k]Reference 45.

[l]Reference 46.

[m]Reference 47.

[n]Reference 48.

[o]Reference 49.

[p]Reference 50.

[q]Reference 51.

[r]Reference 52.

[s]Reference 53.

[t]Reference 54.

[u]Reference 55.

[v]Reference 56.

[w]Reference 57.

[x]References 58 and 59.

[y]The spin-parity assignment is not definite in reference 60. The $^{22}Ne(d,p)\ ^{23}Ne$ results were not sufficient to distinguish between $\ell=0$ and $\ell=1$ transitions.

[z]Reference 60.

[aa]Reference 61.

[bb]Reference 62.

[cc]Reference 63.

[dd]Reference 64.

[ee]Reference 65

[ff]References 66 and 67.

[gg]Reference 68.

[hh]References 68 and 69.

[ii]Reference 69.

[jj]Pre-final calculation showed a douplet of $J^{\pi}=3/2^{+}$ and $5/2^{+}$ for the lowest two states in ^{29}Na, both were fitted to the observed ground-state binding energy.

[kk]Reference 70.

[ll]Reference 71.

[mm]Weighted by $(0.25)^2$.

[nn]Reference 72.

[oo]Reference 31, see text for discussion on $d_{5/2}$-hole strength in ^{39}K.

small change in the interaction in each iteration, and the rapid convergence of the present method of doing the least-squares fit in terms of orthogonal linear combinations of the parameters at a fixed uncertainty level resulted in the adoption of the following fit procedure. Four iterations in all were done to arrive at the final fitted interaction or "Particle" Hamiltonian listed in Table 2. The uncertainty level was kept at a small value in the first iteration and increased slowly for the following three iterations to ensure only a small change in the interactions in each iteration. The data sets in the first and second iterations included only the level energies of A=17-21 and A=22, T=0 systems listed in Table 1. For the third iteration, level energies of A=22, T=1,2 and A=23 systems were added to the data set. The data set was expanded further to include all level energies listed in Table 1 for the fourth and last iteration.

The initial set of 63 two-body matrix elements used is the "K+^{17}O" interaction, which was extensively investigated in reference 1. It is one of the realistic effective interactions calculated by Kuo[16] from the Hamada-Johnston potential.[25] It will be referred to as the KUO14 interaction since a harmonic-oscillator parameter of $\hbar\omega$=14 MeV was used in generating the interaction. The PW interaction was also derived from the KUO14 interaction. The two-body matrix elements of the original KUO14 interaction, the PW

Table 2.--The two-body matrix elements $\langle j_a j_b | V | j_c j_d \rangle_{JT}$ of "Particle", KUO14, and PW Hamiltonians (MeV).[a]

$2j_a$	$2j_b$	$2j_c$	$2j_d$	JT	"Particle"	KUO14[b]	PW[c]
5	5	5	5	01	-2.0094	-2.4381	-2.1243
5	5	5	5	10	-0.8660	-1.0284	-0.9437
5	5	5	5	21	-1.0399	-1.0358	-1.2312
5	5	5	5	30	-1.3434	-0.8589	-1.7788
5	5	5	5	41	0.0208	-0.0502	0.1611
5	5	5	5	50	-4.0307	-3.6640	-4.0232
5	5	5	1	21	-0.6176	-0.8542	-0.6594
5	5	5	1	30	-1.3830	-1.5654	-1.1865
5	5	5	3	10	3.3882	3.1651	3.2056
5	5	5	3	21	-0.4781	-0.3969	-0.4020
5	5	5	3	30	1.9409	1.8746	1.8986
5	5	5	3	41	-1.3293	-1.3626	-1.3801
5	5	1	1	01	-1.3225	-0.9677	-1.4058
5	5	1	1	10	-0.6255	-0.5959	-0.4241
5	5	1	3	10	-0.4242	-0.2368	-0.2399
5	5	1	3	21	-0.9602	-0.8364	-0.8471
5	5	3	3	01	-3.8935	-3.7882	-3.8367
5	5	3	3	10	1.7200	1.6209	1.6417
5	5	3	3	21	-1.2345	-0.9034	-0.9149
5	5	3	3	30	0.8725	0.4996	0.5060
5	1	5	1	20	0.0660	-0.6222	0.1766
5	1	5	1	21	-0.8184	-1.2879	-0.8495
5	1	5	1	30	-3.5513	-3.6919	-3.6603
5	1	5	1	31	0.7762	0.1723	0.7838
5	1	5	3	20	-1.0366	-1.4488	-1.4674
5	1	5	3	21	0.2028	-0.2181	-0.2209
5	1	5	3	30	1.2093	1.1561	1.1709
5	1	5	3	31	-0.3350	-0.0892	-0.0903
5	1	1	3	20	-2.4571	-2.5788	-2.6118
5	1	1	3	21	-1.6881	-1.5511	-1.5710
5	1	3	3	21	-0.9668	-0.7436	-0.7531
5	1	3	3	30	0.0502	0.0269	0.0272
5	3	5	3	10	-5.5217	-5.8276	-5.3692
5	3	5	3	11	0.5267	-0.1257	0.4058
5	3	5	3	20	-3.7876	-4.5271	-4.0520
5	3	5	3	21	0.6659	-0.2037	0.3268
5	3	5	3	30	-0.5305	-1.1313	-0.6127
5	3	5	3	31	0.5476	0.1316	0.6664
5	3	5	3	40	-3.4056	-4.3137	-3.8359
5	3	5	3	41	-1.1427	-1.6603	-1.1485

Table 2.--Continued.

$2j_a$	$2j_b$	$2j_c$	$2j_d$	JT	"Particle"	KUO14[b]	PW[c]
5	3	1	1	10	1.7223	1.7125	1.7345
5	3	1	3	10	-1.6277	-1.9132	-1.9378
5	3	1	3	11	-0.1106	-0.0976	-0.0989
5	3	1	3	20	-1.3218	-1.5404	-1.5602
5	3	1	3	21	-0.2836	-0.7697	-0.7796
5	3	3	3	10	0.1337	0.0383	0.0388
5	3	3	3	21	-0.8424	-1.0101	-1.0230
5	3	3	3	30	2.0286	2.1579	2.1856
1	1	1	1	01	-2.3068	-1.9493	-2.2643
1	1	1	1	10	-3.3275	-3.1839	-3.4227
1	1	1	3	10	0.2719	0.3085	0.3125
1	1	3	3	01	-0.8385	-0.7448	-0.7543
1	1	3	3	10	-0.2569	-0.2127	-0.2154
1	3	1	3	10	-3.0871	-3.2771	-2.7861
1	3	1	3	11	0.2733	0.2167	0.7525
1	3	1	3	20	-1.3414	-1.6099	-1.0974
1	3	1	3	21	-0.1653	-0.3267	0.2022
1	3	3	3	10	0.7599	0.7995	0.8097
1	3	3	3	21	-0.1856	-0.2071	-0.2097
3	3	3	3	01	-0.8119	-0.8076	-0.2849
3	3	3	3	10	-0.4708	-0.4695	0.0576
3	3	3	3	21	0.1747	0.0770	0.6110
3	3	3	3	30	-2.6098	-2.5872	-2.0873

[a]Phase conventions are from reference 1.

[b]Reference 1.

[c]Reference 3.

interaction, and the fitted "Particle" interaction are listed in Table 2.

The initial single-particle energies used were -4.14, -3.27, +1.60 MeV for the $0d_{5/2}$, $1s_{1/2}$, $0d_{3/2}$ orbits respectively. The energies for the $0d_{5/2}$ and $1s_{1/2}$ orbits were taken from the ground and first $1/2^+$ states of ^{17}O. Instead of using the energy of the first $3/2^+$ state in ^{17}O, the centroid of five observed $3/2^+$ resonances in ^{17}O, which contain nearly 100 percent of the $0d_{3/2}$ strength,[30] was used for the energy of the $0d_{3/2}$ orbit. The centroid energy of 5.74 MeV plus the binding energy of the ground state of ^{17}O, relative to ^{16}O, -4.14 MeV, give +1.60 MeV for the energy of the $0d_{3/2}$ orbit.

All 63 two-body matrix elements were varied in all four iterations, although the number of orthogonal parameters varied was in all cases less than 63. The number of orthogonal parameters varied increased with the uncertainty level. The single-particle energies were fixed at the chosen values for the first three iterations. On the final iteration, the energy of the $0d_{3/2}$ orbit was varied together with the 63 two-body matrix elements as free parameters. The fragmentation of the $0d_{3/2}$ strength in ^{17}O raises the question of what is the best energy to use for the $0d_{3/2}$ orbit for this type of shell-model calculation. It was found that the energy shifted to +0.88 MeV, close to the +0.94 MeV which would result if the energy of the first $3/2^+$ in ^{17}O was used.

I.3.C. "Hole" Hamiltonian (A=32-39 fit)

In shell-model theory, there is a complementary relation between a particle and a hole representation of an eigenstate, such that shell-model calculations can be done either in particle or in hole formalism. In certain cases, one formalism may be preferable to the other. For example, in the present study of A=17-39 sd-shell nuclei, the same shell-model eigenstates can be described either by distributing (A-16) particles in the $0d_{5/2}$, $1s_{1/2}$, $0d_{3/2}$ orbits, or by distributing (40-A) holes in the same orbits. For the A=32-39 region, the hole formalism is preferable than the particle formalism for two reasons. First, the number of active holes is smaller than the number of active particles, so the effects of three- or more-body contributions to the interaction should be smaller. Second, it is also more economical of computer time and data storage when doing the least-squares fit. The one- and two-body operator matrix elements defined in equation (3) are only dependent on the model space, the number of active particles or holes, and the angular momentum and isospin of the eigenstate. A single set of operator matrix elements need only be generated once and can then be used for both the "Particle" and the "Hole" least-squares fits. The hole formalism was used for the A=32-39 region and thus the name "Hole" Hamiltonian.

The data set for the "Hole" least-squares fit, composed of 134 corrected binding energies of observed states, is listed in Table 3, together with the excitation energies. The considerations for intruder states are as described previously. The measured binding energies were first corrected as in the "Particle" least-squares fit, and the "Hole" corrected binding energies relative to ^{40}Ca were obtained by simply subtracting the "Particle" corrected binding energy of ^{40}Ca from the "Particle" corrected binding energies. The orders of the Hamiltonians are the same as in the "Particle" case. The fit procedure is also similar. Again, four iterations were done to arrive at the final fitted interaction or "Hole" Hamiltonian listed in Table 4. The same variations on the uncertainty level were also performed. The data set in the first and second iterations included the level energies of only A=34, T=0 and A=35-39 systems listed in Table 3. Level energies of A=34, T=1,2 systems were added to the data set in the third iteration. Finally, all level energies listed in Table 3 were included in the fourth iteration of the fit.

The initial set of 63 two-body matrix elements used was the K12.5P interaction extensively studied in reference 2. As described there, the interaction was generated in the same way as the KUO14 interaction, except that a harmonic-oscillator parameter of $\hbar\omega$=12.5 MeV was used to take into account an increase in nuclear size for increasing A. The two-body matrix elements of the original

TABLE 3.--Binding and excitation energies of states comprising the data used to determine the "Hole" Hamiltonian (MeV).

A	2J	2T	ν	Ex	EB[a]	A	2J	2T	ν	Ex	EB[a]
39	01	01	1	2.50	18.13	35	01	01	1	1.21	65.72
	03	01	1	0.00	15.63				2	3.96	68.47
									3	4.72	69.23[j]
38	02	00	1	0.45	29.11				4	6.63	71.14[j]
			2	1.70	30.36		03	01	1	0.00	64.51
	04	00	1	3.43	32.09[b]				2	2.69	67.20
	06	00	1	0.00	28.66		05	01	1	1.75	66.26
									2	3.00	67.51
	00	02	1	0.00	28.79				3	5.12	69.63[j]
	02	02	1	5.55	34.34[c]				4	5.48	69.99[j]
	04	02	1	2.17	30.96				5	5.59	70.10[j]
			2	4.40	33.19[d]				6	6.03	70.54[j]
									7	6.83	71.34[j]
37	01	01	1	1.40	42.04		07	01	1	2.65	67.16
	03	01	1	0.00	40.64		09	01	1	3.94	68.45
	05	01	1	2.79	43.43						
			2	3.17	43.81[e]		01	03	1	1.56	71.72
	07	01	1	2.22	42.86		03	03	1	0.00	70.16
	01	03	1	1.73	47.36[f]		01	05	1	0.00	79.37[k]
	03	03	1	0.00	45.63						
			2	4.02	49.65[f]	34	02	00	1	0.46	77.61
	05	03	1	3.09	48.72[g]				2	0.67	77.82
			2	4.80	50.43[r]				3	2.59	79.74
									4	3.13	80.28
36	00	00	1	0.00	49.42		04	00	1	1.24	78.39
			2	4.33	53.75				2	1.89	79.04
	04	00	1	1.97	51.39		06	00	1	0.15	77.30
			2	4.44	53.86				2	2.19	79.34
	06	00	1	7.14	56.56				3	2.62	79.77
	08	00	1	4.41	53.83		08	00	1	2.38	79.53
			2	6.36	55.78						
							00	02	1	0.00	77.15
	00	02	1	3.12	59.15				2	3.92	81.07
	02	02	1	1.16	57.19				3	5.23	82.38
			2	1.60	57.63[h,i]		02	02	1	4.08	81.23
			3	2.67	58.70[h,i]				2	5.39	82.54
			4	3.47	59.50[i]		04	02	1	2.13	79.28
	04	02	1	0.00	56.03				2	3.31	80.46
			2	1.96	57.99				3	4.12	81.27
			3	2.49	58.52[i]				4	4.89	82.04
	06	02	1	0.79	56.82[i]				5	5.99	83.14
			2	2.86	58.89[i]		06	02	1	4.88	82.03
							08	02	1	4.69	81.84
	00	04	1	0.00	60.27				2	6.25	83.40
	02	04	1	4.52	64.79						
	04	04	1	3.29	63.56		02	04	1	0.00	87.83

TABLE 3.--Continued.

A	2J	2T	ν	Ex	EB[a]	A	2J	2T	ν	Ex	EB[a]
33	01	01	1	0.84	89.41[ℓ]		00	04	1	0.00	109.26
			2	4.05	92.62[ℓ]				2	4.99	114.25
			3	4.38	92.95[ℓ]		04	04	1	1.94	111.20
	03	01	1	0.00	88.57				2	4.23	113.49
			2	2.31	90.88						
			3	3.93	92.50[m]	31	05	05	1	0.00	131.23[q]
	05	01	1	1.96	90.53						
			2	2.86	91.43[ℓ,m]	29	03	07	1	0.00	172.91[r]
			3	3.83	92.40						
			4	4.14	92.71						
	07	01	1	2.97	91.54						
			2	4.09	92.66[m]						
	09	01	1	4.05	92.62[m]						
	01	03	1	0.00	94.07						
	03	03	1	1.43	95.50						
			2	2.54	96.61						
			3	3.28	97.35						
	05	03	1	1.85	95.92						
			2	3.49	97.56						
			3	4.05	98.12						
			4	4.20	98.27						
	07	03	1	3.63	97.70						
	03	05	1	0.00	104.71[n]						
32	00	00	1	0.00	97.21						
			2	3.78	100.99						
	02	00	1	4.70	101.91						
	04	00	1	2.23	99.44						
			2	4.28	101.49						
			3	5.55	102.76						
	06	00	1	5.41	102.62						
	08	00	1	4.46	101.67						
			2	6.41	103.62[o]						
	00	02	1	0.52	104.73						
			2	3.44	107.65[p]						
	02	02	1	0.00	104.21						
			2	1.15	105.36						
			3	2.24	106.45						
			4	2.75	106.96						
	04	02	1	0.08	104.29						
			2	1.33	105.54						
			3	2.22	106.43[p]						
			4	2.66	106.87[p]						
	06	02	1	1.76	105.97						
			2	2.18	106.39						
			3	3.01	107.22[p]						
	08	02	1	3.15	107.36						

[a]Unless otherwise noted, the ground state binding energies are taken from Reference 28, corrected for Coulomb energies and relative to ^{40}Ca; the spin assignments and excitation energies are taken from Reference 27.

[b]Reference 73.

[c]Reference 74.

[d]Spectroscopic-factors-weighted centroid of second and third observed 2^+ state.

[e]Reference 75.

[f]Reference 76.

[g]Reference 77.

[h]Reference 78.

[i]Reference 79.

[j]Reference 80.

[k]Reference 72.

[ℓ]Reference 81.

[m]Reference 82.

[n]Reference 71.

[o]Reference 83.

[p]Reference 84.

[q]Reference 70.

[r]Reference 85.

Table 4.--The two-body matrix elements $\langle j_a j_b | V | j_c j_d \rangle_{JT}$ of "Hole" and K12.5P Hamiltonians (MeV).[a]

$2j_a$	$2j_b$	$2j_c$	$2j_d$	JT	"Hole"	K12.5P[b]
5	5	5	5	01	-2.1234	-2.2766
5	5	5	5	10	-0.8983	-0.9790
5	5	5	5	21	-0.5549	-0.8799
5	5	5	5	30	-0.6833	-0.7269
5	5	5	5	41	0.4434	-0.0323
5	5	5	5	50	-2.9351	-3.0479
5	5	5	1	21	-0.5527	-0.7416
5	5	5	1	30	-1.3040	-1.3368
5	5	5	3	10	2.6485	2.8734
5	5	5	3	21	-0.1927	-0.3841
5	5	5	3	30	1.5701	1.6060
5	5	5	3	41	-0.8755	-1.1738
5	5	1	1	01	-0.7769	-0.8938
5	5	1	1	10	-0.5285	-0.5859
5	5	1	3	10	-0.2574	-0.2170
5	5	1	3	21	-0.8774	-0.7169
5	5	3	3	01	-3.4471	-3.3550
5	5	3	3	10	1.4097	1.4574
5	5	3	3	21	-0.7272	-0.8010
5	5	3	3	30	0.4723	0.4262
5	1	5	1	20	-0.4291	-0.5203
5	1	5	1	21	-0.3676	-1.1110
5	1	5	1	30	-3.0649	-3.0699
5	1	5	1	31	1.0105	0.1493
5	1	5	3	20	-0.9922	-1.2315
5	1	5	3	21	0.3111	-0.2158
5	1	5	3	30	0.9444	0.9998
5	1	5	3	31	-0.4935	-0.0488
5	1	1	3	20	-2.0269	-2.1718
5	1	1	3	21	-1.3537	-1.3349
5	1	3	3	21	-0.7392	-0.6419
5	1	3	3	30	0.0660	0.0295
5	3	5	3	10	-5.0568	-5.3266
5	3	5	3	11	0.2352	-0.1367
5	3	5	3	20	-3.6694	-3.8860
5	3	5	3	21	0.4477	-0.1664
5	3	5	3	30	-0.9271	-0.9606
5	3	5	3	31	0.6083	0.1122
5	3	5	3	40	-3.3154	-3.5935
5	3	5	3	41	-0.3100	-1.4490

Table 4.--Continued.

$2j_a$	$2j_b$	$2j_c$	$2j_d$	JT	"Hole"	K12.5P[b]
5	3	1	1	10	1.4758	1.6018
5	3	1	3	10	-1.6758	-1.6509
5	3	1	3	11	0.0483	-0.0654
5	3	1	3	20	-0.7370	-1.3372
5	3	1	3	21	-0.3077	-0.6623
5	3	3	3	10	0.0956	-0.0712
5	3	3	3	21	-0.3325	-0.8646
5	3	3	3	30	1.7037	1.8108
1	1	1	1	01	-1.3430	-1.8186
1	1	1	1	10	-2.8093	-2.9245
1	1	1	3	10	0.4661	0.2866
1	1	3	3	01	-0.6696	-0.6906
1	1	3	3	10	-0.2055	-0.1306
1	3	1	3	10	-2.9441	-2.7934
1	3	1	3	11	0.4955	0.1668
1	3	1	3	20	-1.0458	-1.3606
1	3	1	3	21	-0.0240	-0.2924
1	3	3	3	10	0.8651	0.7384
1	3	3	3	21	0.3064	-0.1952
3	3	3	3	01	-0.9707	-0.8197
3	3	3	3	10	-0.4862	-0.4922
3	3	3	3	21	0.0800	0.0571
3	3	3	3	30	-2.1908	-2.1795

[a]Phase conventions are from reference 1.

[b]Reference 2.

K12.5P and the fitted "Hole interactions are listed in Table 4.

The initial single-particle energies used were +22.34, +18.13, +15.63 MeV, for the $0d_{5/2}$, $1s_{1/2}$, $0d_{3/2}$ orbits, respectively. The energies for the $0d_{3/2}$ and $1s_{1/2}$ orbits are taken from the ground and first $1/2^+$ states of ^{39}K. For the $0d_{5/2}$ orbit, a problem arises from the fragmentation of the $0d_{5/2}$ hole strength in ^{39}K. The energy used is taken from recent $^{40}Ca(d, ^3He)$ data by Doll et al.[31] It is the centroid of spectroscopic weighted energies of all states with $\ell=2$ transfer in ^{39}K between 5.27 to 9.75 MeV. The sum of the spectroscopic factors (C^2S), assuming a $d_{5/2}$ pick-up for all the states used, is 4.97, still somewhat smaller than the theoretical total strength of 6.

All 63 two-body matrix elements were varied in the first three iterations as in the "Particle" case. Because of the uncertainty in the $0d_{5/2}$ orbit energy, its energy was varied together with the two-body matrix elements in the last iteration. The energy was then found to shift down slightly, to +21.75 MeV.

I.3.D. Computer Codes

Various computer codes were used in the present study. The Oak Ridge Code[13] and a modified version of the Glasgow Code[14] were used to generate the one- and two-body operator matrix elements ρ's. A modified version of SMIT[1]

was used to combine the operator matrix elements with the eigenvectors to obtain the linear equations (15), and then perform the least-squares fit in terms of orthogonal linear combinations of the parameters. A further modified version of the Oak Ridge Code which uses the Lanczos iterative diagonalization method was used to calculate many of the ground state binding energies and the spectra of A=23,24, 25,26,32 and 33 systems to be discussed in the next section.

I.4. Results

I.4.A. Orthogonal Parameter Fit

Since the Hamiltonian parameters in the transformed representation are linearly independent (orthogonal), it is interesting to ascertain how many of them are well determined by each of the data sets.

The change in the least-squares χ^2 from a change in parameter x_k of Δx_k can be estimated as follows. The definition of χ^2 is:

$$\chi^2 = \sum_{\ell} \left(\sum_{m} \beta_{\ell m} x_m - E_\ell \right)^2 \tag{9}$$

If parameter x_k changes by Δx_k, the new χ^2 is:

$$\chi^2(\Delta x_k) = \sum_{\ell} \left(\sum_{m} \beta_{\ell m} x_m + \beta_{\ell k} \Delta x_k - E_\ell \right)^2 \tag{24}$$

The change in χ^2 is obtained from equations (9) and (24):

$$\Delta(\chi^2) = \chi^2(\Delta x_k) - \chi^2$$

$$\Delta(\chi^2) = \sum_{\ell}\left[\left(\sum_m \beta_{\ell m} x_m + \beta_{\ell k}\Delta x_k - E_\ell\right)^2 - \left(\sum_m \beta_{\ell m} x_m - E_\ell\right)^2\right] \quad (25)$$

Equation (25) can be simplified to:

$$\Delta(\chi^2) = \sum_{\ell}\beta_{\ell k}^2(\Delta x_k)^2 + \Delta x_k\left[2\sum_{\ell}\left(\sum_m \beta_{\ell m} x_m - E_\ell\right)\beta_{\ell k}\right] . \quad (26)$$

The second expression on the right is just $\Delta x_k \frac{\partial \chi^2}{\partial x_k}$, which is equated to zero for the minimization of χ^2. Hence, equation (26) is simply:

$$\Delta(\chi^2) = \sum_{\ell}\beta_{\ell k}^2(\Delta x_k)^2 \text{ , and}$$

$$\Delta(\chi^2) = \gamma_{kk}(\Delta x_k)^2 . \quad (27)$$

The change in χ^2 from a change Δx_k for parameter x_k is just $(\Delta x_k)^2$ multiplied by the corresponding diagonal matrix element of the G matrix. In terms of the diagonal matrix elements d_m of the error matrix D^{-1},

$$\Delta(\chi^2) = \frac{(\Delta x_k)^2}{d_k} \quad (28)$$

or

$$\Delta(\chi^2) = \left(\frac{\Delta x_k}{\varepsilon_k}\right)^2 , \quad (29)$$

where ε_k is the uncertainty of parameter x_k. It should be noted that the x_k affects the χ^2 independently without

affecting the other parameters, as the orthogonal parameters are linearly independent.

The χ^2 of the "Particle" Hamiltonian is 0.22 MeV and for the "Hole" Hamiltonian is 0.28 Mev. It should be noted that the uncertainty in the Coulomb correction of the binding energies can be as much as 200 keV or more. Using the results of the last iterations of the "Particle" and "Hole" fits, the change in χ^2 was calculated for a change in each of the orthogonal parameters. In Figure 2 is plotted on a semi-log scale the percentage change in χ^2 for a 200 keV change in each of the better determined orthogonal parameters. The steepness of the curves is to be noted; only a few orthogonal parameters are extremely well determined by the data in each case. Less than half of the 63-orthogonal parameters affect the χ^2 by more than 1 percent in either the "Particle" case or the "Hole" case for a 200 keV change in their value. The shape of the two curves are similar, though more orthogonal parameters seem to be determined by the data set in the "Particle" case than in the "Hole" case. However, the data set for the "Particle" fit is bigger than for the "Hole" fit.

In the final iteration of the "Particle" fit, thirty orthogonal parameters were varied as free parameters, while twenty were varied in the final iteration of the "Hole" fit. In either case, all the orthogonal parameters kept constant affect the χ^2 by less than 1 percent as shown in Figure 2. Thus, the χ^2 obtained for the "Particle" and

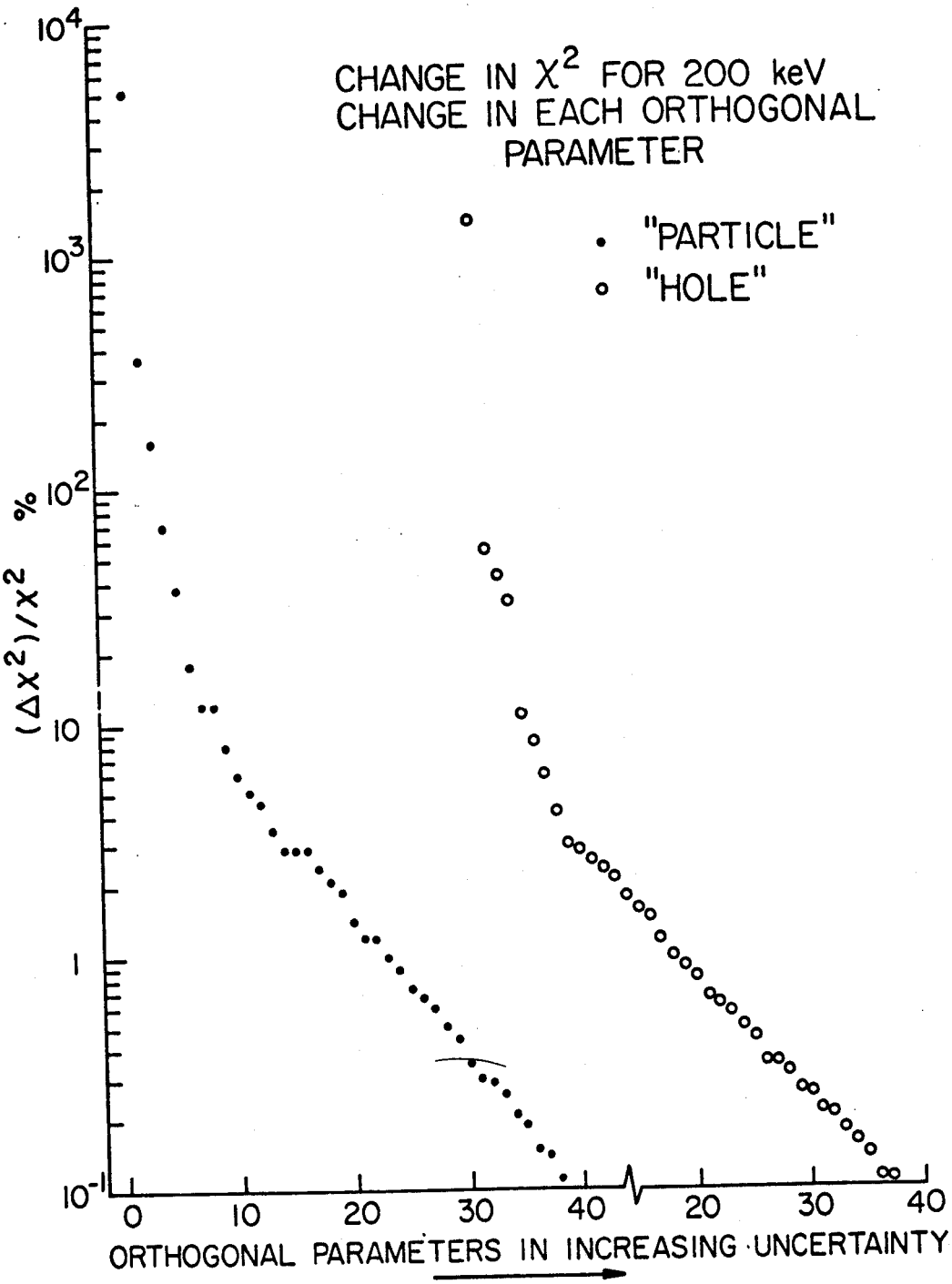

Figure 2. Percentage change in χ^2 for a 200 keV change in each orthogonal parameter.

"Hole" Hamiltonian should not be affected much by varying additional of the less-sensitive orthogonal parameters.

I.4.B. Comparison of Two-Body Matrix Elements

The two-body matrix elements of the "Particle" Hamiltonian, the original KUO14 interaction and the PW interaction are all listed in Table 2. The two-body matrix elements of the "Hole Hamiltonian and the original K12.5P interaction are listed in Table 4. Comparison of the different sets of interactions is now a matter of comparing the different lists of two-body matrix elements. The task is difficult since the least-squares fits were done in terms of orthogonal linear combinations of the two-body matrix elements and hence every two-body matrix element has changed. In Figure 3 are plotted the diagonal two-body matrix elements of the "Particle" Hamiltonian, the "Hole" Hamiltonian, and the original KUO14 and K12.5P realistic Hamiltonians. The off-diagonal two-body matrix elements of the four Hamiltonians are plotted in Figure 4. The dots are the original Kuo matrix elements, and the crosses are the new "Particle" or "Hole" matrix elements. The "Particle" interactions are plotted to the right of the "Hole" interactions. In general, the changes have no clear pattern, though more matrix elements tend to change in the positive direction (become less attractive).

One can compare the strengths of diagonal orbit-orbit interactions for the different Hamiltonians defined as:

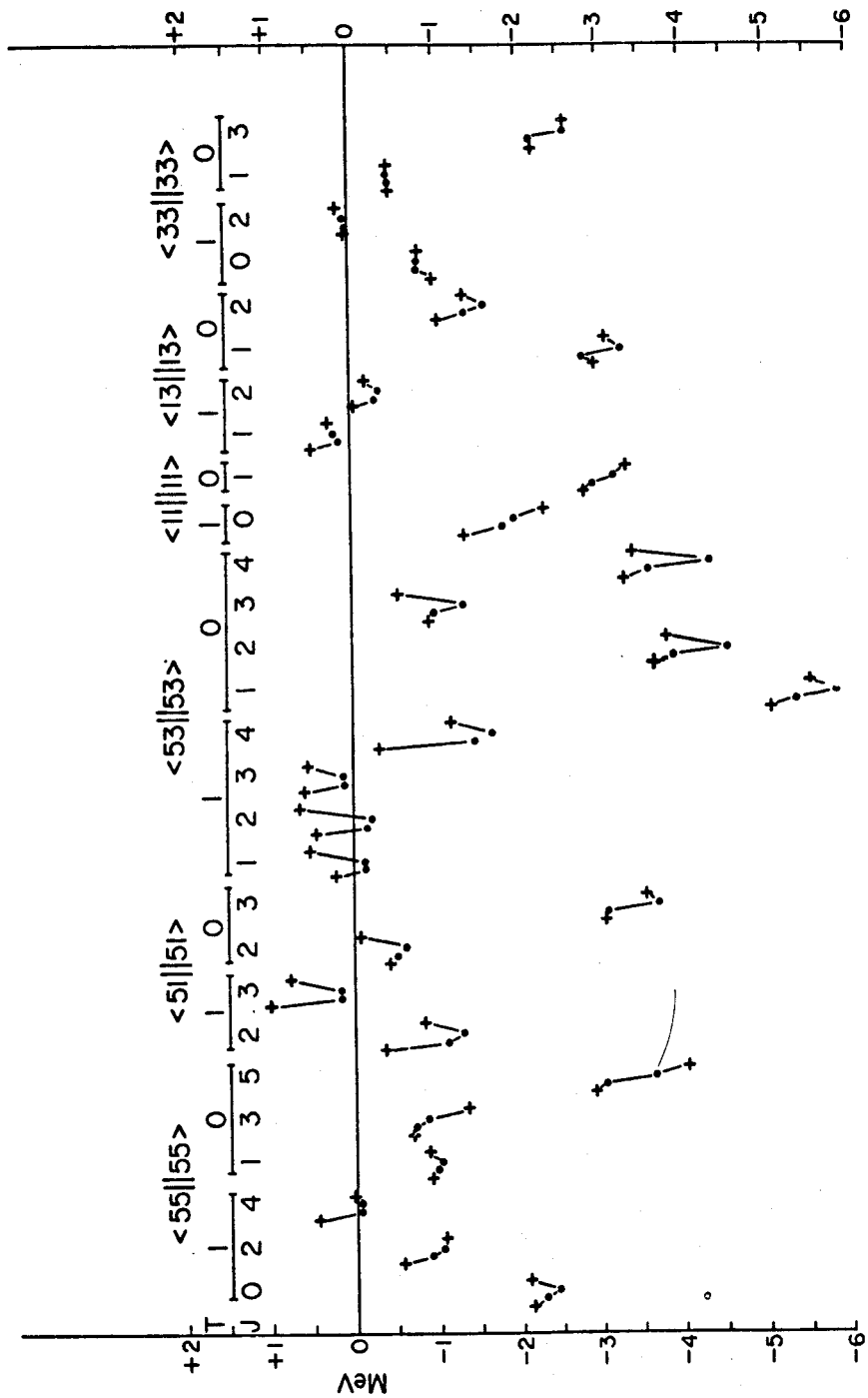

Figure 3. Diagonal two-body matrix elements of the "Particle," "Hole," KUO14 and K12.5P Hamiltonians.

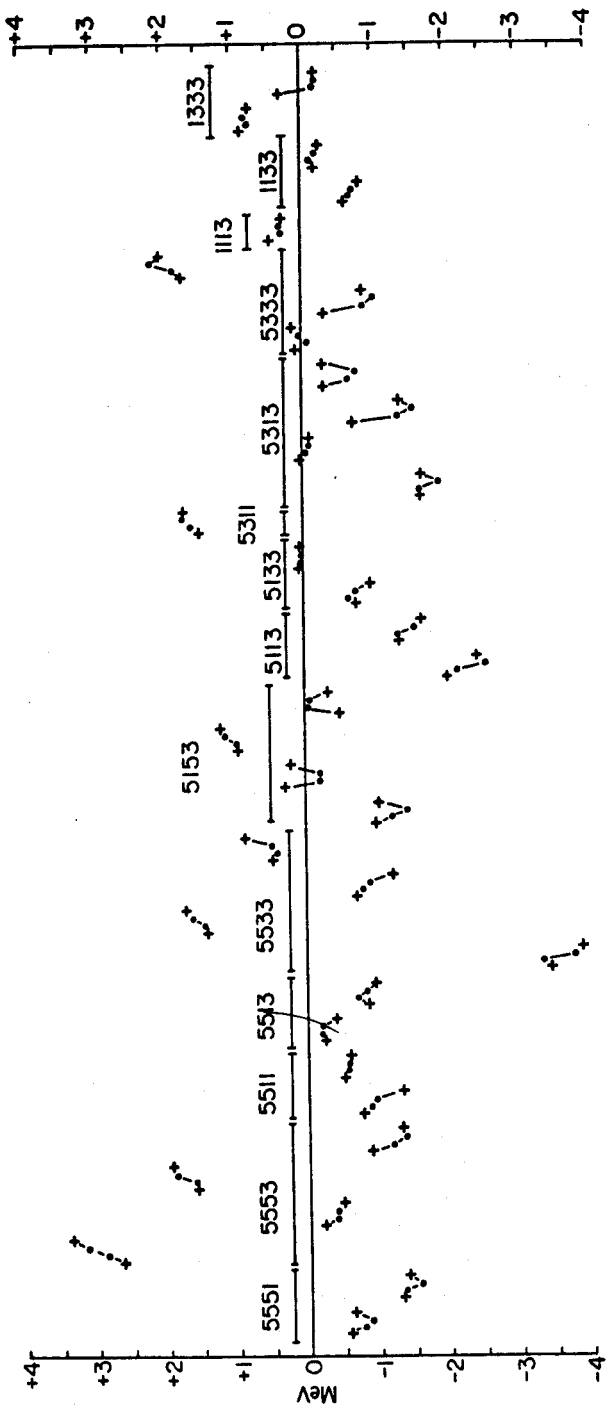

Figure 4. Off-diagonal two-body matrix elements of the "Particle," "Hole," KUO14 and K12.5P Hamiltonians.

$$\sum_{J,T} (2J+1)(2T+1) \langle j_a j_b | V | j_a j_b \rangle_{JT} \quad , \tag{30}$$

where j_a and j_b are single-particle angular momenta and J,T are the coupled angular momentum and isospin. In Table 5 are listed the strengths of the orbit-orbit interactions for the different Hamiltonians. The strength of the $d_{5/2}$-$d_{5/2}$ interaction does not change in the fitted "Particle" and PW Hamiltonians from the original KUO14 Hamiltonian. The strengths of the $d_{5/2}$-$s_{1/2}$ and $d_{5/2}$-$d_{3/2}$ interactions are, however, reduced in both cases by approximately a factor of 2. The strength of the $s_{1/2}$-$s_{1/2}$ interaction is again found to be unchanged by both the present "Particle" fit and the PW fit. The $s_{1/2}$-$d_{3/2}$ and $d_{3/2}$-$d_{3/2}$ interaction strengths are, however, very different for the "Particle" and PW Hamiltonians. Both PW strengths are very much reduced from the KUO14 Hamiltonians. For the present "Particle" Hamiltonian, the $d_{3/2}$-$d_{3/2}$ interaction strength is not changed; the $s_{1/2}$-$d_{3/2}$ interaction strength is slightly reduced, though less than the factor of 2 found for the $d_{5/2}$-$s_{1/2}$ and $d_{5/2}$-$d_{3/2}$ interaction strengths. However, the $s_{1/2}$-$d_{3/2}$ and $d_{3/2}$-$d_{3/2}$ interactions are not well determined from either the PW or "Particle" data set.

Essentially the same picture is obtained in comparing the strengths of the orbit-orbit interactions of the K12.5P and "Hole" Hamiltonians. The $d_{3/2}$-$d_{3/2}$ and $s_{1/2}$-$s_{1/2}$ interaction strengths are not changed, while the $s_{1/2}$-$d_{3/2}$ and $d_{5/2}$-$d_{3/2}$ interaction strengths are reduced

Table 5.--Strengths of orbit-orbit interactions (MeV).
$\sum_{J,T} (2J+1)(2T+1)\langle j_a j_b | V | j_a j_b \rangle_{JT}$

j_a	j_b	KUO14[a]	"Particle"	PW[b]	K12.5P[c]	"Hole"
5/2	5/2	- 75.9	-77.4	-80.0	- 62.5	-42.5
5/2	1/2	- 44.6	-20.5	-21.0	- 37.6	- 7.9
5/2	3/2	-133.1	-74.5	-83.6	-115.0	-56.6
1/2	1/2	- 15.4	-16.9	-17.1	- 14.2	-12.5
1/2	3/2	- 20.8	-16.0	- 4.0	- 18.1	-10.0
3/2	3/2	- 20.8	-19.5	- 6.1	- 18.3	-18.5

[a]Reference 1.

[b]Reference 3.

[c]Reference 2.

by approximately a factor of 2 in the "Hole" Hamiltonian. The $d_{5/2}$-$d_{5/2}$ and $d_{5/2}$-$s_{1/2}$ interactions are the ones not well determined in the "Hole" least-squares fit for the same sort of reasons that the $s_{1/2}$-$d_{3/2}$ and $d_{3/2}$-$d_{3/2}$ interactions are not well determined in the "Particle" least-squares fit. It may be concluded then that the result of both empirical renormalization of the Kuo's realistic Hamiltonians is a lessening of the attractiveness of the $d_{5/2}$-$s_{1/2}$, $d_{5/2}$-$d_{3/2}$, and $s_{1/2}$-$d_{3/2}$ interaction strengths.

Li et al.[32] have recently investigated the $^{17}O(d,p)^{18}O$ reaction at a deuteron bombarding energy of 18 MeV, and observed 12 states in ^{18}O up to an excitation energy of 6.34 MeV. From the observed excitation energies and extracted absolute spectroscopic factors, they deduced the diagonal matrix elements of the effective neutron-neutron interaction for $(d_{5/2})^2$ $0^+,2^+,4^+$ and $(d_{5/2}$-$s_{1/2})$ 2^+, 3^+, T=1 configurations. Their matrix elements are listed in Table 6, together with the corresponding matrix elements of the KUO14, PW and "Particle" Hamiltonians. The uncertainties for the "Particle" Hamiltonian matrix elements are obtained by assuming a 200 keV theoretical error for each calculated energy.

Li et al.[32] pointed out that their deduced matrix elements may be too attractive because of the omission of transitions to higher excited states not seen in the experiment, and made some theoretical estimates of the

TABLE 6.--Matrix elements $\langle d_{5/2}j|V|d_{5/2}j\rangle_{J,(T=1)}$ of the effective neutron-neutron interaction (MeV).

2j	J	Expt.[a]	Est. Error[b]	KUO14[c]	"Particle"[d]	PW[e]
5	0	-2.77	1.00	-2.44	-2.01±0.44	-2.12
5	2	-1.06	0.13	-1.04	-1.04±0.12	-1.23
5	4	-0.35	0.36	-0.05	+0.02±0.04	+0.16
1	2	-0.79	0.20	-1.29	-0.82±0.14	-0.85
1	3	+0.60		+0.17	+0.78±0.09	+0.78

[a]Reference 32.

[b]See text for discussion on error estimates; reference 32.

[c]Reference 1.

[d]See text for discussion on uncertainties.

[e]Reference 3.

error in the deduced matrix elements; these are also listed in Table 6. Li et al.[32] also derived these diagonal matrix elements from the theoretical energies and spectroscopic factors for the two lowest 0^+ and 2^+ levels and the lowest 4^+ level of reference 33 by the same technique they used with their data. These values were then compared to the actual values of the matrix elements used in the calculation of reference 33. The discrepancies are then estimates of error introduced by omitting higher 0^+, 2^+ and 4^+ levels.

These error estimates were found to be model dependent, though the model used is the same as the one for the different Hamiltonians listed in Table 6, i.e., a ^{16}O core with $(sd)^1$ and $(sd)^2$ configurations for ^{17}O and ^{18}O respectively. No estimated error was given for the $\langle 5/2\ 1/2|V|5/2\ 1/2\rangle_{3,1}$ matrix elements because the lowest 3^+ state in ^{18}O is essentially a pure $(d_{5/2}\text{-}s_{1/2})$ configuration. Different $(d_{5/2}\text{-}s_{1/2})\,3^+,(T=1)$ matrix elements merely predict different energies for the lowest 3^+ state.

Comparison of the $(d_{5/2})^2$ diagonal two-body matrix elements shows that the KUO14 realistic matrix elements all agree with the deduced experimental matrix elements within the theoretically estimated errors, with the experimental values being more attractive. The PW matrix elements, however, are in poorer agreement with the experimental values. The present "Particle" matrix elements using the orthogonal least-squares search, on the other hand, are again in good agreement with the experimental

values. The $(d_{5/2})^2{}_{0^+}$ matrix element is even less attractive, but well within the estimated error. The $(d_{5/2})^2{}_{2^+}$ matrix element is not changed from the KUO14 value. The $(d_{5/2})^2{}_{4^+}$ matrix element changes sign, but again the estimated uncertainty of 0.04 MeV is still within the estimated error. In short, the KUO14 and "Particle" $(d_{5/2})^2$ diagonal two-body matrix elements and experimentally deduced values are in rather good agreement, with the observed deviations understandable as mostly due to the omission of higher excited states.

Comparison of the $(d_{5/2}\text{-}s_{1/2})$ diagonal two-body matrix elements gives quite a different picture. The PW and "Particle" matrix elements are in good agreement with the experimental values. The KUO14 matrix elements, however, are much more attractive for both the $(d_{5/2}\text{-}s_{1/2})_{2^+,(T=1)}$ and $(d_{5/2}\text{-}s_{1/2})_{3^+,(T=1)}$ matrix elements than the experimental values. This is consistent with the above conclusion that the result of empirical renormalization is the lessening of the attractiveness of $d_{5/2}\text{-}s_{1/2}$, $d_{5/2}\text{-}d_{3/2}$, and $s_{1/2}\text{-}d_{3/2}$ interaction strengths. The evident question then is why the diagonal $d_{5/2}\text{-}d_{3/2}$, $d_{5/2}\text{-}s_{1/2}$ and $s_{1/2}\text{-}d_{3/2}$ interaction strengths are overattractive in the Kuo realistic interactions while the diagonal $d_{5/2}\text{-}d_{5/2}$, $s_{1/2}\text{-}s_{1/2}$ and $d_{3/2}\text{-}d_{3/2}$ interaction strengths are not.

I.4.C. Ground-State Binding Energies and Spins

The corrected measured ground-state binding energies relative to ^{16}O are listed in Table 7, together with the calculated binding energies of the "Particle" and "Hole" Hamiltonians. The single particle energies used with the "Particle" Hamiltonian are -4.14, -3.27, and +0.88 MeV for the $0d_{5/2}$, $1s_{1/2}$, $0d_{3/2}$ orbits, respectively. For the "Hole" Hamiltonian, they are +21.75, +18.13, +15.63 MeV for the $0d_{5/2}$, $1s_{1/2}$, $0d_{3/2}$ orbits, respectively.

The deviations between calculated and measured ground-state binding energies are also plotted in Figure 5 and Figure 6. The energy deviations for the "Particle" Hamiltonian are plotted in Figure 5 as a function of mass A. For each A, the energy deviations are plotted in order of increasing isospin, starting from the lowest isospin. The ground-state binding energy deviations for the "Hole" Hamiltonian are plotted similarly in Figure 6.

The ground state binding energies are well reproduced in the A=17-24 region with the "Particle" Hamiltonian. The energy deviations are all smaller than 0.5 MeV, except for ^{21}O and ^{22}O, which were not included in the least-squares fit. The observed binding energies of ^{21}O and ^{22}O, however, have large uncertainties. Beyond A=24, the energy deviation increases with A, with a clear isospin dependence, i.e., less binding for higher isospin. The effect of adding seven energy levels from A=35, 38 and 39

TABLE 7.--Ground state nuclear binding energies (MeV) relative to ^{16}O, calculated with the "Particle" and "Hole" empirical Hamiltonians.

Nucleus	J	Expt.[a]	THEORY		(EXPT.-THEORY)	
			Particle	Hole	Particle	Hole
^{16}O	0	0.00	---	30.83	---	-30.83
^{17}O	5/2	- 4.14	- 4.14	21.54	0.00	-25.68
^{18}O	0	- 12.19	- 12.21	9.18	0.02	-21.37
^{19}O	5/2	- 16.14	- 16.31	0.85	0.17	-16.99
^{20}O	0	- 23.75	- 23.98	- 10.50	0.23	-13.25
^{21}O	5/2	$-26.3\ ^{+0.3}_{-0.7}$[b]	- 27.69	- 17.56	1.4	- 8.7
^{22}O	0	$-32.2\ ^{+0.2}_{-0.5}$[b]	- 34.78	- 27.58	2.6	- 4.6
^{23}O	1/2		- 37.13	- 32.48		
^{24}O	0		- 41.54	- 38.28		
^{25}O	3/2		- 40.14	- 38.83		
^{26}O	0		- 40.49	- 41.30		
^{27}O	3/2		- 37.95	- 40.84		
^{28}O	0		- 37.43	- 42.36		
^{18}F	1	- 13.23	- 13.35	9.10	0.12	-22.40
^{19}F	1/2	- 23.68	- 23.87	- 4.54	0.19	-19.14
^{20}F	2	- 30.22	- 30.47	- 15.61	0.25	-14.67
^{21}F	5/2	- 38.39	- 38.51	- 27.02	0.12	-11.37
^{22}F	4	-43.56 ± 0.03[c]	- 43.61	- 35.04	0.05	- 8.52
^{23}F	5/2	-51.10 ± 0.17[d]	- 51.30	- 45.17	0.20	- 5.93
^{24}F	3		- 54.74	- 50.69		
^{25}F	5/2		- 59.62	- 57.05		
^{26}F	1		- 60.47	- 59.76		
^{27}F	5/2		- 61.50	- 62.72		
^{28}F	3,2[e]		- 60.13	- 63.46		
^{29}F	5/2		- 60.02	- 65.42		
^{20}Ne	0	- 40.48	- 40.60	- 23.55	0.12	- 16.99
^{21}Ne	3/2	- 47.24	- 47.29	- 33.94	0.05	- 13.30
^{22}Ne	0	- 57.61	- 57.64	- 47.46	0.03	- 10.15
^{23}Ne	5/2	- 62.80	- 62.88	- 55.40	0.08	- 7.45

TABLE 7.--Continued.

Nucleus	J	Expt.[a]	THEORY		(EXPT.-THEORY)	
			Particle	Hole	Particle	Hole
^{24}Ne	0	- 71.67	- 72.04	- 66.72	0.37	- 5.00
^{25}Ne	1/2	-75.97±0.10[f]	- 75.95	- 72.68	0.03	- 3.21
^{26}Ne	0		- 81.83	- 79.70		
^{27}Ne	3/2		- 82.88	- 82.32		
^{28}Ne	0		- 85.95	- 87.34		
^{29}Ne	3/2		- 84.79	- 88.32		
^{30}Ne	0		- 85.78	- 91.53		
^{22}Na	3	- 58.23	- 58.23	- 47.48	0.00	-10.75
^{23}Na	3/2	- 70.76	- 70.76	- 62.30	0.00	- 8.46
^{24}Na	4	- 77.65	- 77.75		0.10	
^{25}Na	5/2	- 86.66	- 87.04		0.38	
^{26}Na	3	- 92.28±0.02[g]	- 92.50		0.22	
^{27}Na	3/2	- 99.07±0.06[h]	- 99.43	- 97.40	0.36	- 1.67
^{28}Na	1	-102.66±0.08[h]	-102.76	-102.10	0.10	- 0.56
^{29}Na	5/2	-106.94±0.10[h]	-106.63	-107.50	- 0.31	0.56
^{30}Na	1	-109.30±0.20[h]	-107.03	-110.01	- 2.27	0.71
^{31}Na	5/2	-115.14±0.80[h]	-108.46	-113.62	- 6.68	- 1.52
^{24}Mg	0	- 87.11	- 87.49	- 80.23	0.38	- 7.01
^{25}Mg	5/2	- 94.44	- 94.83		0.39	
^{26}Mg	0	-105.51	-106.33	-102.27	0.82	- 3.24
^{27}Mg	1/2	-111.97	-112.68	-109.99	0.71	- 1.98
^{28}Mg	0	-120.48	-121.44	-119.40	0.96	- 1.08
^{29}Mg	3/2,1/2[i]	-124.12±0.40[j]	-124.75	-123.78	0.63	- 0.34
^{30}Mg	0		-130.55	-131.08		
^{31}Mg	3/2		-131.16	-133.65		
^{32}Mg	0		-134.06	-138.71		
^{26}Al	5	-105.80	-106.45		0.65	
^{27}Al	5/2	-118.52				
^{28}Al	3	-126.25				
^{29}Al	5/2	-135.68				

TABLE 7.--Continued.

Nucleus	J	Expt.[a]	THEORY		(EXPT.-THEORY)	
			Particle	Hole	Particle	Hole
^{30}Al	3	-141.43±0.04		-141.01		- 0.42
^{31}Al	5/2	-148.62±0.10[k]	-149.46	-149.14	0.84	0.52
^{32}Al	1		-152.63	-153.96		
^{33}Al	5/2		-156.56	-159.51		
^{28}Si	0	-135.70	-138.03	-134.36	2.33	- 1.34
^{29}Si	1/2	-144.18	-146.37	-143.46	2.19	- 0.72
^{30}Si	0	-154.79	-157.11	-154.59	2.32	- 0.20
^{31}Si	3/2	-161.37	-163.25	-161.09	1.88	- 0.28
^{32}Si	0	-170.59	-171.97	-170.80	1.38	0.21
^{33}Si	3/2	-175.14±0.05[l]	-175.24	-175.29	0.10	0.15
^{34}Si	0		-181.81	-183.28		
^{30}P	1	-155.46	-157.52	-155.09	2.06	- 0.37
^{31}P	1/2	-167.77	-170.36	-167.88	2.59	0.11
^{32}P	1	-175.64	-177.79	-175.74	2.15	0.10
^{33}P	1/2	-185.78	-187.85	-186.34	2.07	0.56
^{34}P	1	-192.02±0.05[l]	-192.75	-192.09	0.73	0.07
^{35}P	1/2	-200.48±0.08[m]	-200.54	-200.96	0.06	0.48
^{32}S	0	-182.64	-185.78	-182.85	3.14	0.21
^{33}S	3/2	-191.28	-194.43	-191.32	3.15	0.04
^{34}S	0	-202.70	-205.54	-203.08	2.84	0.38
^{35}S	3/2	-209.69	-212.22	-209.58	2.53	- 0.11
^{36}S	0	-219.58	-220.99	-219.50	1.41	- 0.08
^{34}Cl	3	-202.55	-205.87	-202.63[n]	3.32	0.08
^{35}Cl	3/2	-215.34	-219.07	-215.69	3.73	0.35
^{36}Cl	2	-223.82	-225.93	-223.84	2.11	0.02
^{37}Cl	3/2	-234.22	-235.65	-234.08	1.43	- 0.14

TABLE 7.--Continued.

Nucleus	J	Expt.[a]	THEORY		(EXPT.-THEORY)	
			Particle	Hole	Particle	Hole
^{36}Ar	0	-230.43	-232.57	-230.75	2.14	0.32
^{37}Ar	3/2	-239.21	-240.72	-238.98	1.51	-0.23
^{38}Ar	0	-251.06	-251.80	-250.67	0.74	-0.39
^{38}K	3	-251.19	-253.04	-251.16	1.85	-0.03
^{39}K	3/2	-264.22	-265.39	-264.22	1.17	0.00
^{40}Ca	0	-279.85	-280.69	---	0.84	---

[a]Unless otherwise noted, the ground-state binding energies are taken from reference 28, corrected for Coulomb energies and relative to ^{16}O. The uncertainties of the uncorrected binding energies are less than 30 keV, except where explicitly specified.

[b]Reference 86.

[c]Reference 5[illegible].

[d]Reference 61.

[e]The "Particle" Hamiltonian gives a $J^{\pi}=3^{+}$ ground-state with a $J^{\pi}=2^{+}$ first excited state at 150 keV. The "Hole" Hamiltonian reverses the two states with a splitting of 80 keV.

[f]References 66 and 67.

[g]References 68 and 69.

[h]Reference 69.

[i]The "Particle" Hamiltonian gives a $J^{\pi}=3/2^{+}$ ground state with a $J^{\pi}=1/2^{+}$ first excited state at 420 keV. The "Hole" Hamiltonian reverses the two states with a splitting of 24 keV.

[j]Reference 87.

[k]Reference 70.

[l]Reference 71.

[m]Reference 72.

[n]For the "Hole" Hamiltonian, the first $J^{\pi}=1^{+}$ state overbinds and is 120 keV below the $J^{\pi}=3^{+}$ ground-state.

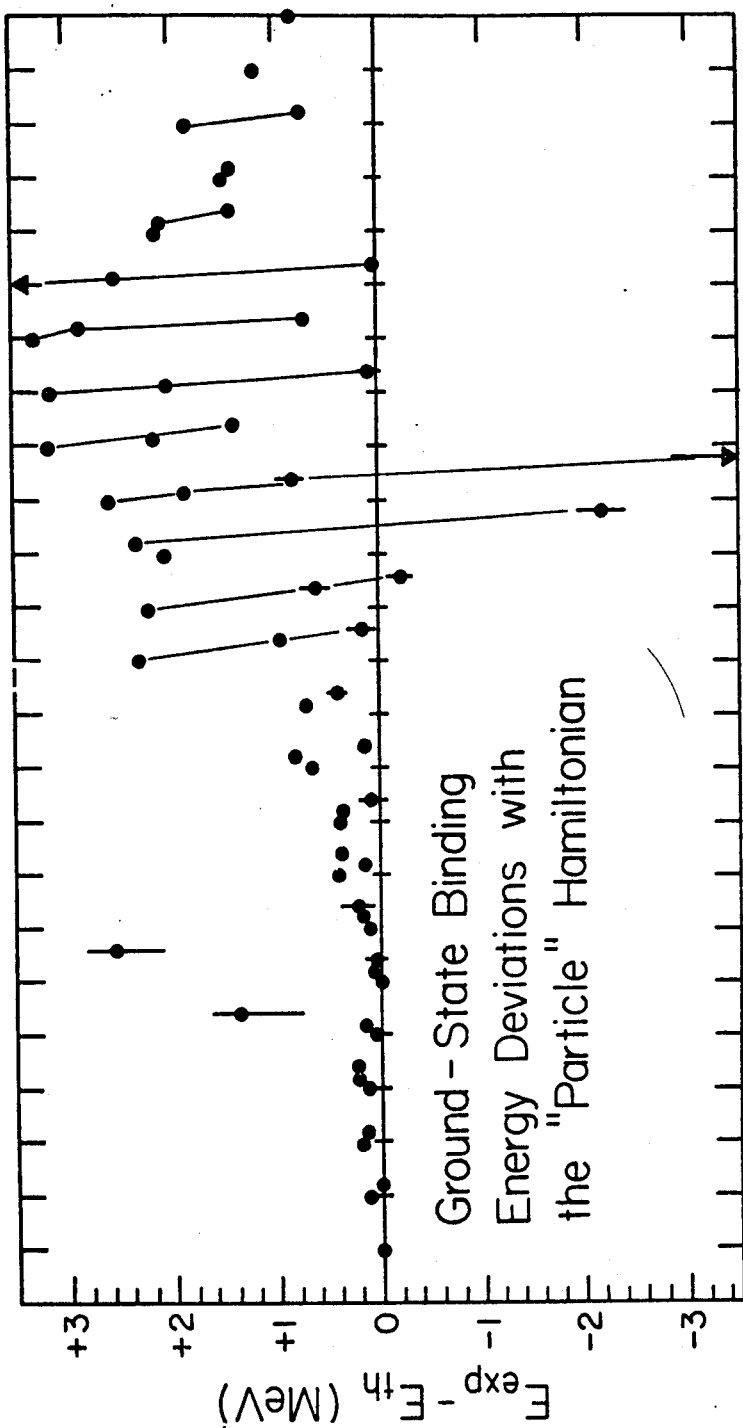

Figure 5. Deviations between measured and calculated ground-state nuclear binding energies for the "Particle" Hamiltonian.

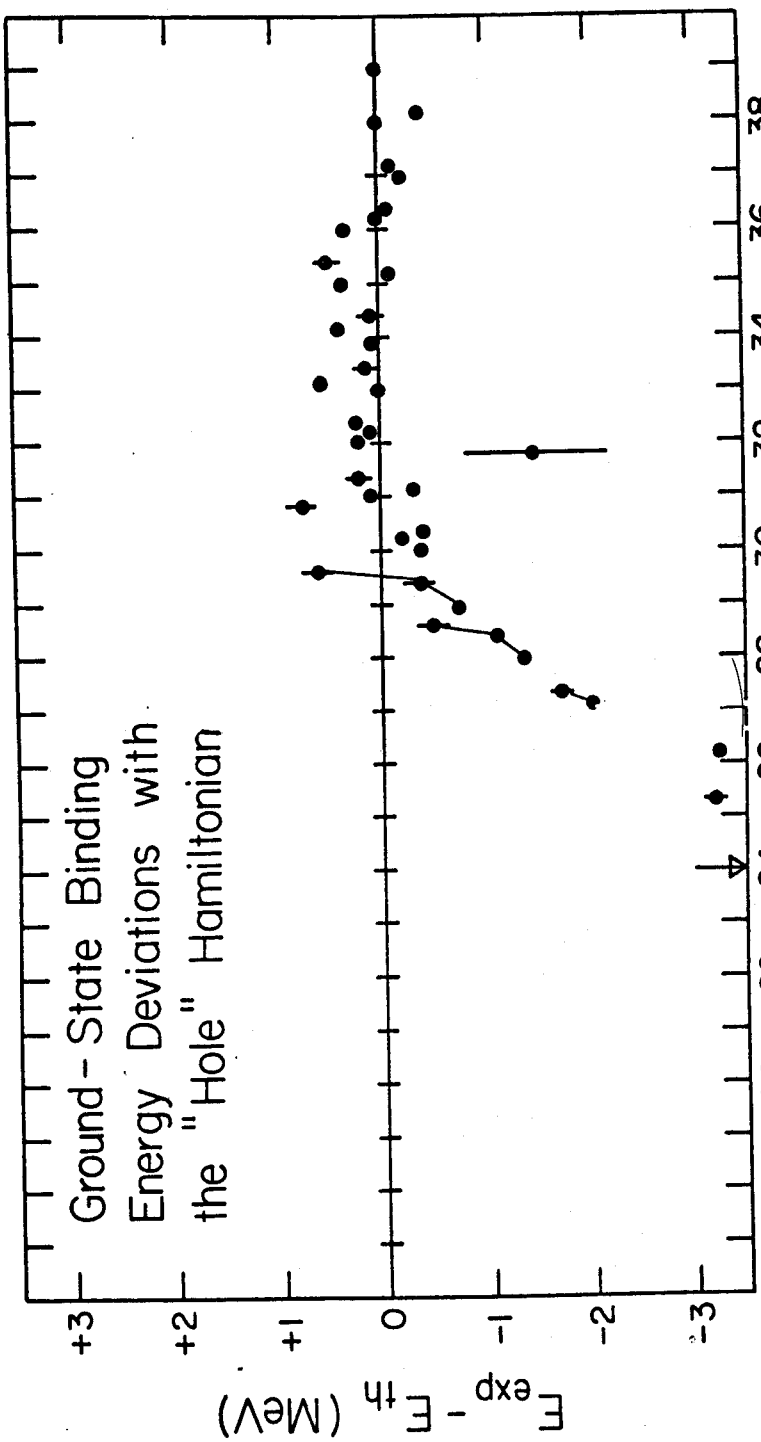

Figure 6. Deviations between measured and calculated ground-state nuclear binding energies for the "Hole" Hamiltonian.

into the fit with a weighted factor of $(0.25)^2$ was to reduce the energy deviations in the upper end, reversing the increase in energy deviation with A. In general, the "Particle" Hamiltonian tends to overbind.

For the "Hole" Hamiltonian, the A=32-39 region ground state binding energies are well-reproduced, consistent with the interaction being fitted to observed energies in these nuclei. Except for ^{33}P, the energy deviations are all smaller than 0.5 MeV. For A<32, the "Hole" Hamiltonian tends to under-bind. The energy deviation increases with decreasing A below A=32, again with a clear isospin dependence which now has the character of more binding energy for higher isospin. The much reduced attractiveness of the $d_{5/2}$-$d_{5/2}$ and $d_{5/2}$-$s_{1/2}$ two-body matrix elements can reasonably be assumed to be responsible for the increasing under-binding in the lower half of the sd-shell. These matrix elements are more and more important as the holes are filling up the $0d_{5/2}$-orbit.

The mass relation formulae of Garvey and Kelson,[34] and later Garvey et al.[35] have been quite successful in predicting masses of nuclei near to stability. The accuracy of using such recurrence relations connecting mass excess values of neighboring nuclei depends upon the accuracy of the input data. Thibault and Klapisch[36] have recomputed mass excesses for light neutron-rich nuclei using the Garvey et al.[35] mass relations with more current

and complete data on $T_z \leq 2$ nuclei. These results are listed in Table 8 under the column TK. Jelley et al.[37] have further extended such fits to include the recently measured mass excesses of $T_z=5/2$ sd-shell nuclei in the input data. Their results are also listed in Table 8 under column G.

Under column M are also listed results obtained with a modified shell-model mass equation employed by Jelley et al..[37] The modified shell-model mass equation differs from that of Garvey et al.[35] mainly in the parameterization of the residual neutron-proton interaction, where shell structure is more explicitly taken into account. The calculated mass excesses of neutron-rich sd-shell nuclei using the "Particle" and the "Hole" Hamiltonians are also listed in Table 8 for comparison.

Comparison of columns TK and G shows that inclusion of the mass excesses of $T_z=5/2$ sd-shell nuclei in the input data for the Garvey et al.[35] mass relations does improve the agreement of the results with experiments, except for ^{21}O, ^{22}O and ^{31}Na. The results of the modified shell-model mass equation of Jelley et al.[37] are very similar to that of Garvey et al.[35] as can be seen from columns G and M. The calculated mass excesses of the "Particle" and "Hole" Hamiltonians combined are in good agreement with the measured mass excesses, i.e., depending on mass A and isospin T_z, either or both Hamiltonians give mass excesses which agree with experiments to within 1 MeV, except again for ^{21}O, ^{22}O and ^{31}Na.

TABLE 8.--Mass-Excesses of Neutron-rich Nuclei (MeV).

Nucleus	Expt.[a]	TK[b]	Jelley et al.[c]		Theory	
			G	M	Particle	Hole
^{20}O	3.80	3.74			3.57	17.05
^{21}O	$9.3^{+0.3}_{-0.7}$[d]	8.82	8.74	8.39	7.93	18.06
^{22}O	$11.5^{+0.2}_{-0.5}$[d]	9.84	9.42	9.35	8.91	16.11
^{23}O		16.44	15.48	15.40	14.64	19.28
^{24}O		20.41	19.70	19.44	18.30	21.56
^{25}O		28.91			27.77	29.08
^{26}O		33.97			35.49	34.68
^{27}O		43.26			46.10	43.21
^{28}O		49.90			54.69	49.76
^{22}F	2.83 ± 0.03[e]	2.83			2.78	11.35
^{23}F	3.36 ± 0.17[f]	3.87	3.40	3.36	3.16	9.29
^{24}F		8.71	8.04		7.79	11.84
^{25}F		12.42	11.75	11.26	10.98	13.55
^{26}F		18.84			18.21	18.92
^{27}F		23.06			25.25	24.03
^{28}F[g]		31.06			34.69	31.36
^{29}F		36.87			42.87	37.47
^{24}Ne	- 5.95	- 5.90			- 6.32	- 1.00
^{25}Ne	-2.18 ± 0.10[h]	- 1.33	- 1.95	- 2.12	- 2.16	1.11
^{26}Ne		0.30	0.17	- 0.27	0.03	2.16
^{27}Ne		5.89	6.52	6.58	7.05	7.61
^{28}Ne		8.82			12.06	10.67
^{29}Ne		15.99			21.29	17.76
^{30}Ne		20.62			28.37	22.62

TABLE 8.--Continued.

Nucleus	Expt.[a]	TK[b]	Jelley et al.[c]		Theory	
			G	M	Particle	Hole
^{26}Na	- 6.90±0.02[i]	- 6.90	- 6.94		- 7.12	
^{27}Na	- 5.62±0.06[j]	- 6.11	- 5.71	- 5.73	- 5.98	- 3.95
^{28}Na	- 1.14±0.08[j]	- 1.81	- 1.02		- 1.24	- 0.58
^{29}Na	2.65±0.10[j]	0.29	2.32	2.66	2.96	2.09
^{30}Na	8.37±0.20[j]	6.28	8.50		10.64	7.66
^{31}Na	10.60±0.80[j]	10.13	12.70	14.38	17.28	12.12
^{28}Mg	-15.02	-15.05			-15.98	-13.94
^{29}Mg[k]	-10.59±0.40[ℓ]	-11.58	-10.70	-10.75	-11.22	-10.25
^{30}Mg		-10.66	- 9.37	- 9.21	- 8.94	- 9.47
^{31}Mg		- 5.45	- 3.73	- 3.17	- 1.48	- 3.97
^{32}Mg		- 2.94			3.69	- 0.96
^{30}Al	-15.89±0.04	-15.89				-15.47
^{31}Al	-15.01±0.10[m]	-15.75	-15.00	-15.05	-15.85	-15.53
^{32}Al		-11.88	-11.14		-10.95	-12.28
^{33}Al		-10.17	- 9.34	- 8.65	- 6.80	- 9.75
^{32}Si	-24.09	-24.13			-25.47	-24.30
^{33}Si	-20.57±0.05[n]	-21.05	-20.71	-20.67	-20.67	-20.72
^{34}Si		-20.66	-20.57	-20.32	-19.17	-20.64
^{34}P	-24.55±0.05[n]	-24.55			-25.28	-24.62
^{35}P	-24.04±0.08[o]	-24.79	-24.90	-24.81	-25.00	-25.42
^{36}S	-30.67	-30.70			-32.08	-30.59

[a] Unless otherwise noted, the mass excesses are taken from reference 28. The uncertainties of the measured mass excesses are less than 30 keV, except where explicitly specified.

[b] Reference 36.

[c] Reference 37; G indicates using Garvey et al.[35] mass relations, and M indicates modified shell-model mass relations.

[d] Reference 86.

[e] Reference 54.

[f] Reference 61.

[g] The ground-state has $J^{\pi}=3^{+}$ and 2^{+} for the "Particle" and "Hole" Hamiltonians, respectively.

[h] References 66 and 67.

[i] References 68 and 69.

[j] Reference 69.

[k] The ground-state has $J^{\pi}=3/2^{+}$ and $1/2^{+}$ for the "Particle" and "Hole" Hamiltonians, respectively.

[ℓ] Reference 87.

[m] Reference 70.

[n] Reference 71.

[o] Reference 72.

It was observed that aside from a mass dependence, the energy deviations between calculated ground-state binding energies and experiments have an isospin dependence, which corresponds to less binding for the "Particle" Hamiltonian, and more binding for the "Hole" Hamiltonian, for increasing isospin. Comparison of calculated mass excesses of neutron-rich nuclei of the "Particle" and "Hole" Hamiltonians with those of Thibault and Kalpisch[36] seems to indicate that the isospin dependences of the "Particle" and "Hole" Hamiltonians complement each other in giving a good description of all sd-shell nuclei. The agreement with the mass excesses of Thibault and Klapisch[36] tends to shift from the "Particle" to the "Hole" Hamiltonian as mass A and isospin T increase. This encourages the hope that the two Hamiltonians will yield overlapping descriptions in the middle of the sd-shell.

The calculated ground state spins are also listed in Table 7. The agreement with all experimentally known states is excellent. The "Particle" and "Hole" Hamiltonians agree for all ground-state spins except for ^{28}F, ^{29}Mg and ^{34}Cl. In ^{28}F, the "Particle" Hamiltonian predicts a 3^+ ground state with a first excited 2^+ state; the "Hole" Hamiltonian reverses the two states. In either case, the splitting between the two states is less than 150 keV. It may be noted that the "Particle" Hamiltonian predicts ^{28}F to be particle unstable by more than 1 MeV; while the "Hole" Hamiltonian predicts a neutron separation energy of

740 keV. Thibault and Klapisch[36] predict a neutron separation energy of 60 keV. In ^{29}Mg, the "Particle" Hamiltonian predicts a $3/2^+$ ground state and $1/2^+$ first excited state; the "Hole" Hamiltonian again reverses the two states. The splitting of the two states is 420 keV for the "Particle" Hamiltonian and 24 keV for the "Hole" Hamiltonian. Both are consistent with a recent observation of $J^\pi=3/2^+$, $1/2^+$ by Goosman et al.[87] In ^{34}Cl, the first 1^+ (T=0) state comes below the lowest 3^+ (T=0) state for the "Hole" Hamiltonian.

The predicted spin of $5/2^+$ for ^{21}O ground state agrees with that of the PW interaction.[6] The recent assignment of $J^\pi=4^+$ for the ^{22}F ground state by Davids et al.[54] was included in the data set for the "Particle" least-squares fit; however, the "Hole" Hamiltonian also reproduces a $J^\pi=4^+$ ^{22}F ground state. The same statement is also true for the $J^\pi=5/2^+$, ^{23}F ground state recently assigned by Goosman and Alburger,[61] and the $J^\pi=1/2^+$, ^{25}Ne ground state experimentally observed by Goosman et al.[66] to have $J^\pi=1/2^+(3/2^+)$. Both the "Particle" and "Hole" Hamiltonians predict a $J^\pi=3/2^+$ ground state for ^{27}Na consistently with $J^\pi=3/2^+$, $5/2^+$ proposed by Alburger et al.[88] The ground state spins of other Na isotopes are calculated to have $J^\pi=1^+$, $5/2^+$, 1^+, $5/2^+$ for ^{28}Na, ^{29}Na, ^{30}Na and ^{31}Na respectively. The $J^\pi=1^+$ ^{28}Na ground state spin was recently assigned by Roeckl et al.[85] and included in the "Particle" fit, however, the "Hole" Hamiltonian also

reproduces a $J^{\pi}=1^{+}$ ground state for ^{28}Na. The ^{29}Na ground state was fitted to the two lowest theoretical eigenstates of $J^{\pi}=3/2^{+}$ and $J^{\pi}=5/2^{+}$ in the "Particle" fit, and to the lowest $J^{\pi}=3/2^{+}$ state in the "Hole" fit. In both cases, a $J^{\pi}=5/2^{+}$ ground state results from the final interaction. The $J^{\pi}=1^{+}$ ^{34}P ground state recently assigned by Goosman et al.[71] is reproduced by the "Particle" Hamiltonian, but was not included in the data set for the least-squares fit.

I.4.D. Ground-State Wave Function of ^{28}Si

As shown in the previous subsection, the ground-state binding energies and spins are well reproduced by the "Particle" and "Hole" Hamiltonians combined. The deviations between calculated and observed binding energies in the regions of nuclei from which the data sets were taken are less than or equal to 0.5 MeV. The improvement in the calculated binding energies further extends beyond the regions of nuclei included in the least-squares fit. It is hoped that the two Hamiltonians will complement each other to give a good description of all sd-shell nuclei, i.e., provide overlapping and similar descriptions of nuclei in the middle of the sd-shell region. To gain some idea of how the Hamiltonians compare in the middle of the sd-shell, we compare the ground-state wave functions of ^{28}Si as generated by the different Hamiltonians.

In Figure 7 are plotted the configuration probabilities of n active particles in the $d_{5/2}$-orbit for the

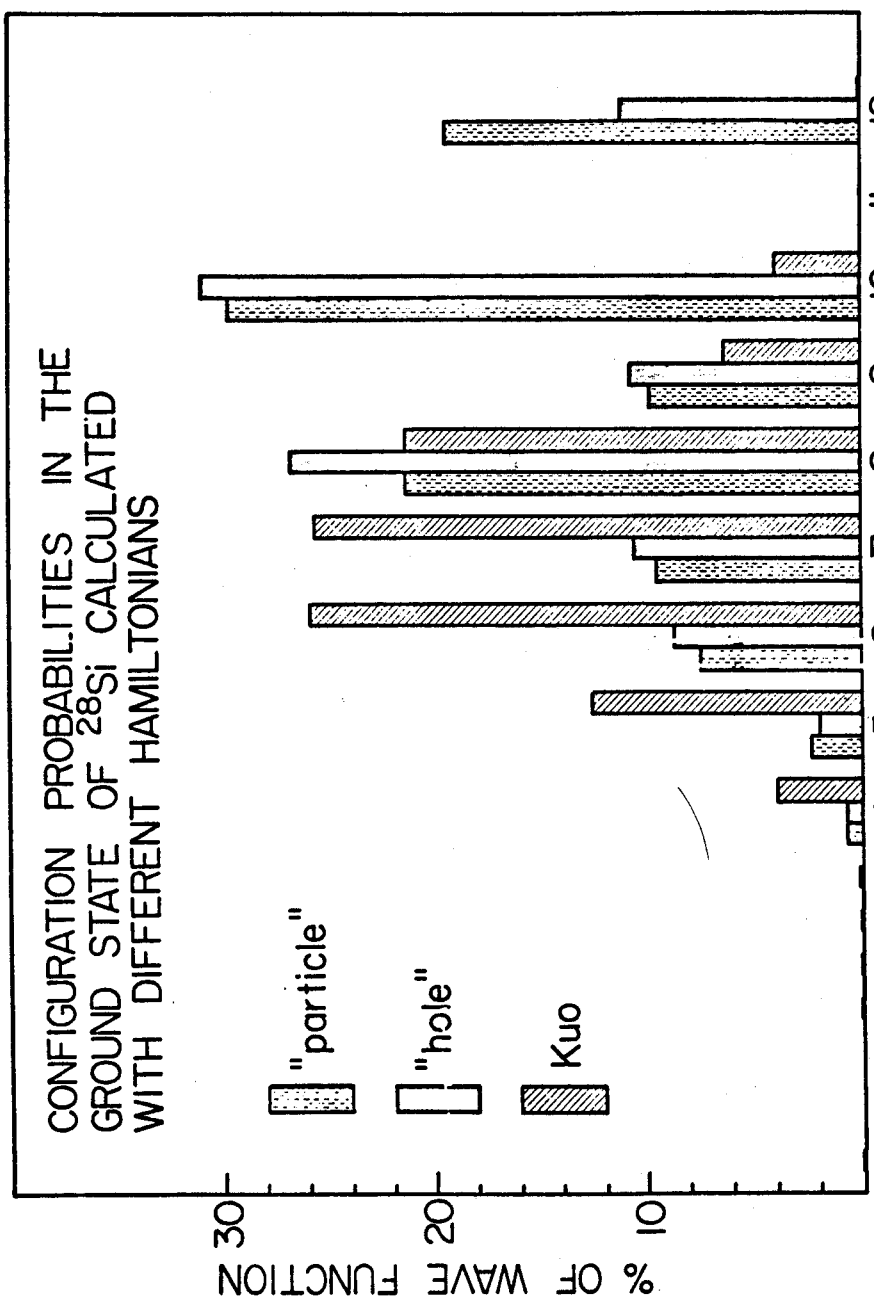

Figure 7. Configuration probabilities in the ground-state of ^{28}Si calculated with "Particle," "Hole" and KUO14 Hamiltonians.

ground state of ^{28}Si, as calculated from the "Particle," "Hole," and KUO14 Hamiltonians. It can be seen that the "Particle" and "Hole" Hamiltonians give similar descriptions of the ground-state of ^{28}Si, one which is quite different from that given by the Kuo interaction.

The KUO14 interaction gives almost no component of $(d_{5/2})^{12}$ configuration in the wave function. The $(d_{5/2})^{10}$ configuration has also a very small component. The large components are those of the $(d_{5/2})^{6}$, $(d_{5/2})^{7}$ and $(d_{5/2})^{8}$ configurations. The (average) occupation numbers are 6.84, 2.68, and 2.48 for the $d_{5/2}$, $s_{1/2}$, and $d_{3/2}$ orbits, respectively. The empirical Hamiltonians give a description of the ^{28}Si ground-state more in keeping with simple expectations. The $(d_{5/2})^{12}$ and $(d_{5/2})^{10}$ configurations are much more heavily occupied than in the Kuo wave function. The (averaged) occupation numbers of 9.13, 1.45, and 1.41 for the "Particle" and 8.79, 1.64, and 1.58 for the "Hole" Hamiltonians, for the $d_{5/2}$, $s_{1/2}$, and $d_{3/2}$ orbits, respectively, are in better agreement with relevant experimental data than are the Kuo values.

The difference between the Kuo and empirical results may be explained by the less attractive $d_{5/2}$-$s_{1/2}$ and $d_{5/2}$-$d_{3/2}$ interactions in the "Particle" and "Hole" Hamiltonians. The same argument may also be used to account for the small differences in the configuration probabilities for $(d_{5/2})^{8}$ and $(d_{5/2})^{12}$ configurations between the "Particle" and "Hole" Hamiltonians. The

$d_{5/2}$-$d_{5/2}$ and $d_{5/2}$-$s_{1/2}$ interactions are more attractive in the "Particle" than in the "Hole" Hamiltonian.

I.4.E. Energy Spectra

The energy spectra calculated with the "Particle" Hamiltonian for A=17-24, 25(T=1/2), 26(T=0) and with the "Hole" Hamiltonian for A=32-39 nuclei are shown in Figures 8-25. The angular momentum labels in the figures give J for even-A nuclei and 2J for odd-A nuclei. Brackets indicate the experimental assignment is tentative. An assignment such as (3) means that the spin is probably 3; and a (3,5) means that the spin is probably 3 or 5. An assignment such as $5^{(+)}$ means that the parity is probably positive; and a $5^{(\ )}$ means that the parity is unknown. A bracket around a line means that the observed level is probably there. A dashed line indicates a negative parity state, and a solid line with no label indicates a positive parity state or a state with only the energy known. All labeled lines with no parity assignment indicate positive-parity states. A dot indicates that above that energy there are levels not shown. All known or calculated levels are included before the first dot. The levels are plotted in terms of calculated or corrected measured binding energy relative to ^{16}O or ^{40}Ca. The spectra are not shifted except for A=26 (T=0) nucleus, where the whole theoretical spectrum is shifted by 0.5 MeV for easier comparison. The spectra plotted do not necessarily reflect

the energy levels included in the data sets for the least-squares fits as listed in Tables 1 and 3. The lines connecting calculated and experimentally observed energy levels are merely to guide the eyes for easier comparison. The experimetnal spectra are taken from references 27, 29, and Tables 1 and 3.

In the following paragraphs we discuss some of the relationships between the model spectra and the experimental data.

(1) A=17, T=1/2 (Figure 8):

The $d_{3/2}$ strength is observed to be fragmented in ^{17}O. The single-particle energy for $d_{3/2}$ was treated as a free parameter in the last iteration of the least-squares fit and was found to move down to +0.88 MeV, close to the energy of the first $3/2^+$ state in ^{17}O.

(2) A=18, T=0 (Figure 8):

The 1^+, 2^+, and 3^+ states at 1.70, 2.52, and 3.36 MeV, respectively, were assumed to be intruder states; otherwise there is good agreement between the calculated and observed spectra in the low-energy region.

(3) A=18, T=1 (Figure 8):

The question of whether the second (3.63 MeV) or third (5.33 MeV) observed 0^+ state in ^{18}O is dominated by core-excited, particle-hole configurations is an unresolved issue in shell-model calculations. The theoretical second 0^+ state was fitted to the spectroscopic-factor-weighted centroid of the energies of the two observed excited 0^+

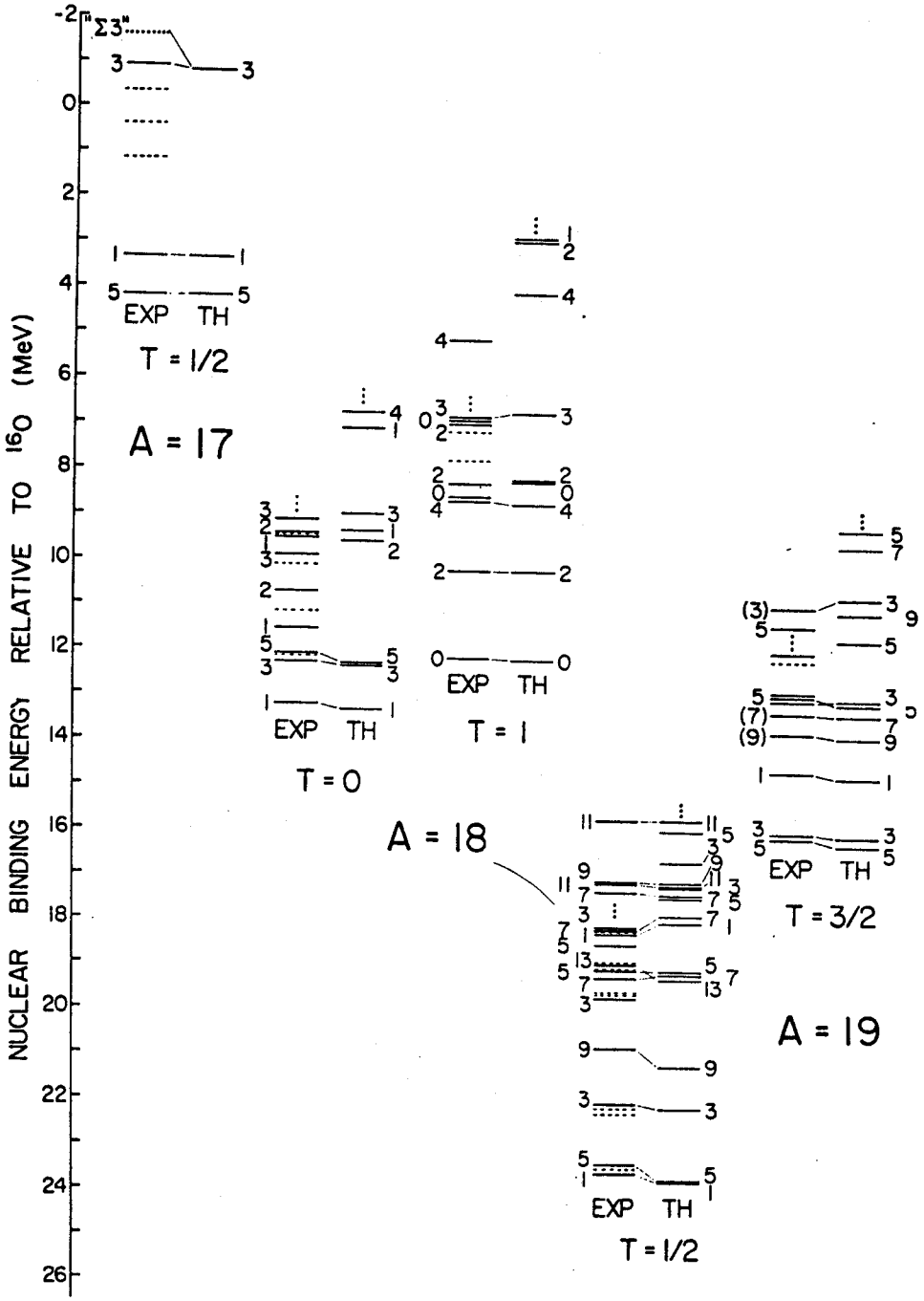

Figure 8. Energy Spectra of A=17 (T=1/2), A=18 (T=0,1), and A=19 (T=1/2, 3/2).

states. The third observed 2^+ state at 5.25 MeV is generally accepted as an intruder state. The theoretical second 4^+ state is always predicted higher than the one experimentally observed at 7.11 MeV.

(4) A=19, T=1/2 (Figure 8):

The observed $3/2^+$ state at 3.91 MeV in ^{19}F is missing in the calculated spectrum. This is very probably an intruder state. A recent weak-coupling particle-hole model calculation by Ellis and Engeland[33] which included $(sd)^3$ configurations also is not able to reproduce this state.

(5) A=19, T=3/2 (Figure 8):

The agreement is good between the calculated and observed spectra, although additional experimental data are required to establish more firmly the correlations between theoretical and observed levels. The observed possible $1/2^+$ state at 3.24 MeV in ^{19}O (not labeled in Figure 8) is missing in the calculated spectrum.

(6) A=20, T=0 (Figure 9):

The ground state rotational band of 0^+, 2^+, 4^+, 6^+, 8^+ states is well-reproduced. Between 6 and 9 MeV, there are three observed 0^+ and three observed 2^+ states, while the calculated spectrum has only one 0^+ and one 2^+ state.

(7) A=20, T=1 (Figure 9):

Below 2.5 MeV, agreement between calculated and observed spectra is good; however above 2.5 MeV more experimental data are needed for a definite comparison

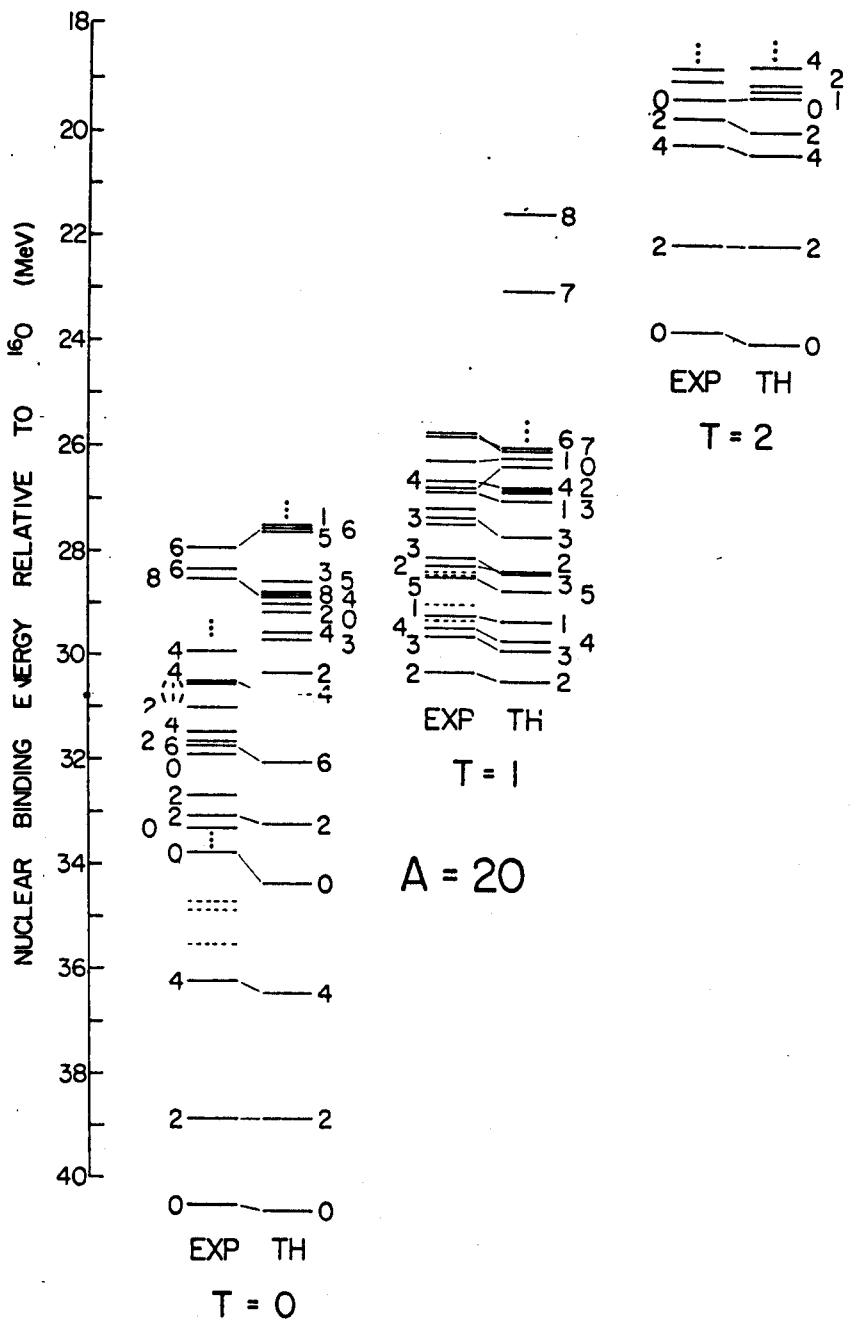

Figure 9. Energy Spectra of A=20 (T=0,1,2).

(8) A=20, T=2 (Figure 9):

The five lowest observed states with known spin-parity assignment are well reproduced.

(9) A= 21, T=1/2 (Figure 10):

The low-lying states are very well reproduced. The first $15/2^+$ state is predicted at 9.76 MeV.

(10) A=21, T=3.2 (Figure 10):

Only the spins of a few states have been uniquely determined experimentally. However, the level density is well reproduced, except for two of the four states observed at about 2 MeV. It is possible that these are negative-parity states.

(11) A=21, T=5/2 (Figure 10):

The ground state of ^{21}O is predicted to have $J^\pi=5/2^+$, although the binding energy is 1.4 MeV larger than the experimental value.

(12) A=22, T=0 (Figure 11):

The 1^+ and 3^+ members of the $K=0^+$, T=0 excited band in ^{22}Na are overbound in the calculated spectrum, although the higher spin members of the same band are not. The extra 2^+ state predicted by the PW interaction near 3 MeV is moved up to around 4 MeV. The observed 4.32 MeV 1^+ state is missing in the calculated spectrum.

(13) A=22, T=1 (Figure 11):

The first excited 0^+ state observed at 6.24 MeV is predicted to come 1 MeV too low in excitation. Otherwise,

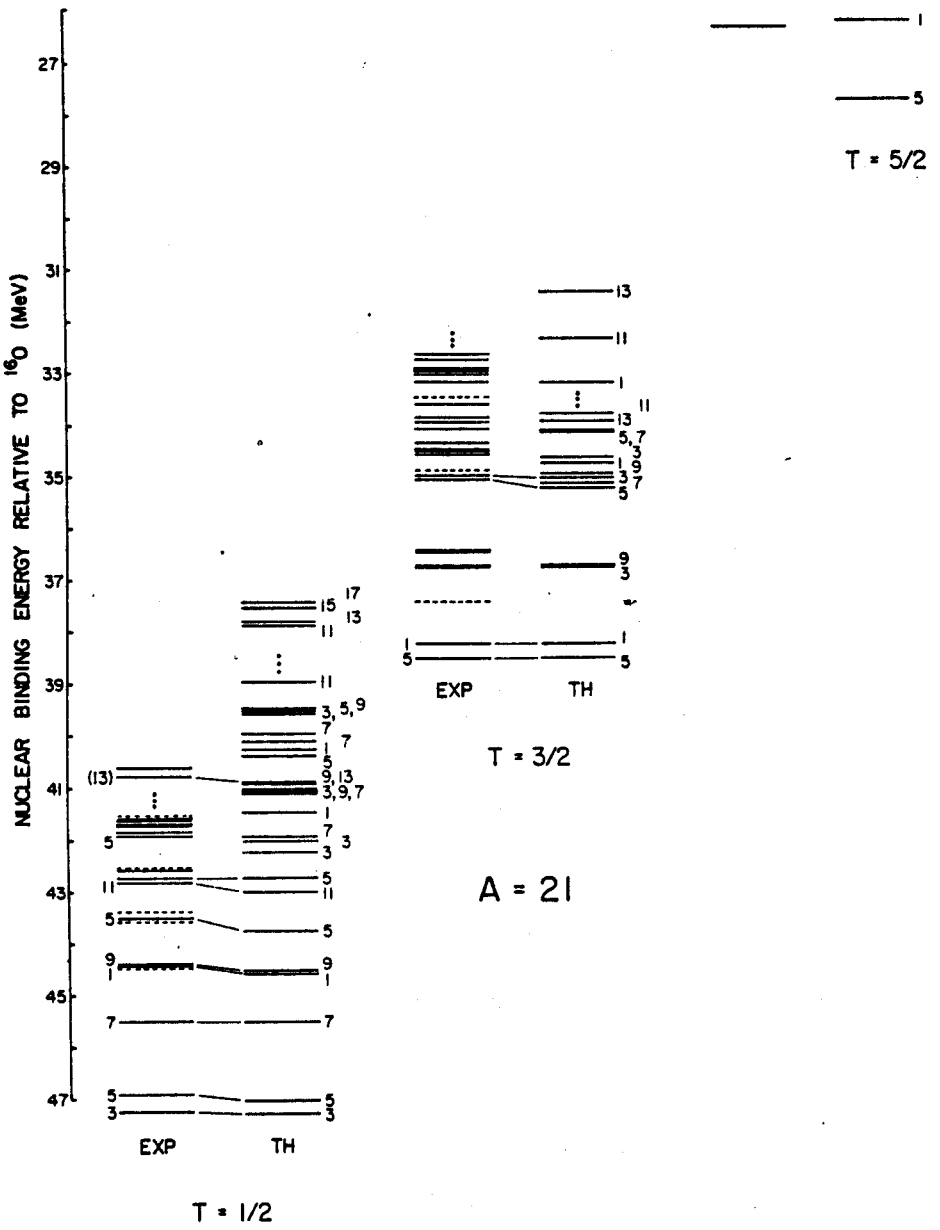

Figure 10. Energy spectra of A=21 (T=1/2, 3/2, 5/2).

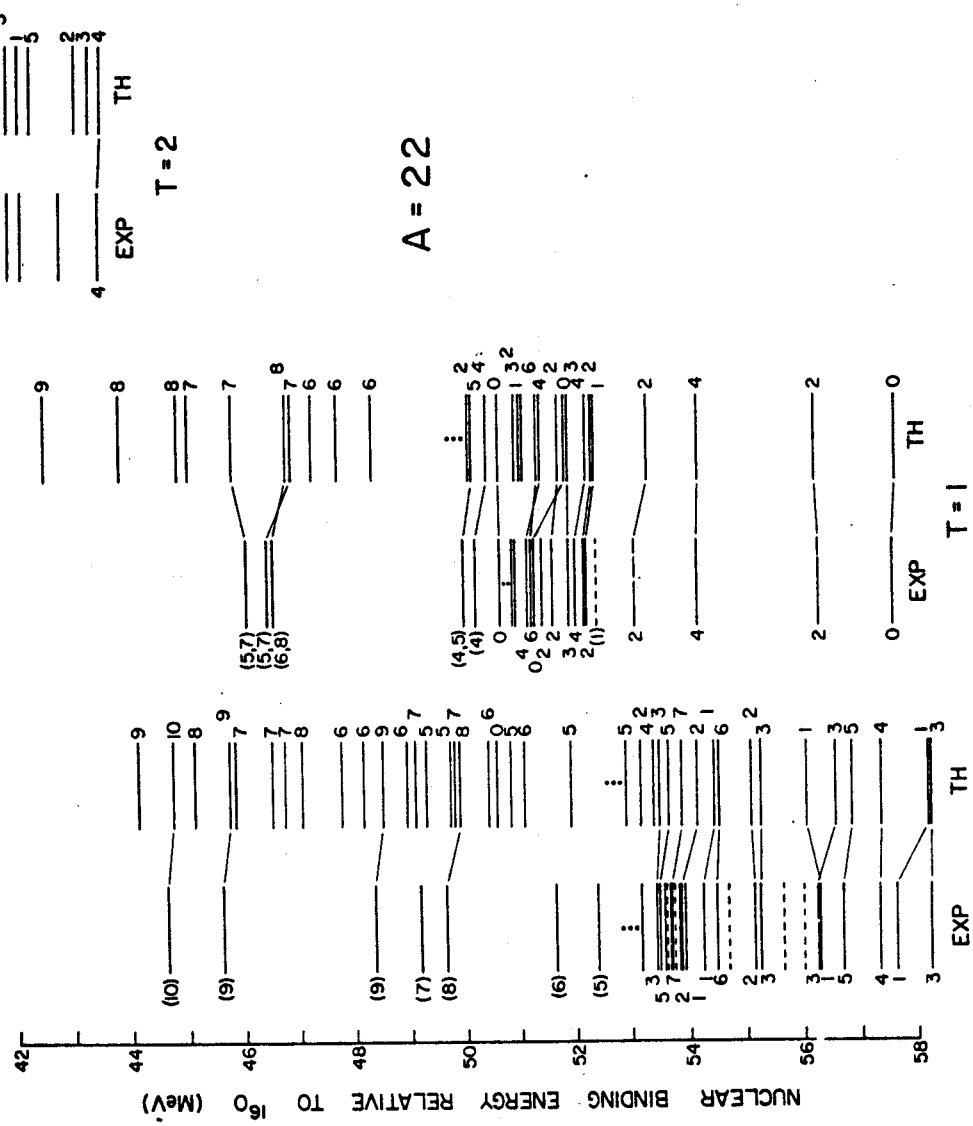

Figure 11. Energy spectra of A=22 (T=0,1,2).

the agreement is good for individual excitation energies and the density of states is also well-reproduced.

(14) A=22, T=2 (Figure 11):

Contrary to the compilation of Endt and Van der Leun,[27] the ground state is predicted to have $J^{\pi}=4^{+}$. This is in agreement with the experimental results of Davids et al.[54]

(15) A=23, T=1/2 (Figure 12):

Compared to the PW interaction, the present calculated spectrum agrees much better with experiment. The low-lying non-ground-state band member observed levels are overbound, but the discrepancies are all less than 250 keV. The 9.04, 9.81, 14.24, and 14.70 MeV excited states were observed recently in $^{12}C(^{12}C,n)^{23}Mg$ by Speer et al.[59] These were proposed to be the $15/2^{+}$, $17/2^{+}$, $19/2^{+}$ and $21/2^{+}$ members of the ground state rotational band. The 9.04 and 9.81 MeV excited states were also observed in $^{12}C(^{12}C,p)^{23}Na$ by Bibber et al.[58] The 9.04 ($15/2^{+}$) and 14.24 ($19/2^{+}$) MeV excited states were fitted to the theoretical counterparts in the "Particle" fit. As shown in Figure 12, the calculated first $15/2^{+}$ state agrees well with the proposed spin assignment for the observed 9.04 MeV state. However, the observed 9.81, 14.24 and 14.70 MeV states are closer in energies to calculated excited states of $15/2^{+}$, $17/2^{+}$ and $19/2^{+}$ spin respectively. The $15/2^{+}$ assignment for the 9.81 MeV state agrees with a recent $^{12}C(^{12}C,p)^{23}Na$ measurement by Kekelis et al.,[57] which eliminated a $17/2^{+}$ assignment

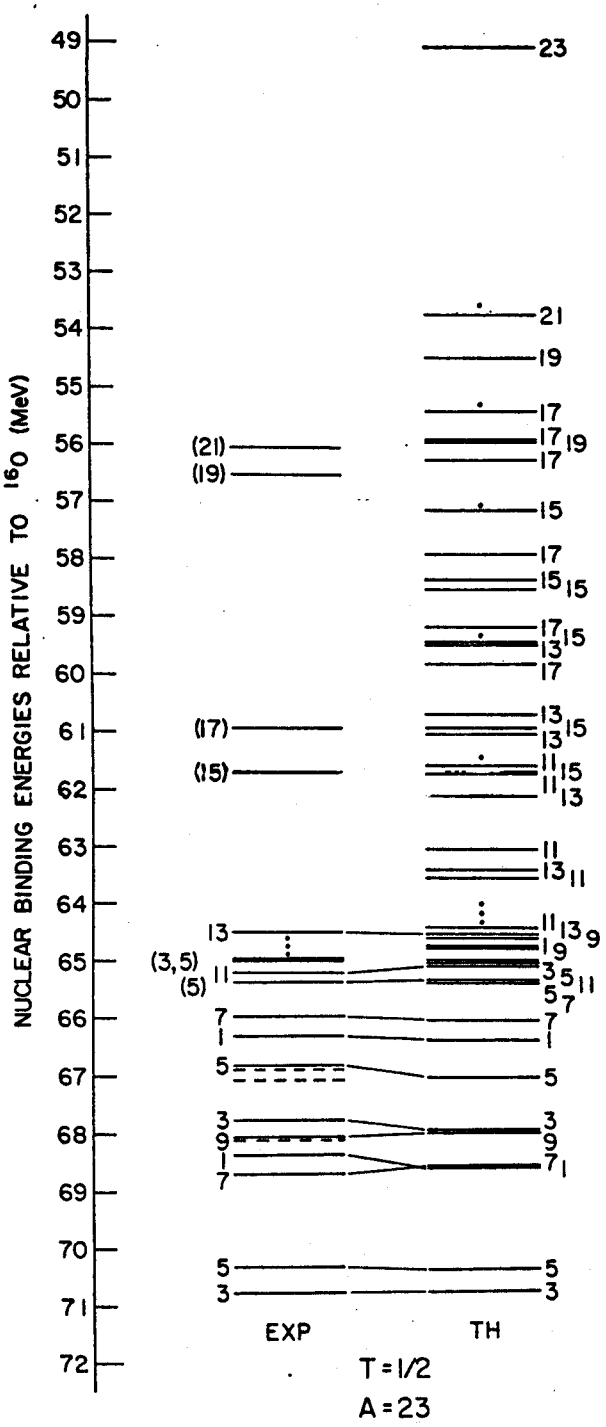

Figure 12. Energy spectra of A=23 (T=1/2).

for this state through angular correlations and lifetime data. The calculated spectrum shows a number of high-spin states rather close together. Following the J(J+1) rule, it is not clear which of the $13/2^+$, $15/2^+$, or $17/2^+$ states are members of the ground-state rotational band. Further investigation of the structure of the ground-state band is needed.

(16) A=23, T=3/2 (Figure 13):

The reversal of the order of the observed $7/2^+$ and $3/2^+$ states at 1.70 and 1.82 MeV by the PW interaction is corrected in the present calculated spectrum.

(17) A=23, T=5/2 (Figure 13):

The ground state of ^{23}F was recently assigned a $J^\pi=5/2^+$ by Goosman and Alburger.[61] The state was included in the "Particle" fit and the binding energy is well reproduced.

(18) A=24, T=0 (Figure 14):

The energies in general are overbound compared with experiment. The K=2 excited band which was predicted 1.5 MeV below its observed position by the KUO14 realistic interaction and 0.5 MeV by the PW interaction is well reproduced in the present case. The first excited 0^+ state is still predicted to be underbound. In the 10-12 MeV region, there are three observed 0^+ states, compared to only two theoretical counterparts.

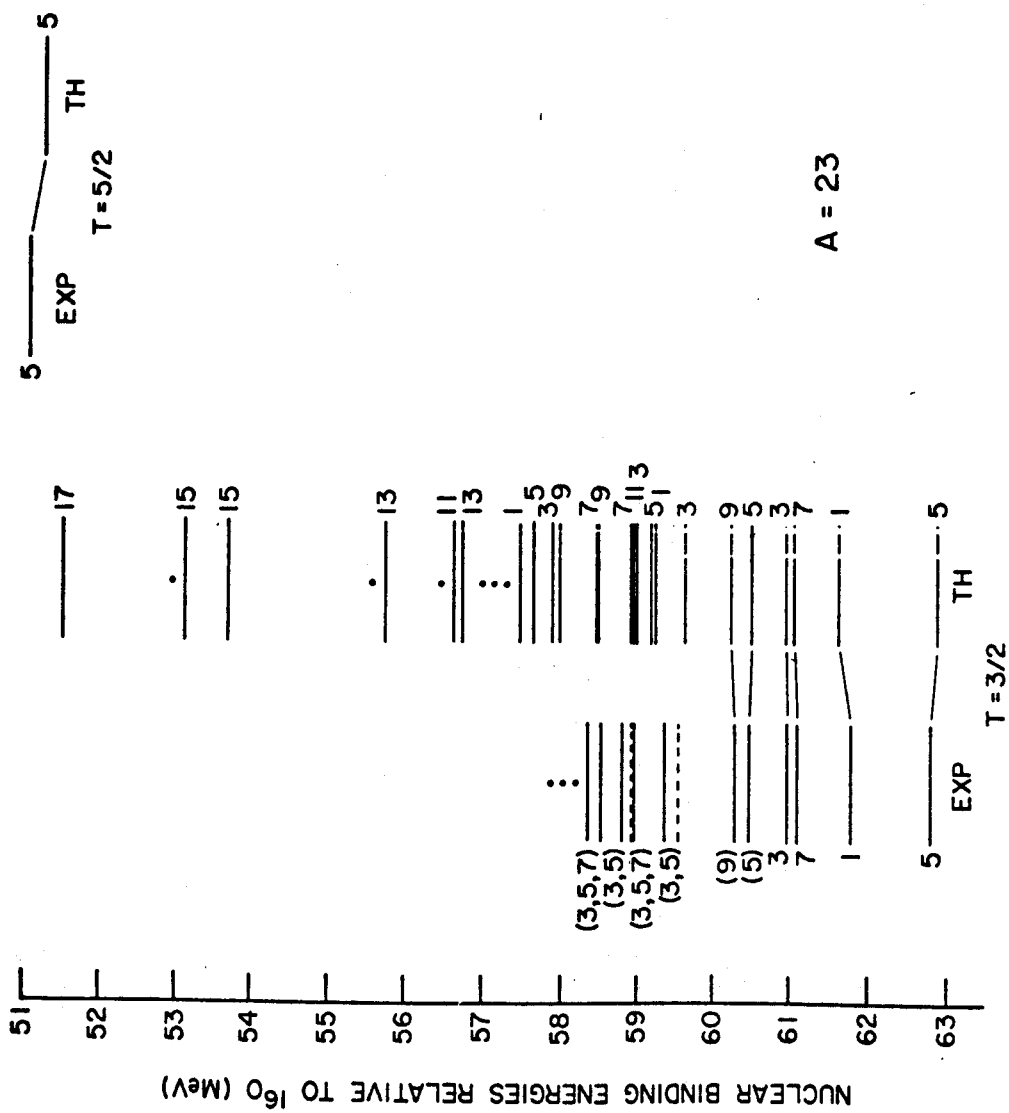

Figure 13. Energy spectra of A=23 (T=3/2, 5/2).

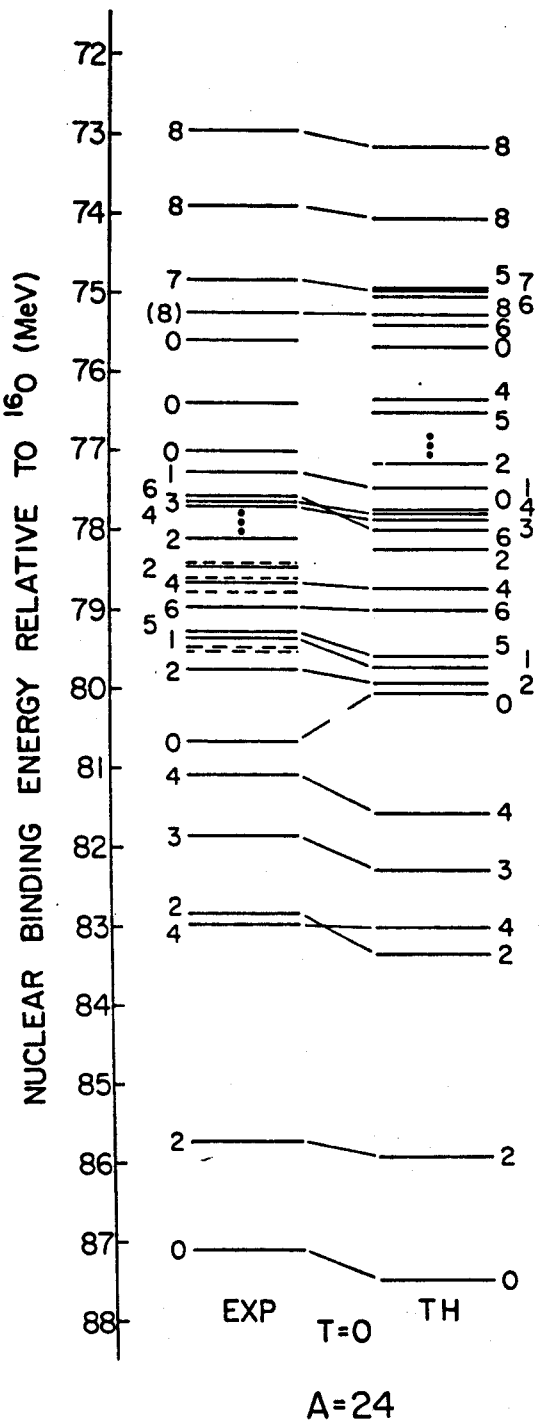

Figure 14. Energy spectra of A=24 (T=0).

(19) A=24, T=1 (Figure 15):

The experimental spectrum is well reproduced below 3 MeV. More experimental data are needed for comparison above 3 MeV.

(20) A=24, T=2 (Figure 15):

The calculated spectrum strongly suggest the 4.89 MeV state to have $J^{\pi}=3^{+}$.

(21) A=25, T=1/2 (Figure 16):

Except for the counterpart of the $1/2^{+}$ excited state observed at 2.56 MeV in ^{25}Mg, all the calculated low-lying states are overbound compared to experiment. The calculated spectrum agrees very well with experiment in terms of sequence and spacings, however.

(22) A=26, T=0 (Figure 17):

The calculated binding energies are too large compared to experiment. In Figure 17, the calculated spectrum has been shifted up by 0.5 MeV for an easier comparison with the experimental spectrum. The agreement is remarkably good, suggesting that the observed 2.66 and 3.07 MeV states have $J^{\pi}=2^{+}$ and 3^{+} respeetively.

(23) A=32, T=0 (Figure 18):

The calculated binding energies are too large compared to experiment. However, the shifting of the excited states down relative to the ground-state by the KUO14 interaction is corrected. The first excited 0^{+} state is also correctly calculated; it is underbound by more than 2 MeV by the KUO14 interaction relative to the ground-state.

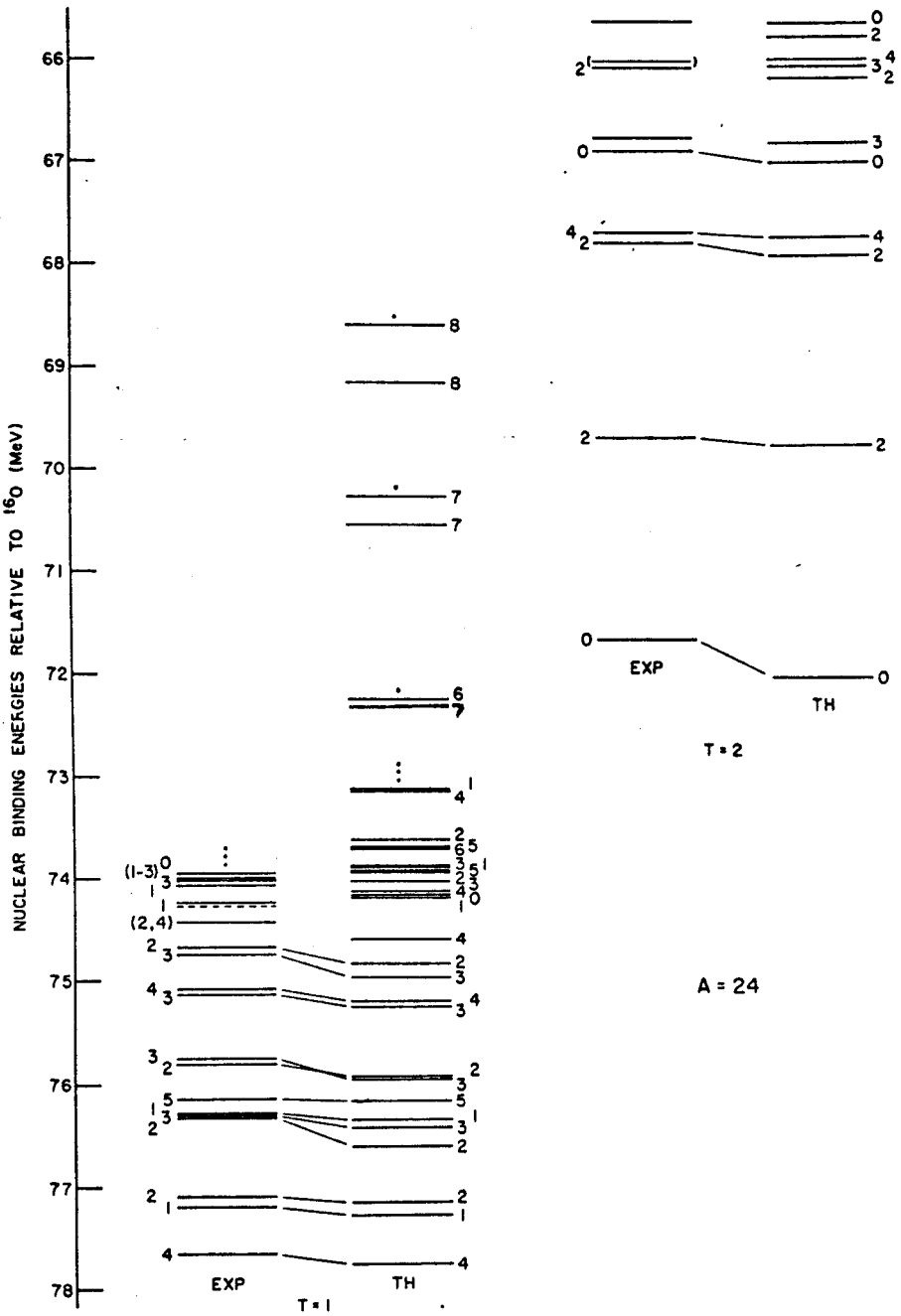

Figure 15. Energy spectra of A=24 (T=1,2).

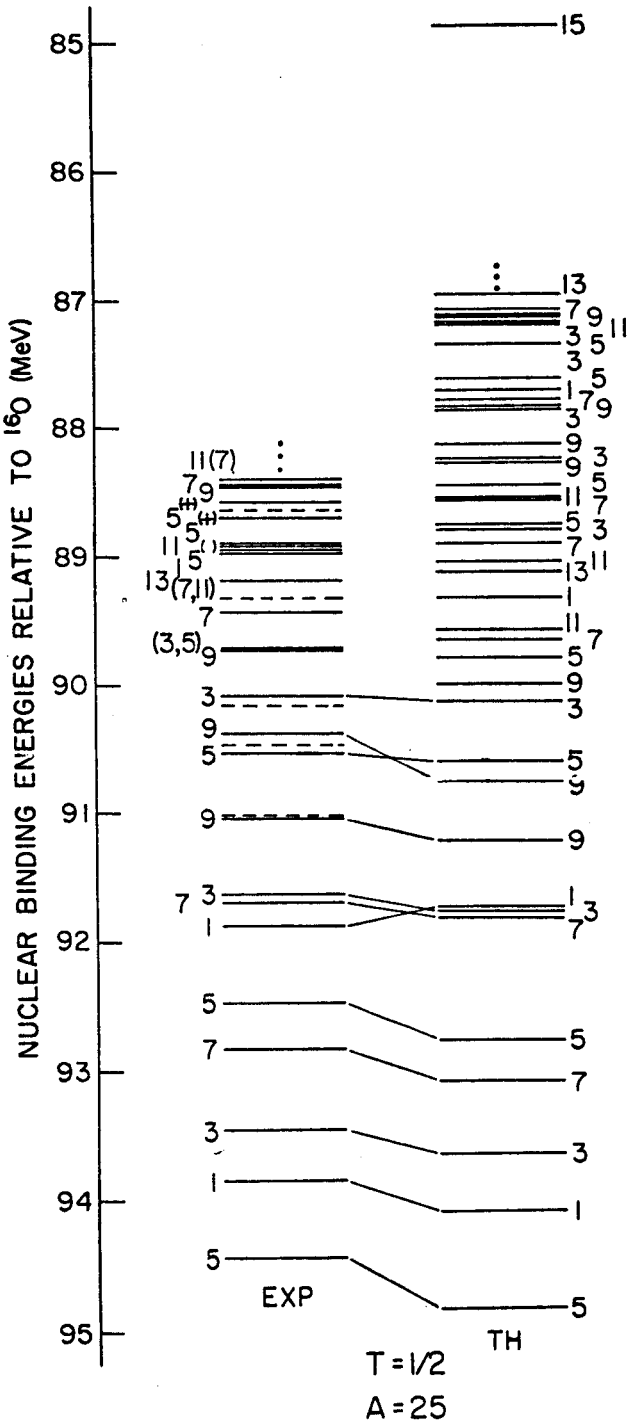

Figure 16. Energy spectra of A=25 (T=1/2).

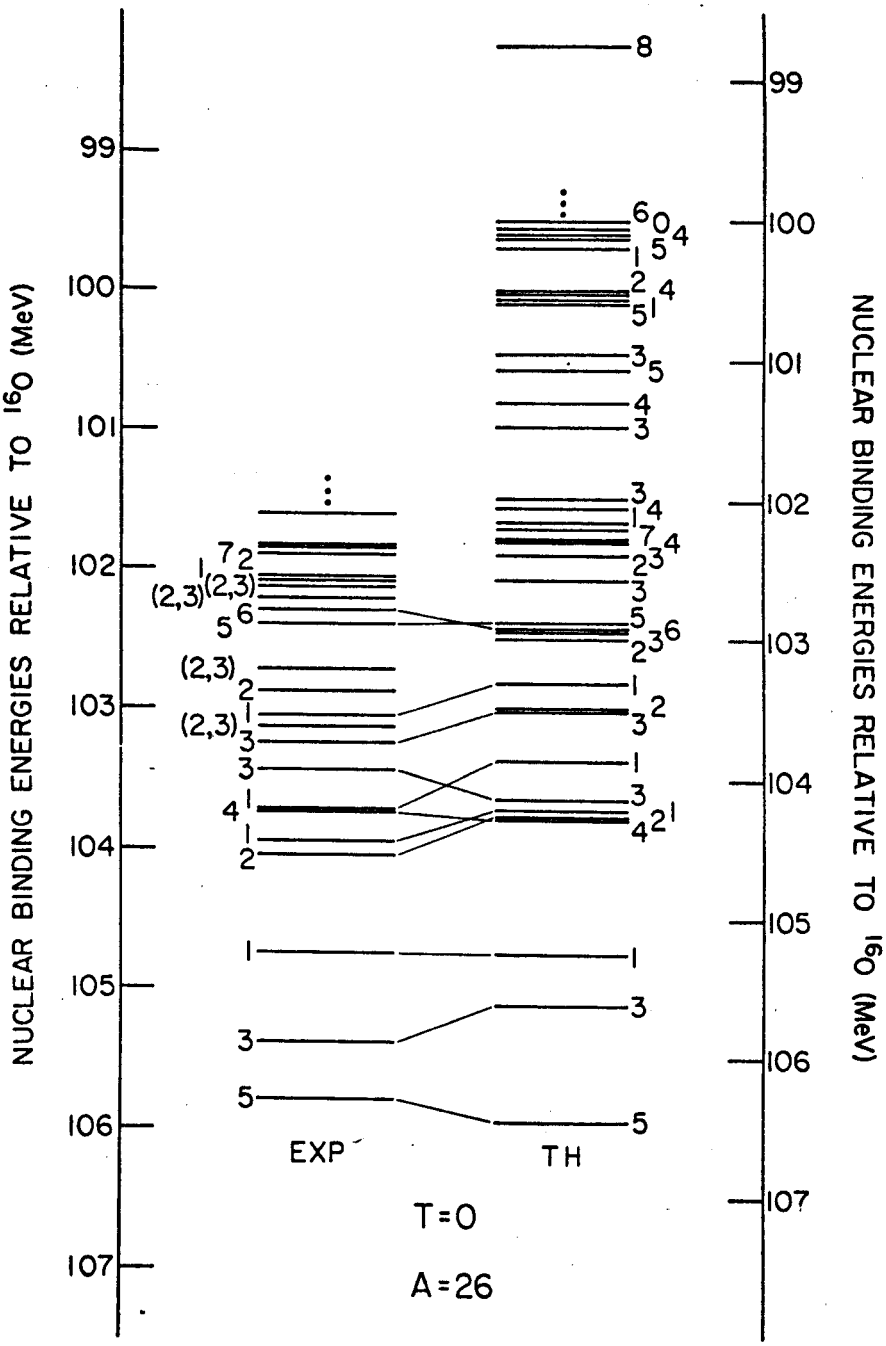

Figure 17. Energy spectra of A=26 (T=0).

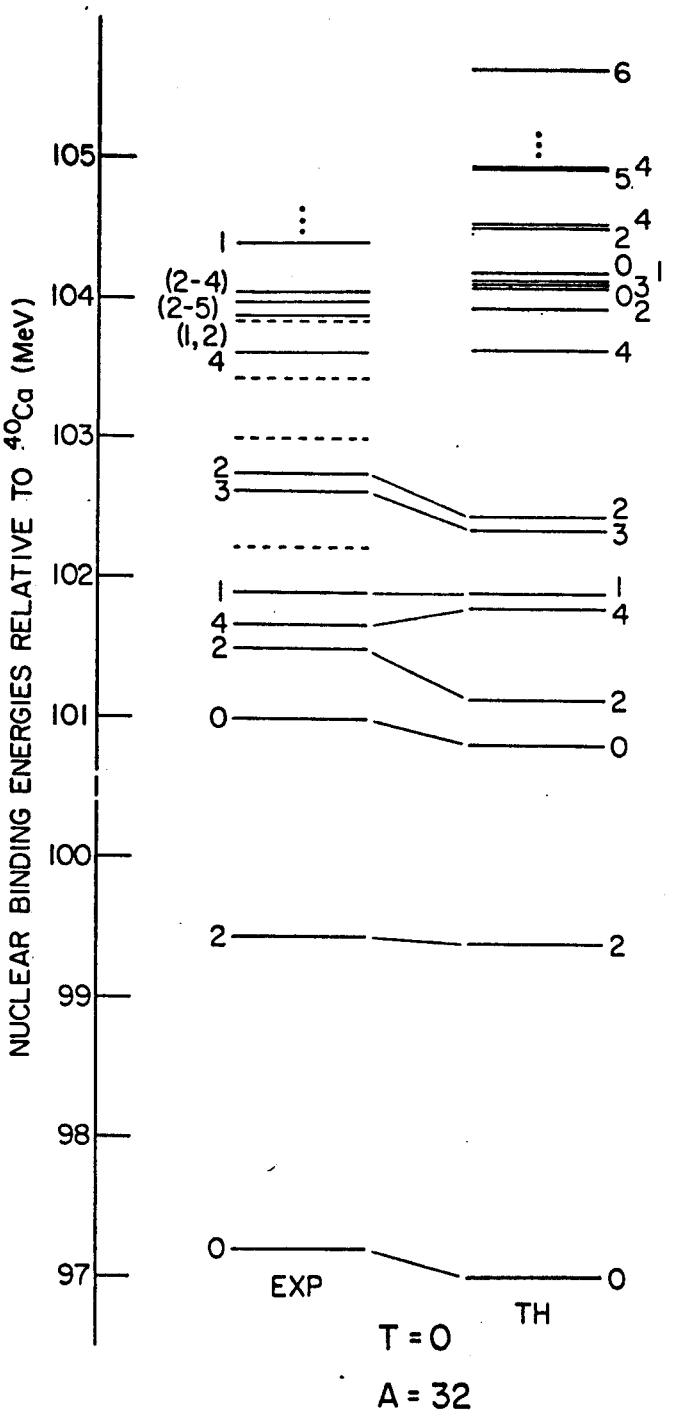

Figure 18. Energy spectra of A=32 (T=0).

(24) A=32, T=1 (Figure 19):

The $J^{\pi}=0^{+}$ and 2^{+} states observed at 0.51 and 1.32 MeV, respectively, are overbound in the calculation. Otherwise the agreement is good for the low-lying states.

(25) A=32, T=2 (Figure 19):

More experimental data are needed for comparison above 4 MeV. Two excited 0^{+} states are predicted near 5 MeV, while only one is observed with a possible assignment of $J^{\pi}=0^{+}$ at 4.98 MeV.

(26) A=33, T=1/2 (Figure 20):

Some of the excited states are calculated to be overbound compared with experiment; the order of the second $5/2^{+}$ and second $3/2^{+}$ states is reversed. The agreement is good in general.

(27) A=33, T=3/2 (Figure 21):

The low-lying states are well reproduced, though more experimental data are needed for comparison above 4 MeV. The observed 3.28 MeV state is suggested to have $J^{\pi}=3/2^{+}$ by our results.

(28) A=33, T=5/2 (Figure 21):

The binding energy of ^{33}Si is well reproduced. The observed energy and J^{π} of $3/2^{+}$ was included in the "Hole" least-squares fit.

(29) A=34, T=0 (Figure 22):

The calculated binding energy of the 3^{+} ground state agrees well with experiment. However, the first excited

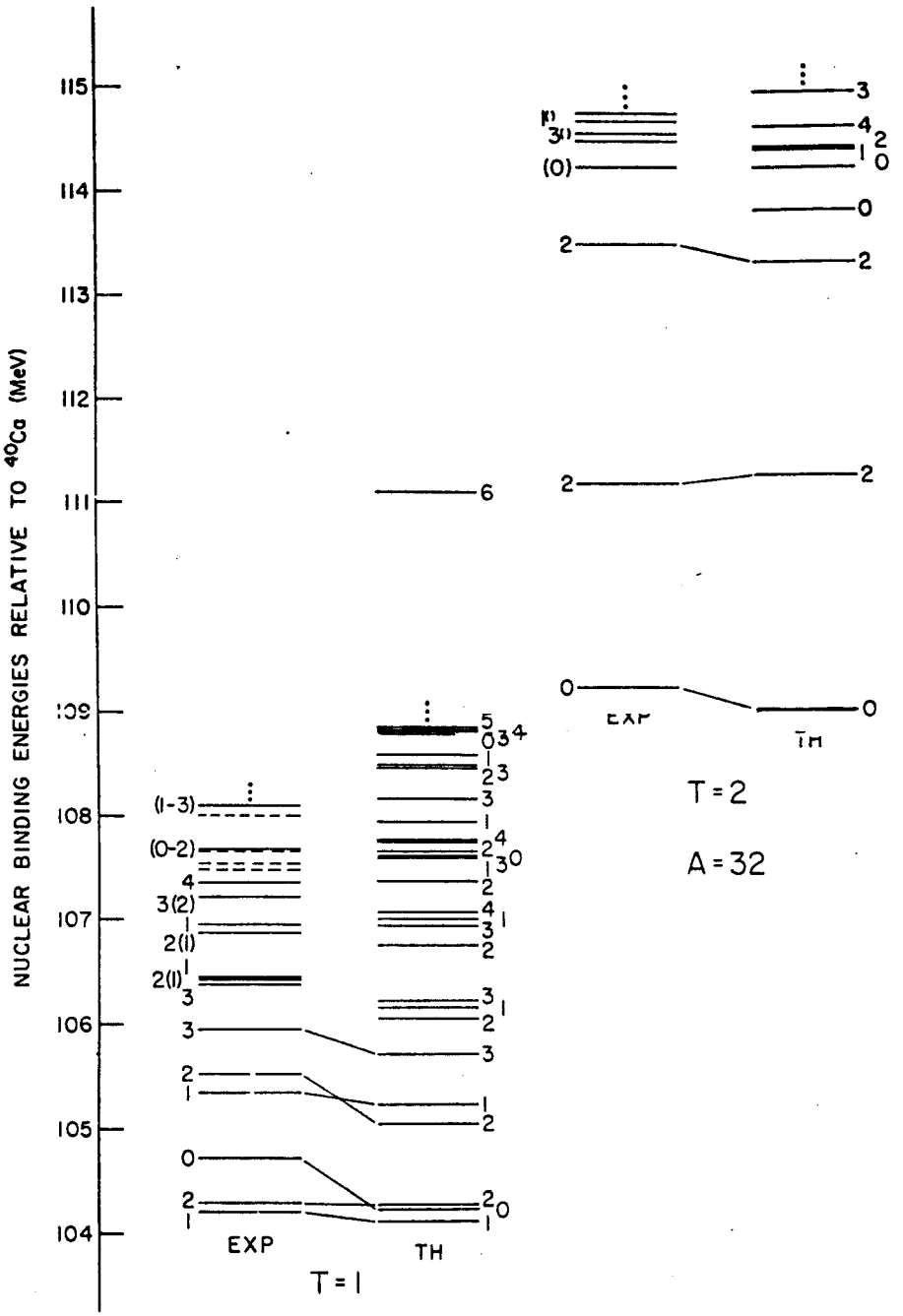

Figure 19. Energy spectra of A=32 (T=1,2).

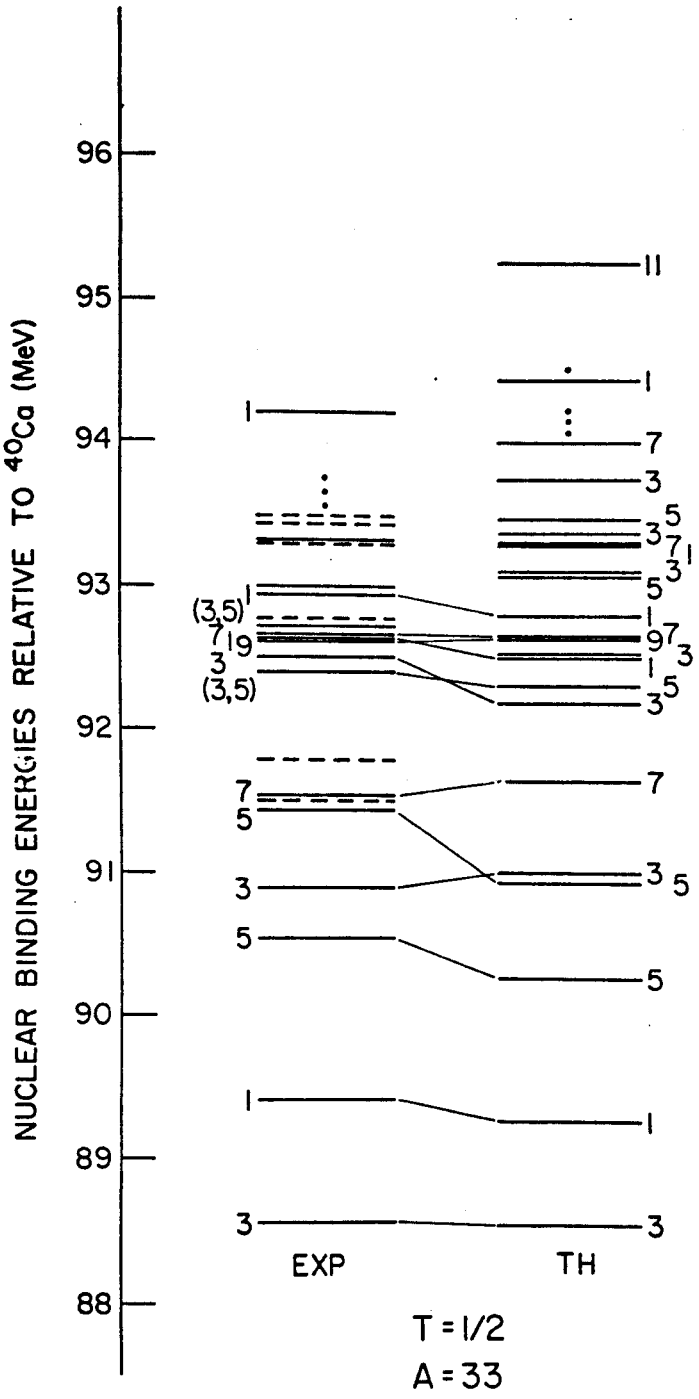

Figure 20. Energy spectra of A=33 (T=1/2).

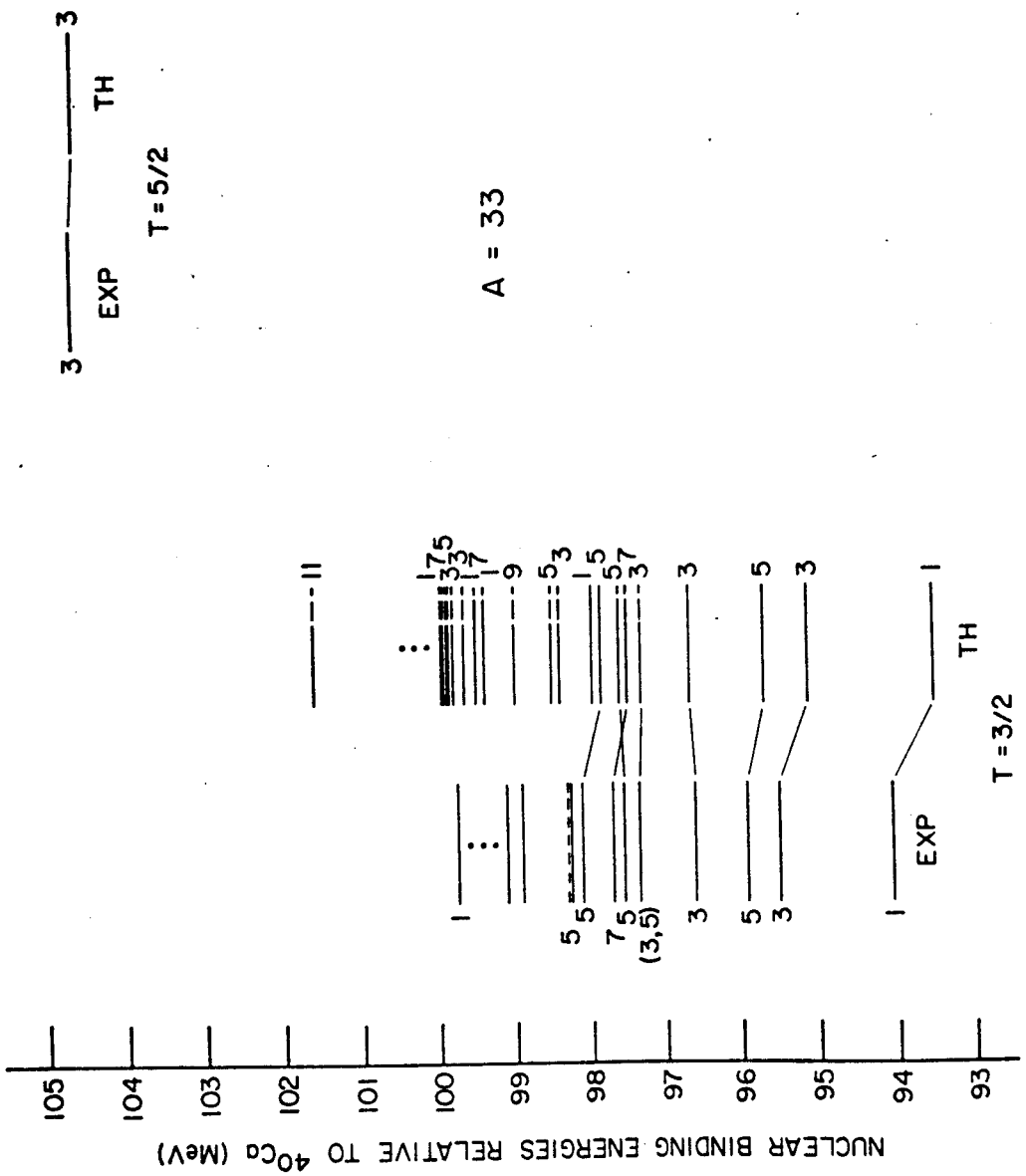

Figure 21. Energy spectra of A=33 (T=3/2, 5/2).

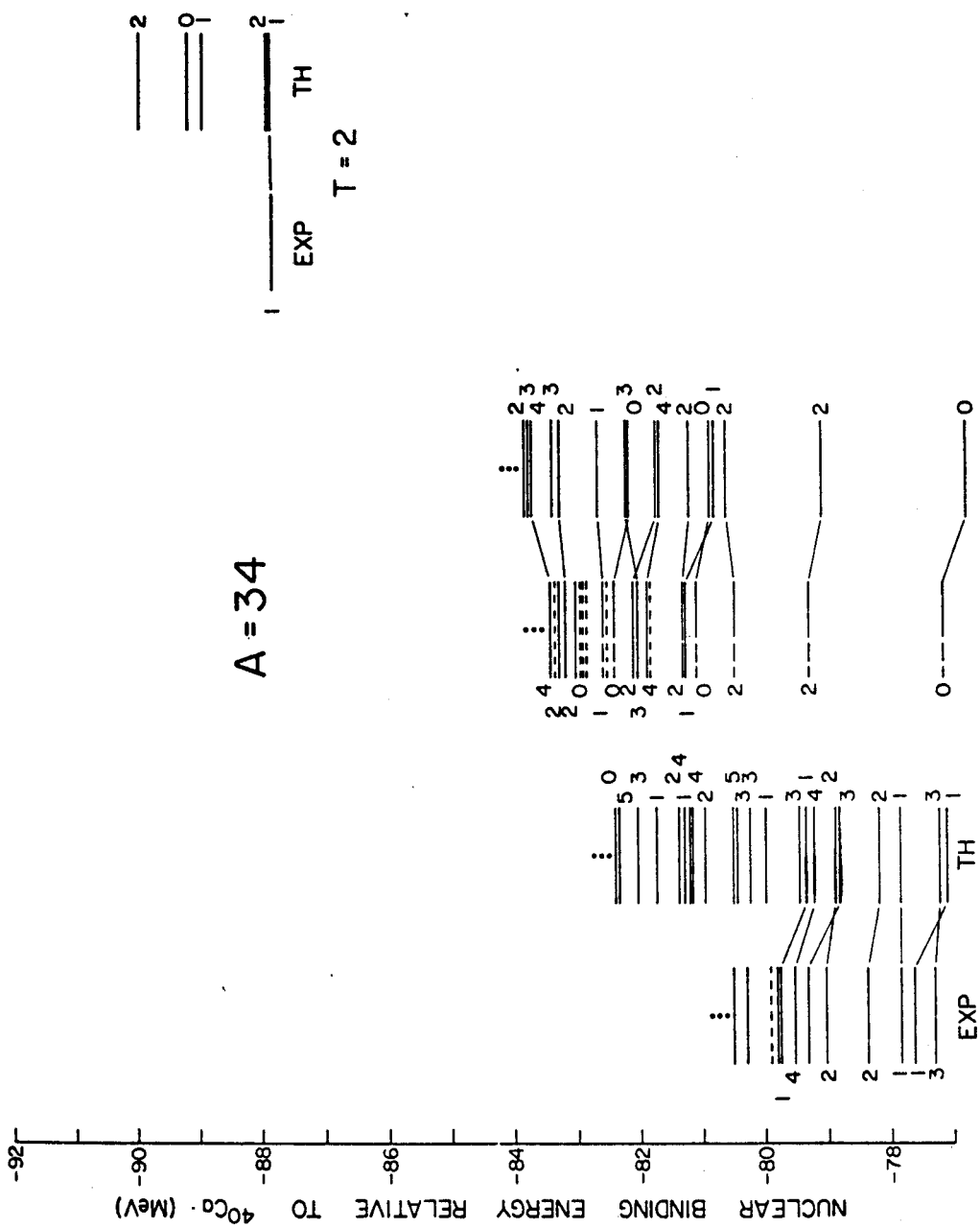

Figure 22. Energy spectra of A=34 (T=0,1,2).

1^+ state is overbound and comes out below the ground state. Some other excited states are also overbound.

(30) A=34, T=1 (Figure 22):

The 0^+, T=1 ground state of ^{34}S is correctly calculated to come below the T=0 states in ^{34}Cl. The calculated spectrum agrees well with experiment except that between 5 and 6 MeV there are two observed 0^+ state while there is only one calculated 0^+ state in this region. The next calculated 0^+ state is at 7.46 MeV.

(31) A=34, T=2 (Figure 22):

The calculated binding energy of the 1^+ ground state agrees very well with experiment. A very close first excited state is predicted to have $J^\pi=2^+$.

(32) A=35, T=1/2 (Figure 23):

The calculated spectrum is somewhat expanded compared with experiment; the agreement is otherwise good.

(33) A=35, T=3/2 (Figure 23):

Only the two lowest observed states have uniquely determined spin and positive parity, so that more experimental data are needed for comparison with the calculated spectrum.

(34) A=35, T=5/2 (Figure 23):

The calculated binding energy for the $J^\pi=1/2^+$ ground state is too large by 0.40 MeV. A $J^\pi=3/2^+$ state is predicted for the first excited state.

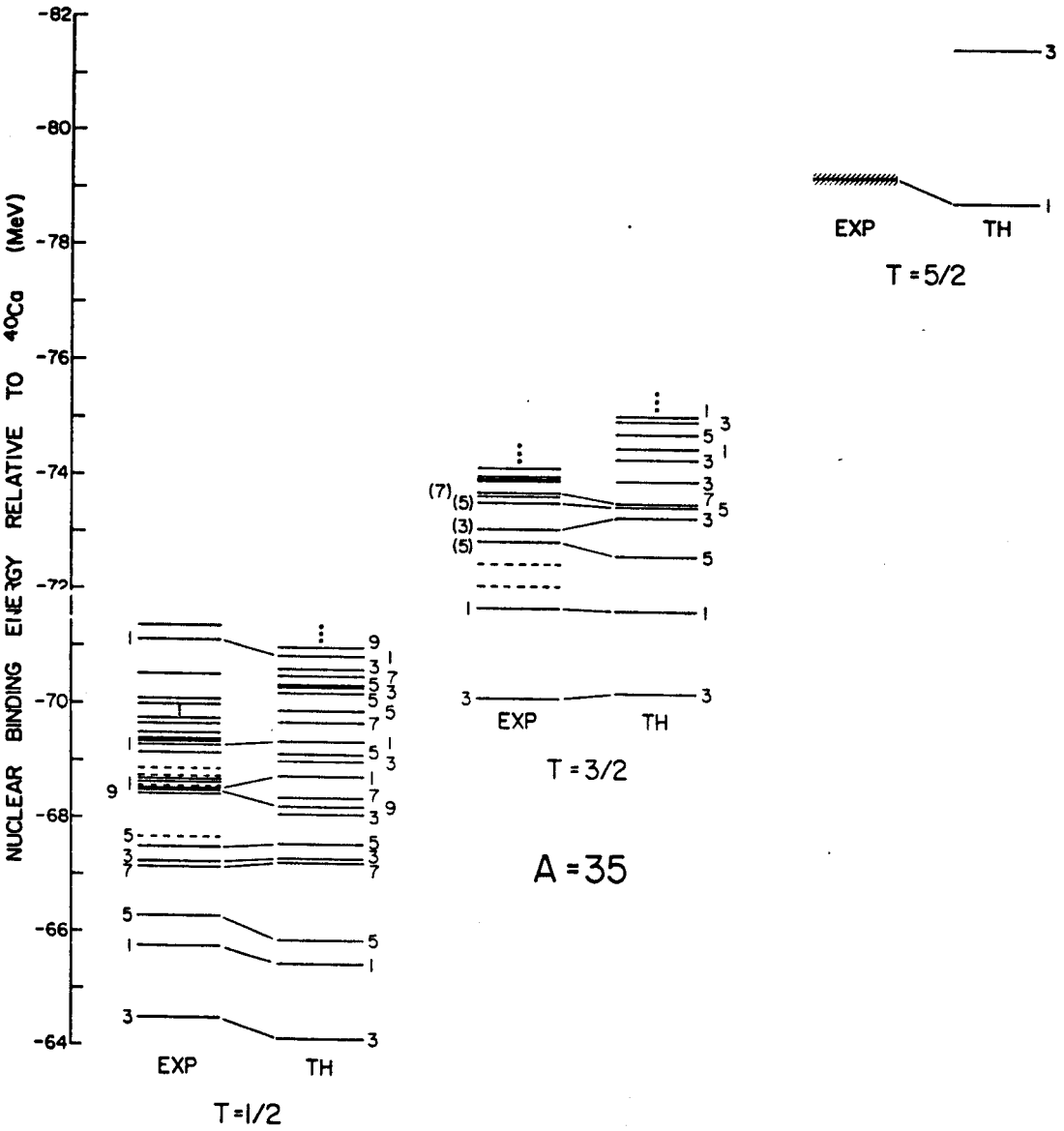

Figure 23. Energy spectra of A=35 (T=1/2, 3/2, 5/2).

(35) A=36, T=0 (Figure 24):

More experimental data above 4.5 MeV are needed for better comparison of calculated and observed spectra. An observed $J^{\pi}=(1,2)^{+}$ state (not labeled in Figure 24) at 4.95 MeV in ^{36}Ar is missing in the calculated spectrum.

(36) A=36, T=1 (Figure 24):

The agreement between calculated and observed spectra is good. The observed 1.60 and 2.86 MeV states in ^{36}Cl have been reassigned to have $J^{\pi}=1^{+}$ and 3^{+}, respectively, following Rice et al.[79]

(37) A=36, T=2 (Figure 24):

The observed first excited 0^{+} state is predicted to be 1.14 MeV underbound, and the observed second 2^{+} state is also predicted to be 1.63 MeV underbound. These two experimental states may be dominated by intruder state configurations.

(38) A=37, T=1/2 (Figure 25):

The five lowest positive parity states are well-reproduced. The results suggests the observed 3.60 MeV state in ^{37}Ar to have $J^{\pi}=3/2^{+}$, consistent with the recent observation by Gadeken et al.[75] of $J^{\pi}=3/2^{+}$ or $5/2^{-}$.

(39) A=37, T=3/2 (Figure 25):

Above 4 MeV, there are many more positive parity states observed than are calculated. These are presumed to be mostly dominated by intruder state configurations.

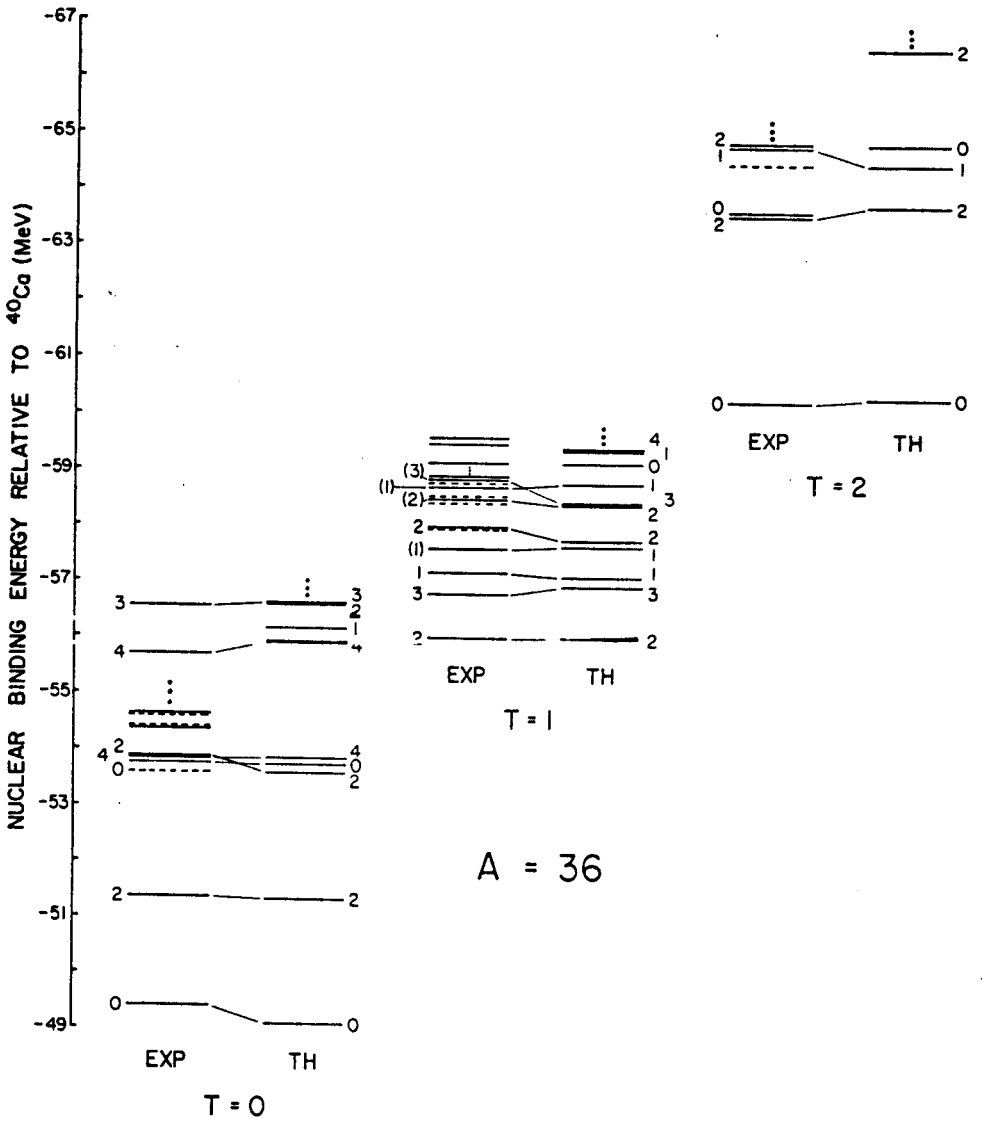

Figure 24. Energy spectra of A=36 (T=0,1,2).

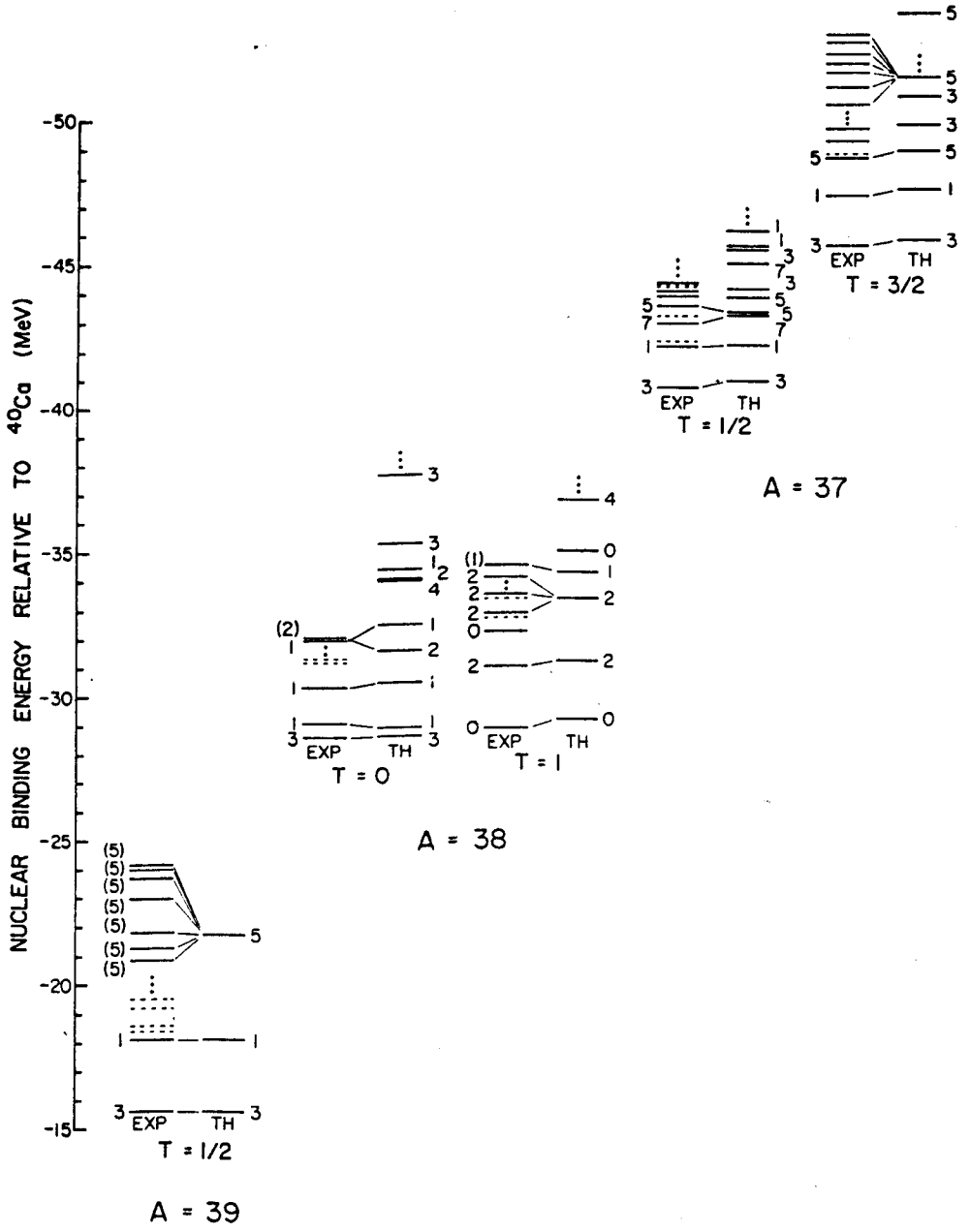

Figure 25. Energy spectra of A=37 (T=1/2, 3/2), A=38 (T=0,1), and A=39 (T=1/2).

(40) A=38, T=0 (Figure 25):

Again intruder states are important in the spectrum. The lowest three states of $J^{\pi}=3^{+}$, 1^{+} and 1^{+} are well reproduced. The first 2^{+} is overbound by approximately 0.5 MeV, while the third 1^{+} is underbound by approximately 0.5 MeV.

(41) A=38, T=1 (Figure 25):

The first excited 0^{+} state is predicted at 5.83 MeV, while there are two excited 0^{+} states observed at 3.38 and 4.71 MeV. There are also more excited 2^{+} states observed between 3 and 6 MeV than are calculated. In analogy to the case of ^{18}O, these states are very probably mixtures of $(sd)^{-2}$ configurations and intruder states.

(42) A=39, T=1/2 (Figure 25):

The $d_{5/2}$-hole strength is observed to be fragmented. The $d_{5/2}$-hole single particle energy was treated as a free parameter in the last iteration of the least-squares fit. The energy was found to be 21.75 MeV.

In summary, the observed spectra are well-reproduced by the "Particle" and "Hole" Hamiltonians in their respective domains, except for some levels which are missing in a few nuclei. These are mostly in "few particle" or "few hole" systems, and can reasonably be assumed to be intruder states. In the extensive studies made by the Glasgow Group,[5-8] the main defect of the KUO14 realistic interaction was the shifting of whole bands of levels relative to each other. The KUO14 interaction predicts

qualitatively correct interband spacings, but the relative positions of the band heads can be wrong by several MeV. The PW interaction gives a good description of $A \leq 22$ nuclei, as is to be hoped since it was derived by a least-squares fit to these nuclei. However, the improvement over the KUO14 interaction diminishes as A increases, as the tendency to shift bands again shows up beyond A=22. The "Particle" Hamiltonian gives very similar spectra for $A \leq 22$ nuclei as the PW interaction. The A=23, and 24 spectra are better described by the "Particle" Hamiltonian than the PW interaction, as these were included in the present least-squares fit and not in the PW derivation. The band shifting is corrected even in A=25 and 26. From the calculated spectra, it appears that the "Particle" Hamiltonian gives a better description of lower sd-shell nuclei than the PW interaction, and definitely better than the KUO14 interaction.

It is hard to compare the "Hole" Hamiltonian with the K12.5P interaction as only the A=35-38 nuclei were studied previously.[2] The KUO14 interaction was found to give a very poor description of the upper sd-shell nuclei, in many cases even predicting the wrong ground state spin. The PW interaction is not expected to show much improvement over the KUO14 interaction in the upper sd-shell nuclei, as the matrix elements involving the $d_{3/2}$-orbit which were least determined in the fit become more dominant. Comparison of A=32 and 33 spectra did bear out this fact, though

the low-lying levels are still predicted in roughly the correct order.[5] The same spectra are very well described by the "Hole" Hamiltonian.

I.5. Summary and Conclusion

Following the success of the PW interaction,[3] an attempt was made to derive a single empirical Hamiltonian for the entire sd-shell region nuclei. The matrix elements were treated as parameters and least-squares fitted to measured binding energies of nuclei in the A=18-24 and A=32-38 regions. It was found that a single set of mass-independent (1+2)-body Hamiltonian was inadequate for the entire sd-shell, presumably because of differing renormalizations at either end of the sd-shell. The data set was divided into two parts and a Hamiltonian was obtained in similar fashion from each part separately.

Starting from the KUO14 realistic interaction, the "Particle" Hamiltonian was obtained by an iterative least-squares fit to measured binding energies in the A=18-24 region. The "Hole" Hamiltonian was fitted to measured binding energies in the A=32-48 region instead, starting from the K12.5P interaction. The least-squares fit was reformulated in terms of orthogonal linear combinations of the matrix elements as parameters. With from 134 to 197 entries in the data sets, it was found that only a few orthogonal parameters were very well determined and that

less than half of the orthogonal parameters were at all well determined by the data.

The dominant result of the empirical renormalization obtained for the Kuo matrix elements is the reduction in attractiveness of the $d_{5/2}$-$s_{1/2}$, $d_{5/2}$-$d_{3/2}$, and $s_{1/2}$-$d_{3/2}$ diagonal two-body matrix elements. Efforts should now be made to understand why the realistic interactions are too attractive for these "unlike orbit" cases.

The ground state binding energies and spins have been calculated using both the "Particle" and "Hole" Hamiltonians. In both cases, the agreement in the region of nuclei from which the data set were taken is very good, with the deviations between calculated and observed binding energies being less than or equal to 0.5 MeV. In both Hamiltonians, the energy deviations increase with increasing number of active particles or active holes, with a further isospin dependence superimposed. Low-lying spectra for a number of nuclei have also been calculated with either the "Particle" or the "Hole" Hamiltonian. The agreement with experiment is good, except for some missing levels in a few active particles or active holes systems which are presumably intruder states. The "Particle" Hamiltonian gives descriptions of $A \leq 22$ nuclei rather similar to the PW interaction. Beyond A=22, the "Particle" Hamiltonian is a better interaction than the PW interaction in that band shifting, the main defect of previous interactions where whole excited bands are predicted overbound

with respect to the ground state, is further corrected. The "Particle" and "Hole" Hamiltonians appear to give a good description of nuclei beyond the region where the Hamiltonians were fitted, overlapping in the middle of the sd-shell. Whether the two sets of Hamiltonians will complement each other to give a good description of all nuclei in the sd-shell region remains to be seen. Further investigations of other nuclear properties, such as spectroscopic factors, electromagnetic transitions and moments, β-decays and so on, specifically for nuclei in the middle of the sd-shell is needed.

II. MAGNETIC DIPOLE MOMENTS OF sd-SHELL NUCLEI

II. 1. Introduction

The deviations of observed magnetic moments of odd-A nuclei from the single-particle Schmidt values have been the subject of many theoretical studies. Modification of the independent-single-particle shell-model wave functions or configuration mixing[89-91] have been thought to explain the majority portion of the deviations, while corrections of the magnetic dipole operator for such effects as mesonic currents[92-94] have generally been considered small, except possibly in high spin states.[94] However, previous studies have mainly been on selected odd-A nuclei with simple configurations, such as one particle or one hole outside a j-j or l-s closed shell. A more quantitative and comprehensive survey, e.g., of all measured dipole moments of sd-shell nuclei, is definitely desirable. The calculations described in section I make such a survey feasible.

The magnetic dipole moment calculations discussed here are carried out with the untruncated $d_{5/2}$-$s_{1/2}$-$d_{3/2}$ shell-model wave functions obtained in the work just

described. The magnetic dipole operator, a one-body operator, does not change the principal nor the orbital quantum numbers of the particle it acts on. A "good" wave function defined in one major shell, e.g., the full 0s-1d model space, should at least be able to account fully to first order for configuration mixing corrections to the observed deviations of measured dipole moments from the Schmidt values. The dipole moments thus provide a sensitive test of the wave functions or the interaction used to generate the wave functions. Conversely, a "good" set of wave functions can be used to find effective dipole operators which may be necessary for other types of corrections which cannot be included in the wave functions.

Magnetic moments of ground and excited states of sd-shell nuclei (except for ^{27,28}Al, ^{30}Si) were first calculated using the wave functions with the "bare"-(or "free"-)nucleon gyromagnetic ratios for the dipole operator. Agreement with experiment was found to be good for A=17-26, but poor for A=28-39. With the same set of wave functions, the dipole operator matrix elements were then treated as parameters and determined from a least-squares fit to available precise values of measured dipole moments. When the magnetic moments were recalculated with this revised operator, the good agreement with experiment for A=17-26 was not changed, while that for A=28-39 was much improved. Subsequently, effective g-factors and

intrinsic moments were derived from the operator matrix elements determined from the fit.

II.2. Details of Calculation

In isospin formalism, the magnetic moment of a state Ψ^{JT} is given by:

$$\mu = \sum_{I=0}^{1} \frac{\langle J\ J\ 1\ 0 | J\ J \rangle \langle T\ T_z\ I\ 0 | T\ T_z \rangle}{\sqrt{2J+1}\quad\sqrt{2T+1}} \langle \Psi^{JT} ||| \vec{\mu}_I ||| \Psi^{JT} \rangle \tag{40}$$

where $\langle \Psi^{JT} ||| \vec{\mu}_I ||| \Psi^{JT} \rangle$ is a double-reduced matrix element with respect to space and isospace. The subscript I equals 0 or 1 for the isoscalar and isovector components respectively of the dipole operator. The operators are defined as follow:

$$\vec{\mu}_0 = \sum_{i=1}^{A} \{ (\frac{g_p^{\ell} + g_n^{\ell}}{2}) \vec{\ell} + (\mu_p + \mu_n) \vec{s} \} \tag{41}$$

$$\vec{\mu}_1 = \sum_{i=1}^{A} \{ (\frac{g_p^{\ell} - g_n^{\ell}}{2}) \vec{\ell} + (\mu_p - \mu_n) \vec{s} \}\ T_z(i) \tag{42}$$

where T_z = +1 for proton and -1 for neutron. The g_p^{ℓ}, μ_p and g_n^{ℓ}, μ_n are the orbital g-factors and intrinsic moments of the proton and neutron respectively. They are, for a bare- or free-nucleon,

$$g_p^{\ell} = 1.0 \text{ n.m.} \quad , \quad \mu_p = 2.79 \text{ n.m.}$$

$$g_n^{\ell} = 0.0 \text{ n.m.} \qquad \mu_n = -1.91 \text{ n.m.}$$

The double-reduced matrix element $\langle \Psi^{JT} |||\vec{\mu}_I|||\Psi^{JT}\rangle$ can be further expressed in terms of single-particle reduced matrix elements and transition density matrix elements

$$\langle \Psi^{JT} |||\vec{\mu}_I|||\Psi^{JT}\rangle = \sum_{ij} \langle i |||\vec{\mu}_I|||j\rangle \rho^{JT}_{ijI} \quad , \tag{43}$$

where i,j denotes single-particle states, and the transition density matrix elements ρ^{JT}_{ijI} are defined as:

$$\rho^{JT}_{ijI} = \frac{\langle \Psi^{JT} |||(a^+_i \times a_j)_{1I}|||\Psi^{JT}\rangle}{\sqrt{3(2I+1)}} \tag{44}$$

The $(a^+_i \times a_j)_{1I}$ is just the single-particle creation (a^+_i) and annihilation (a_j) operators coupled to rank 1 and isospin I. Combining equations (40) and (43), the dipole moment μ can be expressed as a linear expression of the single-particle reduced matrix elements

$$\mu = \sum_{i,j,I} \langle i |||\vec{\mu}_I|||j\rangle \quad C^{JT}_{ijI} \tag{45}$$

with coefficients:

$$C^{JT}_{ijI} = \frac{\langle J\ J\ 1\ 0 | J\ J\rangle \langle T\ T_z\ I\ 0\ |\ T\ T_z\rangle}{\sqrt{(2J+1)(2T+1)}} \rho^{JT}_{ijI} \ . \tag{46}$$

The transition density matrix elements ρ^{JT}_{ijI}, and hence the coefficients C^{JT}_{ijI}, contain all the necessary information from the mixed-configuration wave functions.

For the present calculation, the "Particle" Hamiltonian was used to generate the wave functions for

A=17-28, while the "Hole" Hamiltonian was used to generate the wave functions for A=28-39. As mentioned earlier, the exact overlap of the two Hamiltonians in the middle of the sd-shell remains to be seen from future calculations. However, A=28 where the sd-shell is half-filled is a nautral boundary. And as will be seen, the two sets of Hamiltonians are very similar with respect to reproducing the dipole moment of the first 2^+ state of ^{28}Si. The transition density matrix elements were calculated from the set of wave functions using equation (44), and the dipole moments using equation (45) and (46).

With the linear expression (equation 45) and the coefficients C_{ijI}^{JT} fixed from the generated wave functions, the single-particle reduced matrix elements can be treated as parameters and determined by a least-squares fit to measured dipole moments. This was done by simply minimizing the quantity:

$$(\delta\mu)^2 = (\mu_{theory} - \mu_{expt.})^2 \qquad (47)$$

with respect to the parameters. The measured dipole moments were not weighted by any uncertainties as only the more precise measured moments were included in the fit. In the full 0s-1d model space, l- and j- selection rules limit the number of independent single-particle reduced matrix elements to only eight. The eight parameters were fitted to thirty-seven measured dipole moments, which are listed in Table 9, except where otherwise noted. Where the

TABLE 9.--Magnetic moments of some ground and excited states of sd-shell nuclei.

Nucleus	Ex.E. (keV)	τ^a(s)	J^π	T	$\mu_{expt.}{}^b$ (n.m.)	μ_{calc}(n.m.) bare	fitted
^{17}O	0	stable	$5/2^+$	1/2	-1.89[c]	-1.91	-1.84
^{17}F	0	6.6×10^{1}	$5/2^+$	1/2	±4.72	+4.79	+4.78
^{18}O	1982	3.8×10^{-12}	2^+	1	-0.59±0.03[d,e]	-0.85	-0.82
^{18}Ne	1887	4.9×10^{-13}	2^+	1		3.02	+3.10
^{18}O	3553	$>3\times10^{-12}$	4^+	1	±2.48±0.40[d,f]	-1.99	-2.00
^{18}Ne	3376	4.4×10^{-12}	4^+	1		+6.38	+6.60
^{18}F	0	6.6×10^{3}	1^+	0		+0.85	+0.73
^{18}F	937	6.8×10^{-11}	3^+	0		+1.87	+1.84
^{18}F	1122	2.2×10^{-7}	5^+	0	+2.85±0.03	+2.88	+2.94
^{19}O	0	2.7×10^{1}	$5/2^+$	3/2		-1.50	-1.49
^{19}O	96	2.0×10^{-9}	$3/2^+$	3/2	-0.69±0.09[d,g]	-0.91	-0.84
^{19}F	0	stable	$1/2^+$	1/2	+2.63	+2.90	+2.77
^{19}Ne	0	1.7×10^{1}	$1/2^+$	1/2	-1.89	-2.04	-2.03
^{19}F	197	1.3×10^{-7}	$5/2^+$	1/2	+3.60±0.01	+3.65	+3.53
^{19}Ne	238	2.6×10^{-8}	$5/2^+$	1/2	-0.74±0.01	-0.75	-0.58
^{20}O	1672	1.3×10^{-11}	2^+	2	±0.78±0.08[h]	-0.67	-0.72
^{20}F	0	1.1×10^{1}	2^+	1	+2.09	+2.06	+1.99
^{20}Na	0	4.1×10^{-1}	2^+	1	±0.37	+0.48	+0.47
^{20}Ne	1634	1.2×10^{-12}	2^+	0	+1.08±0.08[i]	+1.02	+1.10
^{20}Ne	4247	9.3×10^{-14}	4^+	0		+2.04	+2.21
^{21}F	0	4.3×10^{0}	$5/2^+$	3/2		+3.84	+3.79
^{21}Ne	0	stable	$3/2^+$	1/2	-0.66	-0.77	-0.66
^{21}Na	0	2.3×10^{1}	$3/2^+$	1/2	+2.39	+2.50	+2.41
^{21}Ne	350	2.0×10^{-11}	$5/2^+$	1/2		-0.61	-0.52
^{21}Na	332	1.4×10^{-11}	$5/2^+$	1/2		+3.38	+3.40
^{22}F	0	4.2×10^{0}	4^+	2		+2.59	+2.50
^{22}Ne	1275	4.9×10^{-12}	2^+	1	+0.65±0.03[j]	+0.76	+0.78
^{22}Ne	3356	3.6×10^{-13}	4^+	1		+1.91	+2.03
^{22}Na	0	2.6 years	3^+	0	+1.75	+1.78	+1.78
^{22}Na	583	3.5×10^{-7}	1^+	0	+0.54±0.01	+0.53	+0.56
^{23}Ne	0	3.8×10^{1}	$5/2^+$	3/2	-1.08±0.01	-1.07	-1.06
^{23}Na	0	stable	$3/2^+$	1/2	+2.22	+2.10	+2.04
^{24}Na	0	5.4×10^{4}	4^+	1	+1.69	+1.59	+1.57

TABLE 9.--Continued.

Nucleus	Ex.E. (keV)	τ^a(s)	J^π	T	$\mu_{expt.}{}^b$ (n.m.)	μ_{calc}(n.m.) bare	fitted
^{24}Na	472	2.0×10^{-2}	1^+	1		-1.77	-1.68
^{24}Mg	1369	1.7×10^{-11}	2^+	0	$+1.02\pm0.04^k$	+1.03	+1.11
^{24}Mg	4238	1.0×10^{-13}	2^+	0		+1.03	+1.10
^{24}Mg	4123	5.5×10^{-14}	4^+	0		+2.06	+2.22
^{25}Na	0	6.0×10^{1}	$5/2^+$	3/2	$+3.67\pm0.03^\ell$	+3.39	+3.51
^{25}Mg	0	stable	$5/2^+$	1/2	-0.85	-0.85	-0.79
^{26}Mg	1809	7.2×10^{-13}	2^+	1	$+1.64\pm0.32^{d,m}$	+1.61	+1.75
^{26}Al	0	7.2×10^{5} years	5^+	0		+2.82	+2.91
^{26}Al	417	1.8×10^{-9}	3^+	0		+1.77	+1.79
^{28}Si	1779	6.8×10^{-13}	2^+	0	$+1.12\pm0.18^{d,m}$	$+1.03^n$	$+1.10^n$
^{28}Si	1779	6.8×10^{-13}	2^+	0	$+1.12\pm0.18^{d,m}$	$+1.03^o$	$+1.10^o$
^{29}Si	0	stable	$1/2^+$	1/2	-0.56	-0.36	-0.55
^{29}P	0	4.2×10^{0}	$1/2^+$	1/2	±1.23	+0.97	+1.18
^{30}P	0	1.5×10^{2}	1^+	0		+0.57	+0.60
^{31}P	0	stable	$1/2^+$	1/2	+1.13	+0.94	+1.12
^{32}P	0	14 days	1^+	1	-0.25	-0.24	-0.27
^{32}S	2230	2.2×10^{-13}	2^+	0		+0.99	+1.07
^{33}S	0	stable	$3/2^+$	1/2	+0.64	+0.50	+0.55
^{33}Cl	0	2.5×10^{0}	$3/2^+$	1/2		+0.86	+0.95
^{34}S	2127	4.1×10^{-13}	2^+	1		+0.85	+1.01
^{34}Cl	146	1.9×10^{3}	3^+	0		+1.33	+1.48
^{35}S	0	87 days	$3/2^+$	3/2	$\pm1.00\pm0.04$	+0.90	+0.90
^{35}Cl	0	stable	$3/2^+$	1/2	+0.82	+0.74	+0.87
^{35}Ar	0	1.8×10^{0}	$3/2^+$	1/2	+0.63	+0.63	+0.64
^{36}Cl	0	3×10^{5} years	2^+	1	+1.29	+1.34	+1.44
^{36}K	0	3.4×10^{-1}	2^+	1	+0.55	+0.35	+0.49
^{36}Ar	1970	4.1×10^{-13}	2^+	0		+0.98	+1.06
^{37}Cl	0	stable	$3/2^+$	3/2	+0.68	+0.32	+0.57
^{37}Ar	0	35 days	$3/2^+$	1/2	$+0.95\pm0.20^d$	+1.39	+1.34
^{37}K	0	1.2×10^{0}	$3/2^+$	1/2	+0.20	-0.13	+0.11
^{38}Ar	2168	5.3×10^{-13}	2^+	1		+0.38	+0.72

TABLE 9.--Continued.

Nucleus	Ex.E. (keV)	τ^a (s)	J^π	T	$\mu_{expt.}{}^b$ (n.m.)	μ_{calc} (n.m.) bare	fitted
^{38}K	0	4.6×10^{2}	3^+	0	+1.37	+1.23	+1.43
^{38}K	461	7.4×10^{-10}	1^+	0		+0.43	+0.50
^{39}K	0	stable	$3/2^+$	1/2	+0.39	+0.13	+0.41
^{39}Ca	0	8.8×10^{-1}	$3/2^+$	1/2	$\pm1.02^p$	+1.15	+1.04

[a] τ is $\tau_{1/2}$ for ground states and τ_m for excited states, except for ^{24}Na (1^+) and ^{34}Cl (3^+) excited states where $\tau_{1/2}$ are specified instead.

[b] Unless otherwise noted, the measured magnetic moments are taken from the compilation in Reference 27.

[c] Reference 29.

[d] Not included in the least-squares fit.

[e] Reference 96, 97.

[f] Reference 98.

[g] Reference 99.

[h] Reference 100.

[i] Reference 101.

[j] Reference 102.

[k] Reference 101, 103.

[l] Reference 104.

[m] Reference 105.

[n] "Particle" Hamiltonian.

[o] "Hole" Hamiltonian.

[p] Reference 106.

sign of the measured dipole moment is not known, it is taken to have the same sign as the bare-nucleon calculated moment.

II.3. Results

In Table 9 are listed the measured dipole moments and calculated dipole moments, both with the bare-nucleon value and the fitted single-particle reduced matrix elements, of some ground and excited states of sd-shell nuclei. Also listed are the excitation energies, life-times, spins, parities, and isospins of each state. The measured and calculated dipole moments for A=17-25 and A=29-39 are also plotted in Figure 26 and Figure 27 respectively. It is clear that good agreement is obtained with either the bare-nucleon or the fitted operators for A=17-25. For A=29-39, agreement is much better with the fitted operator than the bare-nucleon operator. The RMS deviation between measured and calculated dipole moments remains almost unchanged for the 22 dipole moments for A=17-25 included in the least-squares fit, it is 0.11 n.m. and 0.10 n.m. for the bare-nucleon and fitted operators, respectively. On the other hand, the RMS deviation shows a big improvement for the 15 dipole moments for A=29-39 included in the fit with the fitted operators, it is 0.07 n.m. compared to 0.20 n.m. with the bare-nucleon operators. Overall, the RMS deviation changes from

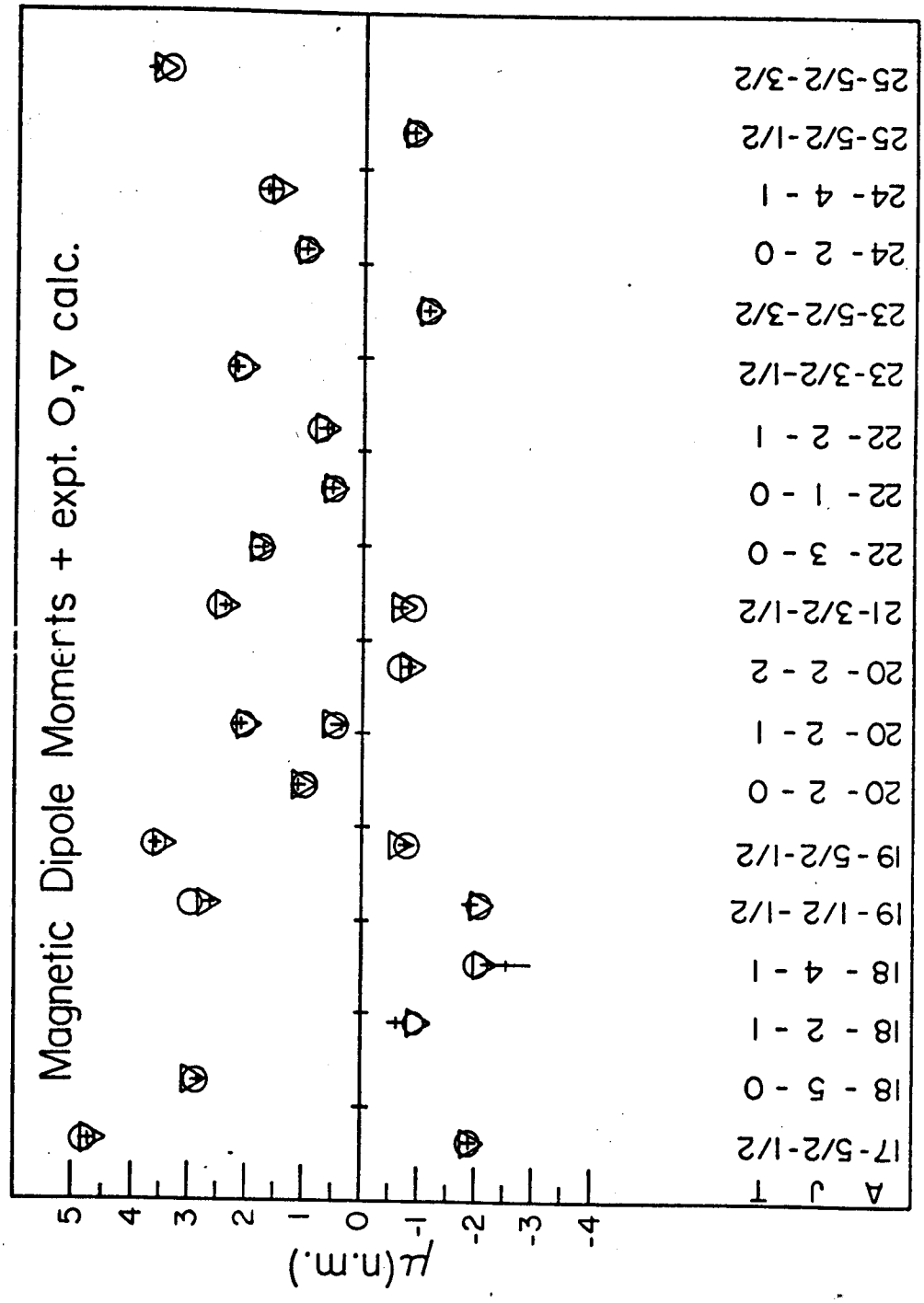

Figure 26. Magnetic dipole moments of some ground and excited states for A=17-25.

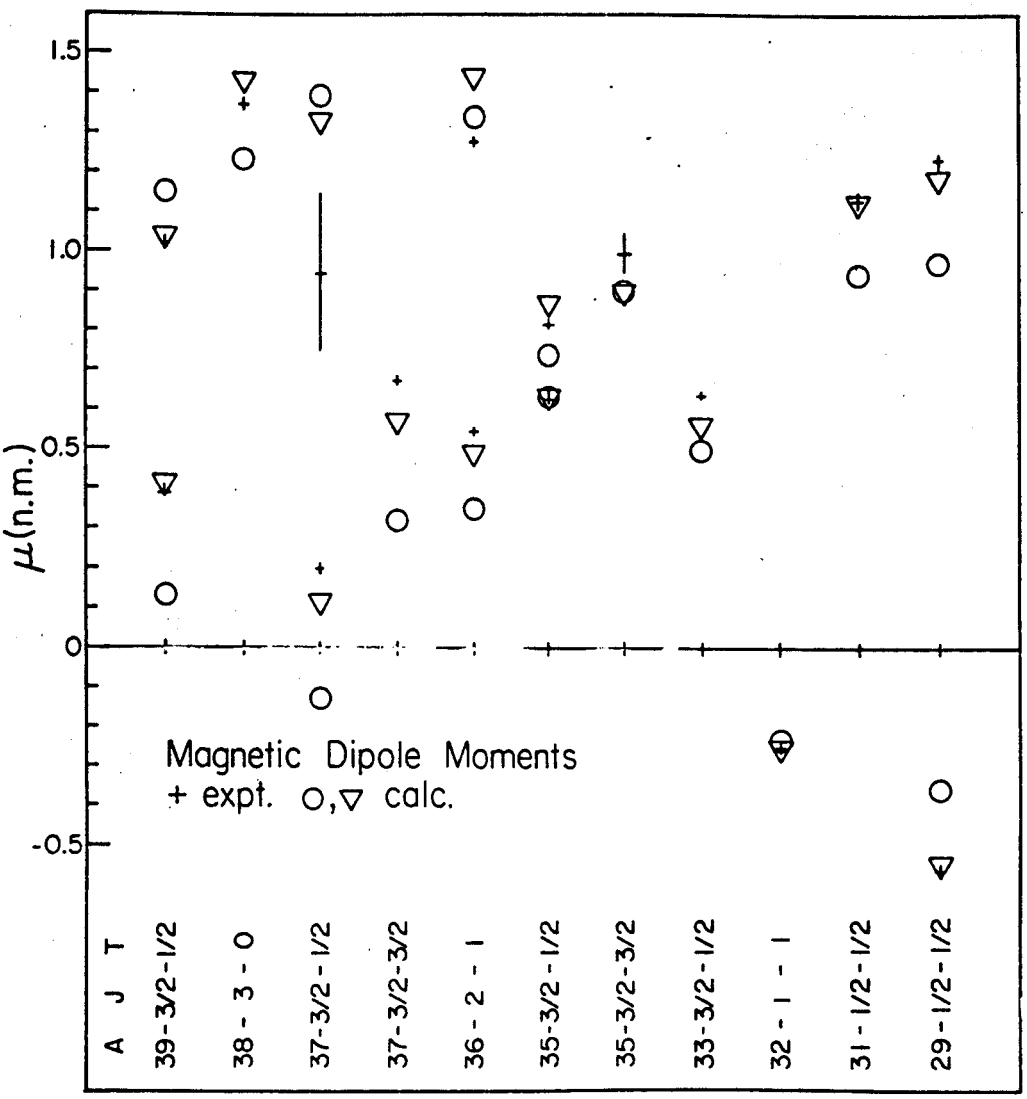

Figure 27. Magnetic dipole moments for some ground and excited states for A=29-39.

0.15 n.m. to 0.09 n.m. for all 37 measured moments included in the least-squares fit.

The fitted single-particle reduced matrix elements are listed in Table 10, together with the bare-nucleon single-particle reduced matrix elements for comparison. The uncertainties were estimated by assuming a 0.09 n.m. (obtained RMS deviation) uncertainty or error for each calculated dipole moment. The $d_{5/2}$-$d_{5/2}$ isoscalar and isovector matrix elements only change very little, presumably due to the already good agreement with the bare-nucleon operators for the lower half of the sd-shell, where the $d_{5/2}$-$d_{5/2}$ matrix elements are more important. In general, except for the $s_{1/2}$-$s_{1/2}$ isoscalar and $d_{5/2}$-$d_{5/2}$ isovector matrix elements, the single-particle reduced matrix elements get more positive.

Obviously, the next question is whether the set of fitted single-particle reduced matrix elements can tell us anything about effective g-factors and intrinsic moments. The isoscalar and isovector single-particle reduced matrix elements are defined explicitly in the following:

$$\langle i|||\vec{\mu}_0|||j\rangle = \left(\frac{g_p^{\ell} + g_n^{\ell}}{2}\right) \langle i|||\vec{\ell}|||j\rangle + (\mu_p + \mu_n) \langle i|||\vec{s}|||j\rangle \qquad (48)$$

TABLE 10.--Comparison between bare-nucleon and fitted single-particle reduced μ matrix elements (n.m.).

$\langle \ell j \vert\vert\vert \vec{\mu}_I \vert\vert\vert \ell' j' \rangle$[a]	Bare	Fitted[b]
$\langle d_{5/2} \vert\vert\vert \vec{\mu}_0 \vert\vert\vert d_{5/2} \rangle$	2.88	2.94±0.06
$\langle d_{5/2} \vert\vert\vert \vec{\mu}_0 \vert\vert\vert d_{3/2} \rangle$	- 0.41	-0.19±0.15
$\langle s_{1/2} \vert\vert\vert \vec{\mu}_0 \vert\vert\vert s_{1/2} \rangle$	0.74	0.69±0.14
$\langle d_{3/2} \vert\vert\vert \vec{\mu}_0 \vert\vert\vert d_{3/2} \rangle$	1.13	1.29±0.04
$\langle d_{5/2} \vert\vert\vert \vec{\mu}_1 \vert\vert\vert d_{5/2} \rangle$	11.62	11.49±0.18
$\langle d_{5/2} \vert\vert\vert \vec{\mu}_1 \vert\vert\vert d_{3/2} \rangle$	- 7.79	-6.52±0.28
$\langle s_{1/2} \vert\vert\vert \vec{\mu}_1 \vert\vert\vert s_{1/2} \rangle$	6.89	7.25±0.25
$\langle d_{3/2} \vert\vert\vert \vec{\mu}_1 \vert\vert\vert d_{3/2} \rangle$	- 1.58	-0.97±0.13

[a] I equals 0 or 1 for isoscalar and isovector components, respectively.

[b] See text for description on uncertainties.

$$\langle i|||\vec{\mu}_1|||j\rangle = \left(\frac{g_p^{\ell} - g_n^{\ell}}{2}\right) \langle i|||\vec{\ell}T_z|||j\rangle$$

$$+ (\mu_p - \mu_n)\langle i|||\vec{s}T_z|||j\rangle \qquad (49)$$

where the reduced matrix elements of $\vec{\ell}$, $\vec{s}$, $\vec{\ell}T_z$, $\vec{s}T_z$ are easily evaluated with angular-momentum algebra. The effective g-factors and intrinsic moments can be treated as unknowns and determined by two separate least-squares fits to the fitted isoscalar and isovector single-particle reduced matrix elements. However, with only two parameters in each case, a graphical representation of the least-squares fits, which is feasible, is more helpful and gives a clearer picture.

In Figure 28(a) and Figure 28(b) are plotted the straight lines corresponding to the eight fitted isoscalar and isovector single-particle reduced matrix elements respectively. The dash lines indicate the uncertainties as listed in Table 10. The cross in each figure corresponds to the bare-nucleon value g-factors and intrinsic moments.

It is seen from Figure 28(a) that the area bounded by the intersections of the four lines is small. In Figure 28(b), the corresponding area is larger with the isovector $s_{1/2}$-$s_{1/2}$ clearly outside the boundary. If the least-squares fits were simply done using Equations (48) and (49) fitted to the four isoscalar and four isovector fitted single-particle reduced matrix elements; the

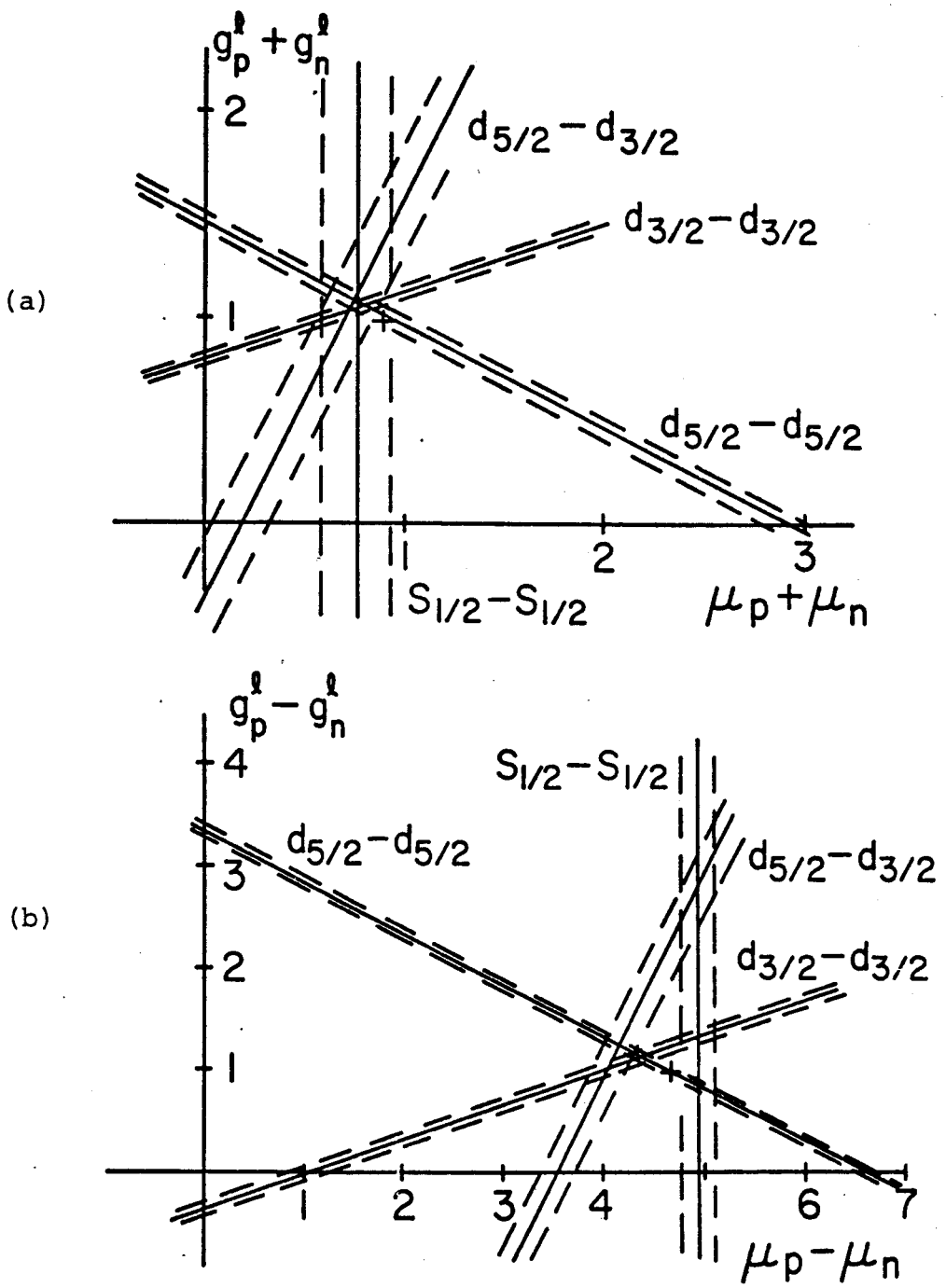

Figure 28. Effective g-factors and intrinsic moments from the fitted single-particle reduced μ matrix elements (n.m.).

isoscalar part would give a good fit, and the isovector part a bad one.

The slopes of the straight lines are fixed by the reduced matrix elements of $\vec{\ell}$ and $\vec{s}$, and $\vec{\ell}T_z$ and $\vec{s}T_z$. The fitted single-particle reduced matrix elements merely translate the lines. In both Figure 28(a) and Figure 28(b), the directions of change of the g-factors and intrinsic moments closely parallel the $d_{5/2}$-$d_{5/2}$ lines. Thus the changes for the $d_{5/2}$-$d_{5/2}$ single particle reduced matrix elements are small compared to the others. It should be noted that in Equations (48) and (49), we have neglected the radial part, i.e., assumed the overlap of radial wave functions in each case to be one. For the $d_{5/2}$-$d_{3/2}$, an overlap less than one would move both lines for the isoscalar and isovector cases in the direction of making the area of intersections smaller. The translation should be larger for the isovector than for the isoscalar. The resulting fits should be better than are shown in Figure 28(a) and 28(b).

The increase in the isovectors $s_{1/2}$ intrinsic moment may be a little surprising. However, it is not inconsistent with what is found for the magnetic moments of ^{3}H and ^{3}He. The Schmidt value for the isovector magnetic moment, i.e., $\mu(^3H)/2-\mu(^3He)/2$, is too small compared to the experimental value. The effective intrinsic moments for a $s_{1/2}$ particle (with $\ell=0$) can be obtained directly from the single-particle reduced matrix

elements listed in Table 10 and equations (48) and (49). The results are:

$$\mu_p^{eff}(s_{1/2}) + \mu_n^{eff}(s_{1/2}) = 0.76 \pm 0.17 \text{ n.m.}$$

$$\mu_p^{eff}(s_{1/2}) - \mu_n^{eff}(s_{1/2}) = 4.95 \pm 0.17 \text{ n.m.}$$

or

$$\mu_p^{eff}(s_{1/2}) = 2.85 \pm 0.17 \text{ n.m.}$$

$$\mu_n^{eff}(s_{1/2}) = -2.09 \pm 0.17 \text{ n.m.}$$

The effective g-factors and intrinsic moments for $d_{5/2}$ and $d_{3/2}$ orbits can be read off Figure 28(a) and Figure 28(b). A more quantitative analysis, i.e., least-squares fits to the four isoscalar and three isovector (excluding $s_{1/2}$-$s_{1/2}$) fitted single-particle reduced matrix elements listed in Table 10 gives:

$$g_p^{\ell,eff} + g_n^{\ell,eff} = 1.07 \text{ n.m.}$$

$$g_p^{\ell,eff} - g_n^{\ell,eff} = 1.12 \text{ n.m.}$$

$$\mu_p^{eff} + \mu_n^{eff} = 0.79 \text{ n.m.}$$

$$\mu_p^{eff} - \mu_n^{eff} = 4.36 \pm 0.01 \text{ n.m.}$$

or

$$g_p^{\ell,eff} = 1.09 \text{ n.m.}$$

$$g_n^{\ell,\text{eff}} = -0.02 \text{ n.m.}$$

$$\mu_p^{\text{eff}} = 2.58 \pm 0.01 \text{ n.m.}$$

$$\mu_n^{\text{eff}} = -1.79 \pm 0.01 \text{ n.m.}$$

The present calculation with the full 0s-1d shell-model space does not include major shell crossing second and higher order configuration mixing corrections for the dipole moments via the mixed-configuration wave functions. The effective g-factors and intrinsic moments are thus due to the combined effects of these higher-order configuration-mixing corrections, mesonic exchange currents and other possible corrections. Mavromatis and Zamick[91] have previously calculated second order configuration-mixing correction for the dipole moments of mass 17 and 39 with up to $2\hbar\omega$ excitations from the ground state. Their results, using the bare-nucleon g-factors and intrinsic moments, show the corrections to be non-negligible. Further studies are needed to untangle the different effects in the effective g-factors and intrinsic moments.

It may be mentioned in passing that the quenching of the intrinsic moments is in agreement with the results of Miyawaza[92] and Drell and Walecka[93] for the effects of mesonic exchange currents. The effective orbital g-factors are close to the empirical estimates of Nagamiya and

Yamazaki[95] over the whole mass region, i.e., $g_p^{\ell,eff}$ = 1.09 ± 0.03 n.m. and $g_n^{\ell,eff}$ = -0.06 ± 0.04 n.m.

II.4. Summary

Magnetic dipole moments in the range A=17-39 have been investigated using mixed-configuration shell-model wave functions generated from empirical Hamiltonians in the full 0s-1d model space. Dipole operators were treated as parameters and determined from a least-squares fit to precise measured moments. Good agreement was found for the whole range with the fitted operators, while the bare-nucleon operators could only give good agreement for A=17-25. Effective g-factors and intrinsic moments were derived from the fitted operators. The intrinsic moments are quenched compared to the bare-nucleon value; while the change in the orbital g-factors are δg_p^{ℓ} = +0.09 n.m. and δg_n^{ℓ} = -0.02 n.m. The isovector intrinsic moment of the $s_{1/2}$-orbit on the other hand increases, however, this is not inconsistent with the observed deviations of the magnetic moments of ^{3}H and ^{3}He from the Schmidt value. It can safely be said only that the effective g-factors and intrinsic moments arise from the combined effects of many different corrections other than the intra-major-shell configuration-mixing corrections included in the present mixed-configuration wave functions. More rigorous and quantitative treatment of the various other corrections to

the magnetic moment, specifically as a renormalization of the g-factors and intrinsic-moments, would be very helpful.

III. SUGGESTIONS FOR FURTHER STUDY

The principal aim of this study was to obtain an empirical Hamiltonian for use in shell-model calculation that would give a good description of all sd-shell nuclei using a full 1s-0d model space. A single set of mass independent (1+2)-body Hamiltonian was found to be inadequate. Instead two Hamiltonians were obtained by iterative least-squares fits to energy-level data in the lower and upper end of the sd-shell. Comparison of calculated ground-state binding energies and spins, and energy spectra with experiments seems to indicate the two Hamiltonians combined will complement each other to give a good description of all sd-shell nuclei. The good agreement of calculated magnetic dipole moments of some ground and excited states in sd-shell nuclei with experiments is an initial confirmation of this expectation. More complete tests are needed, however. Further calculations of energy spectra of nuclei in the middle of the sd-shell, and further tests of the generated wave functions with other nuclear observables such as quadruple moments, electromagnetic transitions, β-decays, spectroscopic amplitudes

and electron scattering form factors will yield a thorough picture of our present level of understanding.

The unambiguous result of the empirical renormalization of the Kuo's realistic Hamiltonians was the reduction in attractiveness of the "unlike orbit" diagonal two-body matrix elements. In the light of the problems that still exist in the theory of effective interactions for shell-model-type calculations derived from the free-nucleon interaction, an understanding of the reduction in attractiveness may provide a key to the solution.

More quantitative treatment of the various effects on orbital g-factors and intrinsic moments of valence nucleon due to higher-order configuration mixings, mesonic exchange currents and others are needed for a better understanding of the effective g-factors and intrinsic moments derived from the fitted single-particle μ reduced matrix elements.

The technique of empirical renormalization of shell-model Hamiltonian in terms of uncorrelated (orthogonal) linear combinations of one- and two-body matrix elements can be applied easily to other regions of nuclei of interest (with manageable orders of Hamiltonians) without the previous problems of too many parameters or insufficiency of data. Examples are shell-model calculations in a $0f_{7/2}$-$1p_{3/2}$ model space, $0p_{3/2}$-$0p_{1/2}$-$0d_{5/2}$-$1s_{1/2}$-$0d_{3/2}$ model space, $0f_{5/2}$-$1p_{3/2}$-$1p_{1/2}$ model space and so on.

Better descriptions of the nuclei of interest should be achieved compared to previous attempts.

However, a shell-model calculation of major interest with the full 0f-1P model space is still prohibitively large even with the present available techniques. The result of the orthogonal parameter fit on the other hand is promising in that it shows only a few orthogonal parameters are important in describing the low-lying spectra. Understanding of such orthogonal linear combinations may provide simplications for shell-model description of low-lying spectra.

LIST OF REFERENCES

REFERENCES

1. E.C. Halbert, J.B. McGrory, B.H. Wildenthal and S.P. Pandya, Advances in Nuclear Physics, Vol. 4, Ed. M. Baranger and E. Vogt (Plenum Press, New York, 1971).

2. B.H. Wildenthal, E.C. Halbert, J.B. McGrory and T.T.S. Kuo, Phys. Rev. C4 (1971) 1266.

3. B.M. Preedom and B.H. Wildenthal, Phys. Rev. C6 (1972) 1633.

4. W.A. Lanford and B.H. Wildenthal, Phys. Rev. C7 (1973) 668.

5. B.J. Cole, A. Watt, and R.R. Whitehead, J. Phys. A7 (1974) 1374.

6. B.J. Cole, A. Watt, and R.R. Whitehead, J. Phys. A7 (1974) 1399.

7. B.J. Cole, A. Watt, and R.R. Whitehead, J. Phys. G1 (1975) 17.

8. B.J. Cole, A. Watt, and R.R. Whitehead, J. Phys. G1 (1975) 213.

9. S. Cohen and D. Kurath, Nucl. Phys. 73 (1965) 1.

10. F.J.D. Serduke, R.D. Lawson, and D.H. Gloeckner, Nucl. Phys. A256 (1976) 45

11. J.B. McGrory and T.T.S. Kuo, Nucl. Phys. A247 (1975) 283.

12. J.B. McGrory, B.H. Wildenthal, and E.C. Halbert, Phys. Rev. C2 (1970) 186.

13. J.B. French, E.C. Halbert, J.B. McGrory and S.S.M. Wong, Advances in Nuclear Physics, Vol. 3, Ed. M. Baranger and E. Vogt (Plenum Press, New York, 1969).

14. R.R. Whitehead, Nucl. Phys. A182 (1972) 290.

15. T.T.S. Kuo and G.E. Brown, Nucl. Phys. 85 (1966) 40.

16. T.T.S. Kuo, Nucl. Phys. A103 (1967) 71.

17. S.K. Shah and S.P. Pandya, Nucl. Phys. 38 (1962) 420.

18. P.W.M. Glaudemans, P.J. Brussaard, and B.H. Wildenthal, Nucl. Phys. A102 (1967) 593.

19. I. Talmi, Rev. Mod. Phys. 34 (1962) 704.

20. J.D. McCullen, B.F. Bayman, and Larry Zamick, Phys. Rev. 134 (1964) B515.

21. B.H. Wildenthal, J.B. McGrory, E.C. Halbert, and P.W.M. Glaudemans, Phys. Lett. 26B (1968) 692.

22. P.W.M. Glaudemans, G. Wiechers, and P.J. Brussaard, Nucl. Phys. 56 (1964) 529 and 548.

23. A. de-Shalit and I. Talmi, Nuclear Shell Theory, (Academic Press, New York, 1963).

24. M.H. Macfarlane, Two-body Force in Nuclei, Ed. S.M. Austin and G.M. Crawley (Plenum Press, New York, 1972).

25. T. Hamada and I.D. Johnston, Nucl. Phys. 34 (1962) 382.

26. R.V. Reid, Ann. Phys. 50 (1968) 411.

27. P.M. Endt and C. Van der Leun, Nucl. Phys. 214 (1973) 1.

28. A.H. Wapstra and N.B. Gove, Nucl. Data Tables, Vol. 9 (1971) 265.

29. F. Ajzenberg-Selove, Nucl. Phys. A166 (1971) 1;
F. Ajzenberg-Selove, Nucl. Phys. A190 (1972) 1.

30. J.L. Fowler, C.H. Johnson, R.M. Feezel, Phys. Rev. C8 (1973) 545;
C.H. Johnson, Phys. Rev C7 (1973) 561.

31. P. Doll et al., private communication.

32. T.K. Li, D. Dehnhard, Ronald E. Brown, and P.J. Ellis, Phys. Rev C13 (1976) 55.

33. P.J. Ellis and T. Engeland, Nucl. Phys. A144 (1970) 161; T. Engeland and P.J. Ellis, Nucl. Phys. A181 (1972) 368.

34. G. T. Garvey and I. Kelson, Phys. Rev. Lett. 16 (1966) 197.

35. G.T. Garvey et al., Rev. Mod Phys. 41 (1969) 51.

36. C. Thibault and R. Klapisch, Phys. Rev. C9 (1974) 793.

37. N.A. Jelley, Joseph Cerny, D.P. Stahel, and K.H. Wilcox, Phys. Rev. C11 (1975) 2049.

38. J.D. Garrett, R. Middleton, H.T. Fortune, Phys. Rev. C2 (1970) 1243.

39. D.J. Crozier, H.T. Fortune, R. Middleton, and J.L. Wiza, Phys. Rev. C11 (1975) 393.

40. J.L. Wiza, H.T. Fortune, Phys. Rev. C7 (1973) 1267.

41. D.J. Crozier and H.T. Fortune, Phys. Rev. C10 (1974) 1697.

42. D.S. Longo, J.C. Lawson, L.A. Alexander, B.P. Hichwa, P.R. Chagnon, Phys. Rev. C8 (1973) 1347.

43. J.N. Bishop, H.T. Fortune, Phys. Rev. Lett. 34 (1975) 1350.

44. D.J. Pullen, private communication.

45. J.C. Lawson, P.R. Chagnon, Phys. Rev. C11 (1975) 643.

46. C. Rolfs, H.P. Trautvetter, E. Kuhlmann, F. Riess, Nucl. Phys. A189 (1972) 641.

47. C. Rolfs, E. Kuhlmann, F. Riess, R. Kraemer, Nucl. Phys. A167 (1971) 449.

48. E.K. Warburton, J.W. Olness, Phys. Rev. C2 (1970) 2235.

49. R. H. Spear, R.A.I. Bell, M.T. Esat, P.R. Gardner, and D.C. Kean, Phys. Rev. C11 (1975) 742.

50. J. Gomez del Campo, J.L.C. Ford Jr., R.L. Robinson, P.H. Stelson, Phys. Rev. C9 (1974) 1258.

51. W. Scholz, P. Neogy, K. Bethge, R. Middleton, Phys. Rev. C6 (1972) 893.

52. P. Neogy, R. Middleton, W. Scholz, Phys. Rev. C6 (1972) 885.

53. C. Broude, W.G. Davies, J.S. Forster, Phys. Rev. Lett. 25 (1970) 944.

54. C.N. Davids, D.R. Goosman, D.E. Alburger, A. Gallmann, G. Guillaume, D.H. Wilkinson, W.A. Lanford, Phys. Rev. C9 (1974) 216.

55. J.R. Powers, H.T. Fortune, R. Middleton, Phys. Rev. C4 (1971) 2030.

56. R.A. Lindgren, R.G. Hirko, J.G. Pronko, A.J. Howard, M.W. Sachs, and D.A. Bromley. Nucl. Phys. A180 (1972) 1.

57. G.J. Kekelis, A.H. Lumpkin, J.D. Fox, Phys. Rev. Lett. 35 (1975) 710.

58. K. Van Bibber, E.R. Cosman, A. Sperduto, T.M. Cormier, and T.N. Chin, Phys. Rev. Lett. 32 (1974) 687.

59. P. Sperr, D. Evers, K. Rudolph, W. Assmann, E. Spindler, P. Konrad, and G. Denhöfer, Phys. Lett. 49B (1974) 345.

60. H.F. Lutz, J.J. Wesolowski, L.F. Hansen, S.F. Eccles, Nucl. Phys. A95 (1967) 591.

61. D.R. Goosman, D.E. Alburger, Phys. Rev. C10 (1974) 756.

62. E. Selin, Physica Scripta 2 (1970) 169.

63. D. Branford, A.C. McGough, and I.F. Wright, Nucl. Phys. A241 (1975) 349.

64. L.K. Fifield, R.W. Zurmühle, D.P. Balamuth, Phys. Rev. C8 (1973) 2217.

65. A.S. Keverling Buisman, P.J.M. Smulders, Nucl. Phys. A228 (1974) 205.

66. D.R. Goosman, D.E. Alburger, J.C. Hardy, Phys. Rev. C7 (1973) 1133.

67. K.H. Wilcox, N.A. Jelley, G.J. Wozniak, R.B. Weisenmiller, H.L. Harney, Joseph Cerny, Phys. Rev. Lett. 30 (1973) 866.

68. E.R. Flynn, J.D. Garrett, Phys. Rev. C9 (1974) 210.

69. C. Thibault, R. Klapisch, C. Rigaud, A.M. Poskanzer, R. Prieels, L. Lessard, W. Reisdorf, Phys. Rev. C12 (1975) 644.

70. D.R. Goosman, D.E. Alburger, Phys. Rev. C7 (1973) 2409.

71. D.R. Goosman, D.E. Alburger, C.N. Davids, Phys. Rev. C8 (1973) 1324.

72. D.R. Goosman and D.E. Alburger, Phys. Rev. C6 (1972) 820.

73. B.H. Wildenthal, J.A. Rice, and B.M. Preedom, Phys. Rev. C10 (1974) 2184.

74. B.H. Wildenthal, E. Newman, Nucl. Phys. A118 (1968) 347.

75. L.L. Gadeken, P.J. Nolan, P.A. Butler, L.L. Green, A.N. James, J.F. Sharpey-Schafer, D.A. Viggars, J. Phys, A7 (1974) 83.

76. P. Doll, H. Mackh, G. Mairle, G.J. Wagner, Nucl. Phys. A230 (1974) 329.

77. J.E. Brock, I.A. Luketina, A.R. Poletti, Phys. Rev. C6 (1972) 1298.

78. S. Fortier, M. Langevin, J.M. Maison, M. Vergnes, and J. Vernotte, Proc. Amsterdam, Vol. I (1974) 81.

79. J.A. Rice, B.H. Wildenthal, B.M. Preedom, Nucl. Phys. A239 (1975) 189.

80. R.R. Betts, H.T. Fortune, R. Middleton, Phys. Rev. C8 (1973) 660.

81. A. Moalem, B.H. Wildenthal, Phys. Rev. C11 (1975) 654.

82. P.A. Butler, A.J. Brown, P.E. Carr, L.L. Green, A.N. James, C.J. Lister, J.D. MacArthur, P.J. Nolan, and J.F. Sharpey-Schafer, J. Phys. G1 (1975) 543.

83. H. Nann and B.H. Wildenthal, to be published.

84. F.E.H. Van Eijkern, G. Van Middlekoop, J. Timmer, and J. A. Van Luijk, Nucl. Phys. A210 (1973) 38.

85. E. Roeckl, P.F. Dittner, C. Detraz, R. Kaplisch, C. Thibault, and C. Rigaud, Phys. Rev. C10 (1974) 1181.

86. A.G. Artukh, G.F. Gridnev, V.L. Mikheev, V.V. Volkov, and J. Wilczynski, Nucl. Phys. A192 (1972) 170.

87. D.R. Goosman, C.N. Davids, D.E. Alburger, Phys. Rev. C8 (1973) 1331.

88. D.E. Alburger, D.R. Goosman, C.N. Davids, Phys. Rev. C8 (1973) 1011.

89. A. Arima and H. Horie, Progr. Theor. Phys. 11 (1954) 509; 12 (1954) 623.

90. R.J. Blin-Stoyle, Proc. Phys. Soc. A66 (1953) 1158.

91. H.A. Mavromatis and L. Zamick, Nucl. Phys. A104 (1967) 17; H.A. Mavromatis, L. Zamick, and G.E. Brown, Nucl. Phys. 80 (1966) 545; H.A. Mavromatis and L. Zamick, Phys. Lett. 20 (1966) 171.

92. H. Miyazawa, Progr. Theor. Phys. 6 (1951) 801.

93. S.D. Drell and J.D. Walecka, Phys. Rev. 120 (1960) 1069.

94. M. Chemtob, Nucl. Phys. A123 (1969) 449.

95. S. Nagamiya and T. Yamazaki, Phys. Rev. C4 (1971) 1961.

96. M. Forterre, J. Gerber, J.P. Vivien, M.B. Goldberg, K.H. Speidel, Phys. Lett. 55B (1975) 56.

97. J. Asher, J. of Phys. G, to be published.

98. Z. Berant, C. Broude, S. Dima, G. Goldring, M. Hass, Z. Shkedi, D.F.H. Start, Y. Wolfson, Nucl. Phys. A235 (1974) 410.

99. Z. Shkedi, Private Communication.

100. Z. Berant, C. Broude, G. Engler, M. Hass, R. Levy, B. Richter, Nucl. Phys. A243 (1975) 519.

101. R.E. Horstman, J.L. Eberhardt, H.A. Doubt, C.M.E. Otten, G.Van Middelkoop, Nucl. Phys. A248 (1975) 291.

102. R.E. Horstman, Nucl. Phys., to be published.

103. J.L. Eberhardt, R.E. Horstman, H.W. Heeman, G. Van Middlekoop, Nucl. Phys. A229 (1974) 162.

104. R. Kalish, Physica Scripta 11 (1975) 190.

105. J.L. Eberhardt, R.E. Horstman, H.A. Doubt, and G. Van Middlekoop, Nucl. Phys. A244 (1975) 1.

106. J.W. Hugg, T. Minamisono, D.G. Mavis, T.K. Saylor, H.F. Glavish, S.S. Hanna, Bulletin of American Physical Society 20 (1975) 1163.